

MISTRÀ

version v9.0_beta006

Description of the 1D MBL chemistry model

Roland von Glasow, Josué Bock

May 12, 2021

This manual is licenced under Creative Common licence BY-NC-ND v2.0,
whose text is available at:
<https://creativecommons.org/licenses/by-nc-nd/2.0/legalcode>

Contents

Preface	4
1 Introduction	5
2 Description of the MBL model	9
2.1 Meteorology, microphysics and thermodynamics	9
2.2 Chemistry	13
2.2.1 Gas phase and uptake	13
2.2.2 Aqueous phase	14
2.2.3 Photolysis	16
2.2.4 Emissions and deposition	17
2.3 Model initialisation	19
2.4 Model resolution and integration scheme	21
3 Model structure	23
3.1 *.f90 and *.f files	25
3.1.1 str.f90	25
3.1.2 kpp.f	30
3.2 *.h files	30
3.3 Additional files	30
3.3.1 euler.in.dat	30
3.3.2 namelist mistra_cfg	30
3.3.3 gas_species.csv	31
3.4 Integration of chemical reaction scheme with KPP	31
3.5 How to run the model	33
3.6 How to change the model	34
4 Description of the nucleation module	36
4.1 Physical concept	36
4.1.1 Apparent nucleation	36
4.1.2 Real nucleation	38
4.2 Treatment in MISTRA	39
4.3 Drawbacks, limitations, and unsolved problems	42

5 Photolysis	44
5.1 Theory	44
5.2 Calculation of the effective values	46
5.2.1 Structure of the programs to calculate the effective values for the band model	47
5.2.2 Introducing a new species in the programs for the effective values	48
5.2.3 Introducing a new species in the band model	49
5.3 Multiple scattering and photolysis rates	52
A Treatment of turbulent transport	53
B Calculation of the aqueous fraction	55
C List of symbols	57
C.1 Variable names	57
C.2 Names in the source code	59
D Tables of reaction rate coefficients	66
D.1 Iodine chemistry	83
E File unit numbers	90
F Cross sections	92
G Photolysis frequencies	103
H Routines documentation	107
H.1 claf	107
I Change log	108
J Troubleshooting and FAQ	113
J.0.1 Issues when producing the mechanism files	113
Bibliography	113
List of Tables	131

Preface

The meteorological kernel of this model is the microphysical stratus model MISTRA developed by Andreas Bott (*Bott et al.*, 1996). For his Ph.D. thesis work, Roland von Glasow (hereafter RvG) included a detailed chemical submodule where the reaction mechanism is based on the box model MOCCA (*Sander and Crutzen*, 1996; *Vogt et al.*, 1996). This combined model used to be called MISTRA-MPIC, where MPIC stands for “Max-Planck-Institute for Chemistry” version, but is now referred to as MISTRA for simplicity. All versions up to version **u6** have been developed at the MPIC, version **u7.1.x** was developed while RvG was at Scripps, **v7.2.x** and **v7.3.x** were developed at the Institute for Environmental Physics at the University of Heidelberg. An update for **v7.3.3** uses the integrator ROS3 and is called **v7.3.3_ROS3**. Version **v7.4.0** is the first version released at UEA. It uses the integrator ROS3 as standard, has a number of minor updates and includes the latest version of a nucleation routine developed by Susanne Pechtl. Version **v7.4.1** was released in March 2009 and includes several updates in the chemical mechanism. A version **v8** was developed with major changes in the number of chemical bins, but is abandoned. Version **v9.0** is the first public version, and includes an important number of technical improvements and bugfix that were implemented between 2015 and 2021. See appendix I for a change log.

The kinetic preprocessor KPP that was used to implement the chemical differential equation system was developed by Valeriu Damian-Iordache and Adrian Sandu (*Damian et al.*, 2002). Up to Mistra **v7.4.1**, the oldest version of KPP (version **v1.0**) was used. The latest released version of KPP (version **v2.2.3**) was adapted for Mistra in 2016, and this derived version is provided along with Mistra **v9.0**. It is distributed with its own licence. The photolysis module is courtesy of Jochen Landgraf (*Landgraf and Crutzen*, 1998) while the module for the calculation of the activity coefficients was provided by Beiping Luo. Rolf Sander, Paul Crutzen, Rainer Vogt and John Crowley contributed with ideas and support to the MPIC version of MISTRA. Susanne Pechtl wrote a new module for aerosol nucleation and dramatically improved the iodine chemistry (*Pechtl et al.*, 2006, 2007), Matthias Piot has extended the model for polar conditions (*Piot and von Glasow*, 2008b) and Linda Smoydzin included an ocean model for studies of the Dead Sea (*Smoydzin*, 2008). MISTRA has also been used to model ship (*von Glasow*, 2001) and volcanic plumes (*Bobrowski et al.*, 2007; *Aiuppa et al.*, 2007). From version **v9.0** onwards, this model is publicly available, and is distributed under the European Public Licence EUPL-v1.1.

Chapter 1

Introduction

This model was designed for process studies of the physics and chemistry of the marine boundary layer (MBL). The MBL is the lowest part of the troposphere that is in direct contact with the sea surface. It is separated from the free troposphere by a temperature and humidity inversion and is generally well mixed. As a consequence, the absolute humidity is constant with height in a cloud-free MBL. In the MBL the temperature decreases with height and therefore the relative humidity increases with height (see e.g. *Stull*, 1988). Below the inversion, stratiform clouds occur frequently. Figure 1.1 shows schematically the structure of the MBL with typical vertical profiles of the relative humidity, temperature and potential temperature. When the potential temperature is constant with height, this indicates a well mixed MBL. For the cloudy MBL also a typical profile of liquid water content of the cloud is shown. In the cloud the potential temperature increases with height due to the release of latent energy during condensation.

Approximately 70 % of the earth's surface is covered by oceans, making processes in the MBL potentially significant for the whole troposphere and atmosphere, as trace gases and aerosol can be exchanged between the MBL and the free troposphere. The net radiative forcing of stratiform clouds in the MBL is negative, which is important for the total radiation budget of the atmosphere (e.g. *Albrecht*, 1989). *Lelieveld et al.* (1989) provided values for the latitudinally averaged cloud coverage for different types of clouds, which show that in the latitude bands of the southern hemisphere where the fraction of land is below 4 %, the coverage by stratiform clouds is in all seasons greater than 20 % and often greater than 40 %. *Peixoto and Oort* (1991) list the total global cloud coverage (i.e. not distinguished between different cloud types). Over the oceans the cloud coverage is almost always greater than 50 %. (*Houze*, 1993, Fig. 5.9) gives seasonal averages for cloud cover by cloud type. But even when no clouds are present in the MBL, the relative humidity is usually high enough to allow aerosol particles to be deliquescent, and therefore active aqueous chemistry to occur.

Chemical reactions on and inside atmospheric particles (e.g. aerosol particles and cloud droplets) can have a significant influence on the chemistry of the gas phase (see, e.g., *Jacob*, 2000, for a review). The aerosol particles in the unpolluted MBL are usually particles with sulfate as a main component as well as aerosol

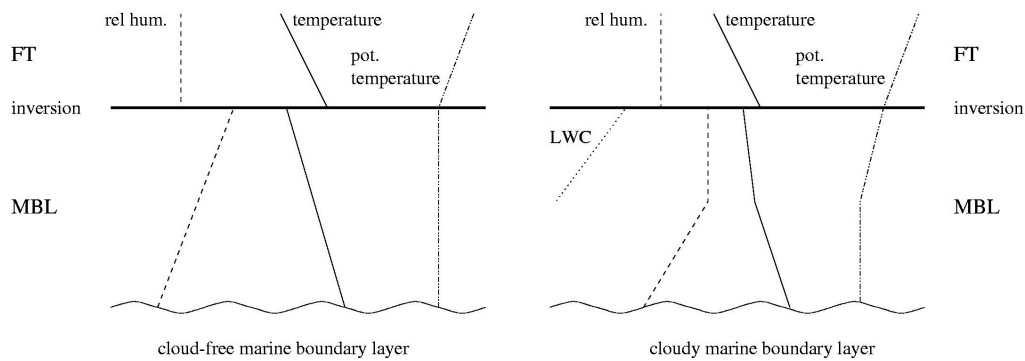


Figure 1.1: Schematic depiction of the vertical profiles of relative humidity, temperature, potential temperature (Θ) and liquid water content (LWC) in the cloud-free and cloudy MBL, FT stands for free troposphere. The LWC is only shown where a cloud is present.

particles produced from wind acting on the ocean surface, the so-called sea salt aerosols. During episodes of strong influence of continental air, e.g. dust outbreak from deserts or biomass burning, those particles can significantly contribute to the aerosol loading. Usually the number of aerosols in the MBL is dominated by sulfate particles, whereas the mass is dominated by the sea salt fraction.

Traditionally it was thought that cloud condensation nuclei (CCN) in the MBL are predominantly sulfate aerosol particles but more recent data suggests that under remote conditions, small sea salt particles can be very important as CCN or even dominate their number (*O'Dowd and Smith, 1993; Mason, 2001*).

Sea salt aerosols are produced at the sea surface by the bursting of air bubbles that had been entrained from the atmosphere at wave crests. This process produces small droplets from the film of the air bubbles and large jet droplets (see Figure 1.2). Even larger droplets are produced by strong winds blowing over wind crests and producing spray droplets (*Pruppacher and Klett, 1997*). When these droplets remain airborne, they evaporate partly to form sea salt aerosol particles. Sea salt aerosol consists mainly of sea water, often an organic film is present on the sea surface ('surface microlayer') which might get incorporated into the particles. The major component of sea salt aerosol is NaCl, but other components are also included (see Table 1.1), e.g. the halogen bromine which is very reactive once it is liberated from the sea salt aerosol. The composition of the major ions in sea water is very constant due to the long residence times of the ions in the oceans (about 10^8 years for Na^+ and Cl^- , *Andrews et al. (1996)*, p. 124).

Sea salt aerosol is important on a global scale because it contributes about 2/3 of the total natural sources of aerosol particles (by mass). If gas-to-particle conversion is included as particle source, it still contributes more than 40 % – 60 % (different estimates) to the total naturally produced aerosol mass (*Pruppacher and Klett, 1997*).

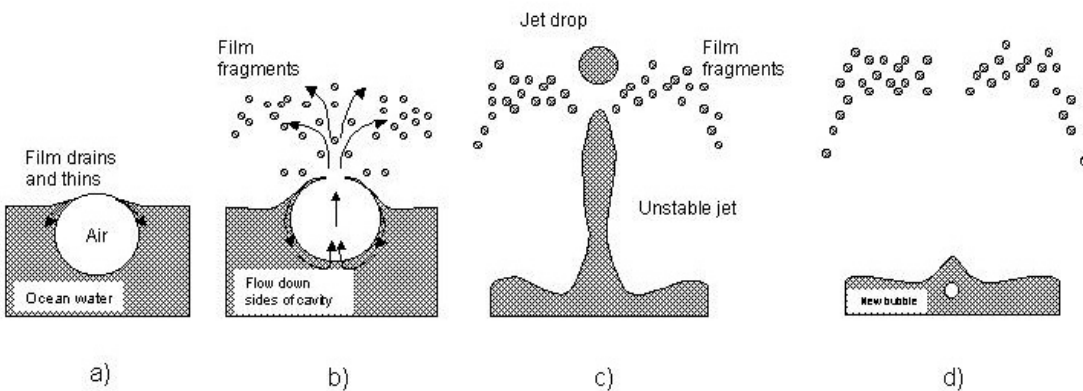


Figure 1.2: Four stages in the production of sea salt aerosol by the bubble-burst mechanism. (a) A bubble rises to the ocean surface thereby forming a thin film at the interface which begins to thin. (b) Flow of water down the sides of the cavity further thins the film which eventually ruptures into many small sea spray particles. (c) An unstable jet, produced from water flowing down the sides of the cavity, releases a few large sea spray drops. (d) Tiny salt particles remain airborne as drops evaporate; a new bubble is formed. Note the scale change between Figures (a) to (c) and Figure (d). After Pruppacher and Klett (1997).

Table 1.1: Ionic composition of sea water.

ion	Cl^-	Na^+	Mg^{2+}	SO_4^{2-}	K^+	Ca^{2+}	HCO_3^-	Br^-	I^-
conc. [mmol/l]	550	470	53	28	10	10	2	0.85	10^{-3}

The data is after Andrews *et al.* (1996), p. 121, except for Br^- and I^- which are calculated after Jaenicke (1988).

Apart from the halogens chlorine and bromine, the halogen iodine is also present in the MBL. It is mainly emitted in the form of biogenic alkyl iodides and molecular iodine that are rapidly photolysed in the MBL.

Reactions of halogens in the atmosphere received most attention in the study of the “ozone hole” that occurs in the Antarctic stratosphere during spring. This very strong O_3 destruction could be explained by fast, catalytic reactions involving halogen (mainly chlorine and bromine) radicals. The importance of interactions between the gas and the particulate phase was shown to be of particular importance (see e.g. Brasseur *et al.* (1999) for an overview).

The basic reaction mechanisms responsible for the destruction of O_3 in the stratosphere are not restricted to the stratosphere as shown by the occurrence of sudden O_3 destructions during spring (“polar sunrise”) in the Arctic boundary layer. See von Glasow and Crutzen (2007) for a description of the reaction cycles including gas and aerosol phase. Note that these cycles cause very quick autocatalytic O_3 destruction and that radicals that are present at very small con-

centrations (the BrO to O₃ ratio is about 1:1000 to 1:10000) can have a large impact.

As halogen compounds as well as particles are present in the MBL, the question arose, if similar reaction cycles with influence on O₃ or other species can be important in the MBL as well. Being the source for the OH radical, O₃ strongly influences the oxidative capacity of the atmosphere which determines, for example, the lifetime of most short and some long lived (e.g., CH₄) trace gases. Many measurements of the ionic composition of sea salt aerosol have shown that it is usually depleted in Cl⁻ but even more so in Br⁻. Typically the ratio of Br⁻/Na⁺ in the aerosol compared to the same ratio in sea water is used to quantify the Br⁻ deficit. Using Br⁻/Cl⁻ would lead to errors as Cl⁻ is also depleted from sea salt and therefore not a passive tracer unlike Na⁺. Small aerosol particles (mainly sulfate but also sea salt) are often found to be enriched in Br⁻. This could, however, also be an analytical problem due to the absence of Na⁺ in non-sea salt particles. This topic is reviewed by *Sander et al. (2003)*.

To further elucidate the role of halogens in the MBL, RvG extended the one-dimensional boundary layer model MISTRA to include chemical reactions in the gas phase as well as in and on aerosol (sea salt and sulfate particles) and cloud particles that grew on each type of aerosol. The resulting model is designed for detailed process studies; it is presented in chapter (2). In chapter (3) the model structure is explained and technical details on how to run the model are given. The nucleation module, developed by Susanne Pechtl, is described in chapter (4). The treatment of photolysis as well as how to modify the Band Model for the inclusion of new species is explained in chapter (5). In the appendix, additional information on the treatment of turbulence in the model (appendix A) and the calculation of the aqueous fraction (appendix B) is provided. The variables and the names of variables as they are used in the source code are listed in appendix C and the chemical reaction system is listed in appendix D.

In the text, “aqueous phase chemistry” is used as a generic term for all reactions involving aqueous particles. Aqueous particles in this context are deliquescent aerosols or cloud droplets. The reactions involving aqueous particles are uptake from the gas phase, reactions on the surface of particles, chemical reactions and equilibria within the particles.

Results using MISTRA are discussed in *von Glasow (2001)*, *von Glasow and Sander (2001)*, *Wagner et al. (2002)*, *von Glasow et al. (2002a,b)*, *von Glasow and Crutzen (2004)*, *Pechtl et al. (2006)*, *Bobrowski et al. (2007)*, *von Glasow (2006)*, *Stutz et al. (2007)*, *Aiuppa et al. (2007)*, *Pechtl et al. (2007)*, *Smoydzin and von Glasow (2007)*, *Keene et al. (2007)*, *Pechtl and von Glasow (2007)*, *Piot and von Glasow (2008a)*, *Piot and von Glasow (2008b)* and *von Glasow (2008)*.

Chapter 2

Description of the MBL model

2.1 Meteorology, microphysics and thermodynamics

MISTRA is a one-dimensional model of the MBL. The meteorological and microphysical part is the boundary layer model MISTRA described in detail by *Bott et al.* (1996) and *Bott* (1997). Apart from dynamics and thermodynamics it includes a detailed microphysical module that calculates particle growth explicitly and treats feedbacks between radiation and particles. Figure 2.1 shows schematically the most important processes that are included in the model for a cloudy MBL. Gas phase chemistry is active in all model layers, aerosol chemistry only in layers where the relative humidity (of which a typical vertical profile is shown) is greater than the deliquescence/crystallisation humidity (see discussion on page 15). When a cloud forms, cloud droplet chemistry is also active. Fluxes of sea salt aerosol and gases from the ocean are included and the main meteorological processes (turbulence, radiation) are also shown.

The set of prognostic variables comprises the horizontal components of the wind speed u , v , the specific humidity q , and the potential temperature Θ :

$$\frac{\partial u}{\partial t} = -w \frac{\partial u}{\partial z} + \frac{\partial}{\partial z} \left(K_m \frac{\partial u}{\partial z} \right) + f(v - v_g) \quad (2.1)$$

$$\frac{\partial v}{\partial t} = -w \frac{\partial v}{\partial z} + \frac{\partial}{\partial z} \left(K_m \frac{\partial v}{\partial z} \right) - f(u - u_g) \quad (2.2)$$

$$\frac{\partial q}{\partial t} = -w \frac{\partial q}{\partial z} + \frac{\partial}{\partial z} \left(K_h \frac{\partial q}{\partial z} \right) + \frac{C}{\rho} \quad (2.3)$$

$$\frac{\partial \Theta}{\partial t} = -w \frac{\partial \Theta}{\partial z} + \frac{\partial}{\partial z} \left(K_h \frac{\partial \Theta}{\partial z} \right) - \left(\frac{p_0}{p} \right)^{R/c_p} \frac{1}{c_p \rho} \left(\frac{\partial E_n}{\partial z} + LC \right) \quad (2.4)$$

where f is the Coriolis parameter, u_g and v_g are the geostrophic wind components, K_m and K_h are the turbulent exchange coefficients for momentum and heat, L is the latent heat of condensation, C the condensation rate, ρ the air density, p

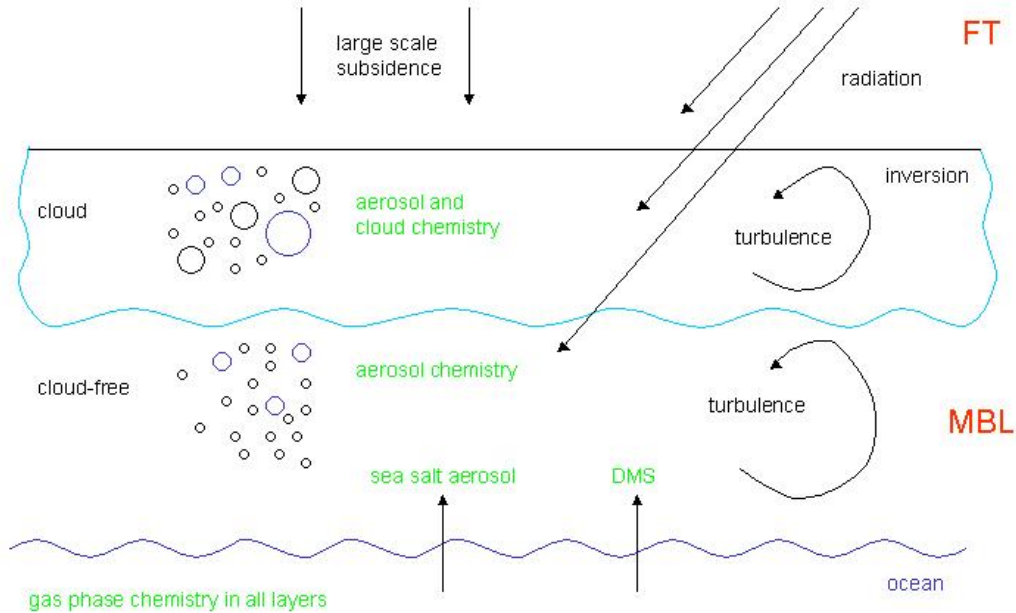


Figure 2.1: Schematic depiction of the most important processes included in the one-dimensional boundary layer model MISTRAL. The free troposphere is denoted as FT.

the air pressure, p_0 the air pressure at the surface, R the gas constant for dry air, c_p the specific heat of dry air at constant pressure, and E_n the net radiative flux density, respectively. The first term on the right of each equation is the large scale subsidence. Strictly, in a one-dimensional framework the vertical velocity $w = 0$ everywhere as this implies downward mass transport (for $w < 0$) without lateral outflow at the bottom of the 1D model column as would occur in the real atmosphere. Therefore the mass balance is violated if subsidence is included. To correctly model the evolution of stratiform clouds subsidence is, however, essential, as pointed out by several authors (e.g. *Driedonks and Duynkerke (1989)*). In runs where only aerosol chemistry is studied, i.e. in runs without clouds, the vertical velocity is set to zero ($w = 0$) in the model to avoid this problem, for the cloud runs subsidence is usually included.

Turbulence is treated with the level 2.5 model of *Mellor and Yamada (1982)* with the modifications described in *Bott et al. (1996)*. The turbulent exchange coefficients K_m and K_h are calculated via stability functions $S_{m/h}$ and $G_{m/h}$. The prognostic equation for the turbulence kinetic energy e is:

$$\frac{\partial e}{\partial t} = -w \frac{\partial e}{\partial z} + \frac{\partial}{\partial z} \left(K_e \frac{\partial e}{\partial z} \right) + \frac{(2e)^{3/2}}{l} \left(S_m G_m + S_h G_h - \frac{1}{16.6} \right) \quad (2.5)$$

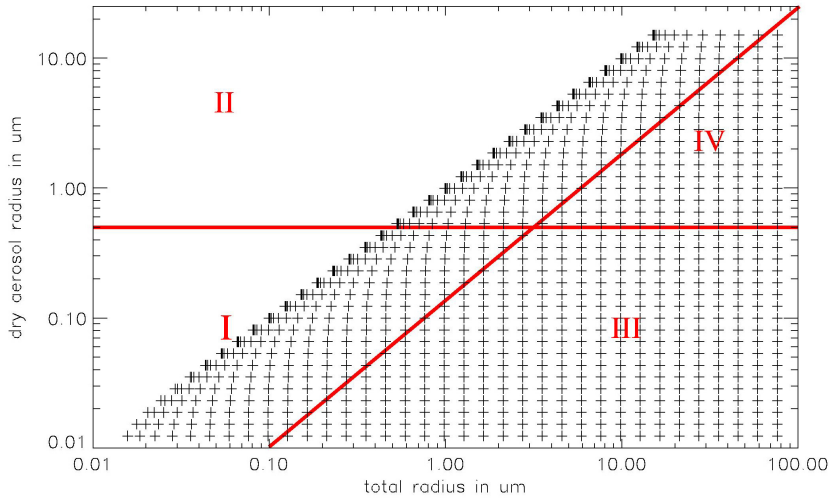


Figure 2.2: The two-dimensional particle spectrum as function of the dry aerosol radius a and the total particle radius r . Added are the chemical bins. I: sulfate aerosol bin, II: sea salt aerosol bin, III: sulfate cloud droplet bin, IV: sea salt droplet bin. For simplicity a 35×35 bin grid is plotted, in the model 70×70 bins are used.

assuming a constant dissipation ratio (last term on the right). For more details and an explanation of the calculation of the mixing length l , the exchange coefficient K_e for the turbulent kinetic energy, and the functions $S_{m/h}$ and $G_{m/h}$ see *Mellor and Yamada (1982)* and *Bott et al. (1996)*.

The microphysics is treated using a joint two-dimensional particle size distribution function $f(a, r)$ with the total particle radius r and the dry aerosol radius a the particles would have, when no water were present in the particles. The two-dimensional particle grid (see Figure 2.2) is divided into 70 logarithmically equidistant spaced dry aerosol classes, with the minimum aerosol radius being $0.005 \mu\text{m}$ and the maximum radius $15 \mu\text{m}$. Chosing these values allows to account for all accumulation mode particles and most of the coarse particles. All these numbers are adjustable.

Each of the 70 dry aerosol classes is associated with 70 total particle radius classes, ranging from the actual dry aerosol radius up to $60 \mu\text{m}$ ($150 \mu\text{m}$ in cloud runs). The prognostic equation for $f(a, r)$ is:

$$\begin{aligned} \frac{\partial f(a, r)}{\partial t} &= -w \frac{\partial f(a, r)}{\partial z} + \frac{\partial}{\partial z} \left(K_h \rho \frac{\partial f(a, r)}{\partial z} \right) \\ &\quad - \frac{\partial}{\partial z} \left(w_t f(a, r) \right) - \frac{\partial}{\partial r} \left(\dot{r} f(a, r) \right) \end{aligned} \quad (2.6)$$

Again, subsidence is the first term on the right, followed by turbulent mixing, particle sedimentation (w_t is the sedimentation velocity) and changes in f due to particle growth ($\dot{r} = dr/dt$). Upon model initialisation the particles are initialized

with a water coating according to the equilibrium radius of the dry nucleus at the ambient relative humidity. During the integration, particle growth is calculated explicitly for each bin of the 2D particle spectrum using the growth equation after *Davies* (1985) (see also *Bott et al.* (1996)):

$$r \frac{dr}{dt} = \frac{1}{C_1} \left[C_2 \left(\frac{S_\infty}{S_r} - 1 \right) - \frac{F_d(a, r) - m_w(a, r)c_w dT/dt}{4\pi r} \right] \quad (2.7)$$

with the ambient supersaturation S_∞ and the supersaturation at the droplet's surface S_r according to the Köhler equation¹:

$$S_r = \exp \left[\frac{A}{r} - \frac{Ba^3}{r^3 - a^3} \right]. \quad (2.8)$$

The change in particle radius is not determined by changes in water vapor saturation alone, but also by the net radiative flux at the particle's surface $F_d(a, r)$, that leads to temperature changes and therefore to condensation or evaporation. The constants C_1 and C_2 in equation (2.7) are:

$$C_1 = \rho_w L + \frac{\rho_w C_2}{D'_v S_r \rho_s} \quad C_2 = k' T \left[\frac{L}{R_v T} - 1 \right]^{-1}, \quad (2.9)$$

$m_w(a, r)$ is the liquid water mass of the particle, c_w and ρ_w are the specific heat and density of water, ρ_s is the saturation vapor density and R_v the specific gas constant for water vapor. The thermal conductivity k' of moist air and the diffusivity of water vapor D'_v have been corrected for gas kinetic effects following *Pruppacher and Klett* (1997) (their equation 13.14). For the accommodation coefficient of water (condensation coefficient), a value of $\alpha_c = 0.036$ is used (see table 5.4 in *Pruppacher and Klett* (1997) for a compilation of measured α_c values; in table 13.1 they use $\alpha_c = 0.036$ as “best estimate”).

The condensation rate C in equation (2.4) is determined diagnostically from the partical growth equation (2.7).

Collision-coalescence processes are not included in the model because this leads to great difficulties for describing the redistribution of the chemical species in the particles. However a version of MISTRAL including collision-coalescence without considering chemistry does exist (*Bott*, 2000).

For the calculation of the radiative fluxes, a δ -two stream approach is used (PIFM2, *Zdunkowski et al.* (1982), *Loughlin et al.* (1997)). The radiative fluxes are used for calculating heating rates and the effect of radiation on particle growth. The radiation field is calculated with the aerosol/cloud particle data from the microphysical part of the model, so feedbacks between radiation and particle growth are fully implemented. The calculation of photolysis frequencies is described in section (2.2.3) and chapter (5).

¹Please note a typo in *Bott et al.* (1996), a^3 is missing in the numerator of the second right hand side argument

2.2 Chemistry

The multiphase chemistry module comprises chemical reactions in the gas phase as well as in aerosol and cloud particles. Transfer between gas and aqueous phase and surface reactions on particles are also included. Tables D.2 to D.6 show a complete listing of the reactions. The reaction set is based on *Sander and Crutzen* (1996) plus some organic reactions from *Lurmann et al.* (1986a). It has been updated and expanded to include a better description of the oxidation of DMS (*von Glasow and Crutzen*, 2004). In the following the term aqueous phase is used as generic term for sub-cloud aerosol, interstitial aerosol (i.e. non-activated aerosol particles in cloudy layers), and cloud particles.

2.2.1 Gas phase and uptake

The prognostic equation for the concentration of a gas phase chemical species c_g (in mol/m³_{air}) including subsidence, turbulent exchange, deposition on the ocean surface, chemical production and destruction, emission and exchange with the aqueous phases is:

$$\begin{aligned} \frac{\partial c_g}{\partial t} = & -w \frac{\partial c_g}{\partial z} + \frac{\partial}{\partial z} \left(K_h \rho \frac{\partial c_g / \rho}{\partial z} \right) - D \\ & + P - L c_g + E - \sum_{i=1}^{n_{kc}} \left[\overline{k_{t,i}} \left(w_{l,i} c_g - \frac{c_{a,i}}{k_H^{cc}} \right) \right]. \end{aligned} \quad (2.10)$$

Again subsidence is included only in runs with clouds. P and L are chemical production and loss terms, respectively, k_H^{cc} is the dimensionless Henry constant obtained by $k_H^{cc} = k_H RT$, where k_H is in mol/(m³Pa), $w_{l,i}$ is the dimensionless liquid water content (m³_{aq}/m³_{air}) of bin i (see explanation on p. 14). The emission E as well as dry deposition D are effective only in the lowermost model layer. The calculation of the dry deposition velocity v_g^{dry} , that is needed for the determination of D , is explained at the end of this section. Note that both, E and D , are not inserted as fluxes in equation 2.10. For example the dry deposition flux $F_{dep} = c_g v_g^{dry}$ (in mol/(m² s)) has to be divided by the thickness of the lowermost model layer Δz to yield D . The last term in equation (2.10) describes the transport from the gas phase into the aqueous phases according to the formulation by *Schwartz* (1986) (see also *Sander* (1999)), n_{kc} is the number of the aqueous classes as explained below. For a single particle, the mass transfer coefficient k_t is defined as

$$k_t = \left(\frac{r^2}{3D_g} + \frac{4r}{3\bar{v}\alpha} \right)^{-1} \quad (2.11)$$

with the particle radius r , the mean molecular speed $\bar{v} = \sqrt{8RT/(M\pi)}$ (M is the molar mass), the accommodation coefficient α (see Table D.6), and the gas

phase diffusion coefficient D_g . D_g is approximated as $D_g = \lambda\bar{v}/3$ (e.g. *Gombosi* (1994), p. 125) using the mean free path length λ .

Chameides (1984) points out that the time needed to establish equilibrium between the gas and aqueous phase differs greatly for individual species and that soluble species never reach equilibrium in cloud droplets, emphasizing the importance of describing phase transfer in the kinetic form that is used here. *Audriffen et al.* (1998) and *Chaumerliac et al.* (2000) point out, that for reactive species like H_2O_2 the use of the Henry equilibrium assumption instead of the detailed description of mass transfer in the kinetic form that is used here would lead to significant errors in cloud droplet concentrations.

Ambient particle populations are never monodisperse, i.e. one has to account for particle with different radii. The mean transfer coefficient \bar{k}_t for a particle population is given by the integral:

$$\bar{k}_t = \frac{4\pi}{3w_l} \int_{lgr_{min}}^{lgr_{max}} \left(\frac{r^2}{3D_g} + \frac{4r}{3\bar{v}\alpha} \right)^{-1} r^3 \frac{\partial N}{\partial lgr} dlgr, \quad (2.12)$$

where the size distribution function $\partial N/\partial lgr$ is defined in Table 2.3.

2.2.2 Aqueous phase

Aqueous chemistry is calculated in four bins (see Figure 2.2): deliquescent aerosol particles with a dry radius less than $0.5 \mu m$ are included in the “sulfate aerosol” bin, whereas deliquescent particles with a dry aerosol radius greater than $0.5 \mu m$ are in the “sea salt aerosol” bin. Although the composition of the particles changes over time the terms “sulfate” and “sea salt” aerosol are used to describe the origin of the particles. The particles get internally mixed by exchange with the gas phase but, as mentioned earlier, not by particle collisions.

When the total particle radius exceeds the dry particle radius by a factor of 10, i.e. when the total particle volume is 1000 times greater than the dry aerosol volume, the particle and its associated chemical species are moved to the corresponding sea salt or sulfate derived cloud particle class. This threshold roughly coincides with the critical radius derived from the Köhler equation. When particles shrink they are redistributed from the droplet to the aerosol bins.

Therefore in a cloud-free layer there are 2 ($n_{kc} = 2$) aqueous chemistry classes (sulfate and sea salt aerosol) and in a cloudy layer 2 cloud droplet (sulfate and sea salt derived) and 2 interstitial aerosol (sulfate and sea salt) classes, giving a total of 4 ($n_{kc} = 4$) aqueous chemistry classes. In each of these classes the following prognostic equation is solved for each chemical species $c_{a,i}$ (in mol/m $_air^3$), where the index i stands for the i-th aqueous class:

$$\begin{aligned}\frac{\partial c_{a,i}}{\partial t} = & -w \frac{\partial c_{a,i}}{\partial z} + \frac{\partial}{\partial z} \left(K_h \rho \frac{\partial c_{a,i}/\rho}{\partial z} \right) - D \\ & + P - Lc_{a,i} + E + P_{pc} + \overline{k_{t,i}} \left(w_{l,i} c_g - \frac{c_{a,i}}{k_H^{cc}} \right)\end{aligned}\quad (2.13)$$

The individual terms have similar meanings as in equation (2.10). The calculation of the sedimentation velocity $v_{a,i}^{dry}$, that is needed for the calculation of the dry deposition D , is explained at the end of this section. The additional term P_{pc} accounts for the transport of chemical species from the aerosol to the cloud droplet regimes and vice versa when droplets are formed or when they evaporate. If only phase transfer is considered, equation (2.13) reduces in steady state conditions ($\partial c_{a,i}/\partial t = 0$) to the Henry equilibrium $c_{a,i} = w_{l,i} c_g k_H^{cc}$.

The concentration of H^+ ions is calculated like any other species, i.e. no further assumptions are made. The charge balance (sometimes used to derive the pH) is satisfied implicitly.

Cloud-processing, i.e. the change of aerosol mass due to uptake of gases, is included in the model based on *Bott* (1999). Due to uptake (mainly of sulfur) the sulfate aerosol particles grow into the size range occupied by sea salt aerosol. Shrinking of sea salt particles (see section 2.3) leads to the presence of Na^+ in sulfate particles. The implementation of the aerosol processing has to be improved in further versions, however, because shrinking of particles leads to the accumulation of particles at the lower end of the particle spectrum (due to errors that lead to shrinking in the first place??). Important issues in this respect are number *and* mass conservation, where the number is a critical parameter for the microphysics and mass for the chemistry.

It has been observed in many laboratory experiments that soluble aerosol remain in a highly concentrated metastable aqueous state when they are dried below their deliquescence humidity. Only when they reach the crystallisation humidity they can be regarded as “dry”. This effect is called the hysteresis effect. For $NaCl$ the crystallisation point is about 45 % relative humidity (*Shaw and Rood* (1990), *Tang* (1997), *Pruppacher and Klett* (1997), and *Lee and Hsu* (2000)). The crystallisation humidity for many mixed aerosol particles containing sulfate or nitrate is below 40 % relative humidity (*Seinfeld and Pandis* (1998) and references therein), implying that aerosol particles that already had been involved in cloud cycles will also be in an aqueous metastable state. Therefore most soluble aerosol particles will be present in the atmosphere as metastable aqueous particles below their deliquescence humidity. Upon model initialisation all aerosol particles are regarded as “aqueous” when the ambient relative humidity is above the respective crystallisation humidity. If the humidity drops during integration below the crystallisation humidity, these particles can only reactivate when the deliquescence humidity is reached (controlled via the logical *cloud*).

Aerosol particles are usually highly concentrated solutions. Laboratory measurements show that $NaCl$ molalities can be in excess of 10 mol/kg (*Tang*, 1997) implying also very high ionic strengths. Therefore it is necessary to account for

deviations from ideal behaviour, i.e. to include activity coefficients. The Pitzer formalism (*Pitzer*, 1991) is used to calculate the activity coefficients for the actual composition of each aqueous size bin. We use the implementation by Luo (*Luo et al.* (1995) and pers. comm. 1999). Note that it is important to change units as the activity coefficients are calculated for molalities ([mol]/[kg_{solvent}]) but used are molarities ([mol]/[dm³_{solution}]). The conversion factor is *cm/cw*.

In the atmosphere each aerosol or cloud particle is a closed “reaction chamber” with its own pH and concentrations of the species. In models the particles have to be lumped in bins where the individual properties of the particles vanish. In the model freshly emitted, alkaline sea salt particles are put into the same chemistry bin as aged acidic particles leading to mean conditions and reaction paths that can be distinctly different from what is happening in the atmosphere. Especially in the case of high wind, when sea salt aerosol production and therefore also sea salt aerosol loadings are high, the pH might be overestimated and reactions involving acidity might be underestimated because the buffer capacity of the few large particles would dominate the smaller, more acidic particles. In future versions of this model a finer resolution for the aqueous chemistry bins will be achieved.

Many reactions are pH dependent and the range of pH values in aerosol particles ranges from around 0 to 8 and even more. Some expressions for the rate coefficients, especially for third order reactions, can lead to reaction rates that are faster than the physical limit - the diffusion rate. In order to avoid that these artificial numbers are used, the reaction rate coefficient is limited to the diffusion value for reactions where this problem might arise. See *Pechtl et al.* (2007) and *Espenson* (1995) for details.

2.2.3 Photolysis

Photolysis is calculated online using the method of *Landgraf and Crutzen* (1998). Here an overview of the calculation of the photolysis rates is given, for a detailed description see chapter 5. The photolysis rate (or photo dissociation coefficient) J_x for a gas X can be calculated from the spectral actinic flux $F(\lambda)$ via the integral:

$$J_x = \int_I \sigma_x(\lambda) \phi_x(\lambda) F(\lambda) d\lambda \quad (2.14)$$

where λ is the wavelength, σ_x the absorption cross section, ϕ_x the quantum yield and I the photochemically active spectral interval. If the integral in equation (2.14) would be approximated with a sum, the number of wavelength bins needed for an accurate approximation of the integral would be in the order of 100 which would lead to excessive computing times. *Landgraf and Crutzen* (1998) suggested a method using only 8 spectral bins (see Table 2.1) approximating (2.14) by:

$$J_x \approx \sum_{i=1}^8 J_{i,x}^a \cdot \delta_i \quad (2.15)$$

Table 2.1: Subdivision of the spectral range of the photolysis module.

interval	1	2	3	4	5	6	7	8
λ_a [nm]	178.6	202.0	241.0	289.9	305.5	313.5	337.5	422.5
λ_b [nm]	202.0	241.0	289.9	305.5	313.5	337.5	422.5	752.5
λ_i [nm]	see LC98	205.1	287.9	302.0	309.0	320.0	370.0	580.0

The spectral range $178.6 \text{ nm} \leq \lambda \leq 752.5 \text{ nm}$ is subdivided into eight intervals, λ_a and λ_b are the initial and the final, and λ_i the fixed wavelength in interval I_i (after *Landgraf and Crutzen* (1998)). The intervals 1 and 2 are important only for the stratosphere, as only light with wavelengths greater than about 290 nm reaches the troposphere.

where $J_{i,x}^a$ is the photolysis rate for a purely absorbing atmosphere. The factor δ_i :

$$\delta_i := \frac{F(\lambda_i)}{F^a(\lambda_i)} \quad (2.16)$$

describes the effect of scattering by air molecules, aerosol and cloud particles, which is significant in the spectral range $202.0 \text{ nm} \leq \lambda \leq 752.5 \text{ nm}$. $F^a(\lambda_i)$ is the actinic flux of a purely absorbing atmosphere. For the Schumann-Runge band (spectral range $178.9 \text{ nm} \leq \lambda \leq 202.0 \text{ nm}$), scattering effects can be neglected because of the strong absorption by O_2 ($\delta_1 = 1$). The factor δ_i is calculated online for one wavelength for each interval (see λ_i in Table 2.1).

The $J_{i,x}^a$ are precalculated with a fine spectral resolution and are approximated during runtime from lookup tables or by using polynomials. The advantage of this procedure is that the fine absorption structures that are present in σ_x and ϕ_x are considered and only Rayleigh and cloud scattering, included in $F(\lambda_i)$, are treated with a coarse spectral resolution which is justified.

For the calculation of the actinic fluxes a four stream radiation code is used in addition to the two stream radiation code used for the determination of the net radiative flux density E_n because different spectral resolutions and accuracies are needed for these different purposes. Based on the findings of *Ruggaber et al.* (1997) a factor 2 is applied to photolysis rates inside aqueous particles to account for the actinic flux enhancement inside the particles due to multiple scattering.

2.2.4 Emissions and deposition

Constant emission fluxes for the gases DMS and NH_3 from the sea surface are applied with $2 \times 10^9 \text{ molec}/(\text{cm}^2\text{s})$ (*Quinn et al.*, 1990) and $4 \times 10^8 \text{ molec}/(\text{cm}^2\text{s})$ (*Quinn et al.* (1990)), scaled to model their measured gas phase mixing ratios of 19 nmol/mol in clean air masses), respectively.

Sea salt particles are emitted by bursting bubbles at the sea surface (e.g. *Woodcock et al.* (1953), *Pruppacher and Klett* (1997)). The parameterisation of *Monahan et al.* (1986) is used that estimates the flux F of particles with radius r at a relative humidity of 80 % per unit area of sea surface, per increment of droplet radius and time (in particles $\text{m}^{-2} \text{ s}^{-1} \mu\text{m}^{-1}$):

$$\frac{dF}{dr} = 1.373 u_{10}^{3.41} r^{-3} (1 + 0.057 r^{1.05}) \times 10^{1.19 \exp(-B^2)} \quad (2.17)$$

where $B = (0.380 - \log_{10} r)/0.65$ and u_{10} is the windspeed at 10 m height. *Monahan et al.* (1986) also parameterize the emission for particles with radii larger than $r=10 \mu\text{m}$ by additional terms, but only the bubble burst mechanism and not the spume production terms are included in Mistra because, as pointed out by e.g. *Wu* (1993), *Gong et al.* (1997) and *Andreas* (1998), these additional terms lead to an overestimation of the particle flux compared to measurements.

Large sea spray droplets ($r=10 - 300 \mu\text{m}$) can contribute to the transport of heat and moisture between ocean and atmosphere. According to *Andreas et al.* (1995) this is important for high windspeeds above about 15 m/s. As the model studies are mainly for moderate wind speeds where only very small amounts of particles in this size range are produced this process is neglected.

For each dry aerosol radius bin of the 2D microphysical spectrum the equilibrium radius for the current relative humidity is calculated and the appropriate number of particles according to equation (2.17) is added in the lowermost model layer in the respective total aerosol bin. The *Monahan et al.* (1986) estimate of the sea salt aerosol flux based on wind tunnel experiments is believed to yield good results for small particles (*Andreas*, 1998). For higher wind speeds the resulting mass flux of sea salt particles is less realistic, so for the model runs with high wind speed the parameterisation of *Smith et al.* (1993) that is based on measurements off the Scottish coast is used.

The dry deposition velocity for gases v_g^{dry} at the sea surface is calculated using the resistance model described by *Wesely* (1989):

$$v_g^{dry} = \frac{1}{r_a + r_b + r_c}. \quad (2.18)$$

The aerodynamic resistance r_a is calculated using:

$$r_a = \frac{1}{\kappa u_*} \left[\ln \left(\frac{z}{z_0} \right) + \Phi_s(z, L) \right], \quad (2.19)$$

with the friction velocity u_* , the von Kármán constant $\kappa = 0.4$, and the stability function Φ_s which depends on the Monin-Obukhov length L , the roughness length z_0 and a reference height z . The quasi-laminar layer resistance r_b is parameterized as:

$$r_b = \frac{1}{u_* (Sc^{-2/3} + 10^{-3/St})}. \quad (2.20)$$

The Stokes number St can be written as $St = w_t u_*^2 / (g\nu)$ and the Schmidt number as $Sc = \nu/D$ with the dynamic viscosity of air ν and the aerosol diffusion coefficient D_a . The surface resistance r_c is calculated using the formula by *Seinfeld and Pandis* (1998) (their equation (19.30)):

$$r_c = \frac{2.54 * 10^4}{H^* Tu_*}, \quad (2.21)$$

with the effective Henry constant H^* .

The dry deposition velocity of particles $v_{a,i}^{dry}$ is calculated after *Seinfeld and Pandis* (1998):

$$v_{a,i}^{dry} = \begin{cases} \frac{1}{r_a + r_b + r_a r_b w_t} + w_t & \text{lowest model layer} \\ w_t & \text{rest of model domain.} \end{cases} \quad (2.22)$$

The particle sedimentation velocity w_t is calculated in the microphysical module assuming Stokes flow and taking into account the Cunningham slip flow correction for particles with $r < 10\mu\text{m}$ and after Beard for larger particles (see *Pruppacher and Klett* (1997)).

2.3 Model initialisation

Tables 2.2 and 2.3 list the initial gas phase mixing ratios and parameters for the initial lognormal aerosol size distribution that were used in *von Glasow* (2001), *von Glasow et al.* (2002a), and *von Glasow et al.* (2002b). A vertical profile for the initial gas mixing ratios can be prescribed in file `initca.dat`; The initial aerosol size distribution is assumed to be the same throughout the model column, however this can easily be changed.

Particles larger than $r=0.5\mu\text{m}$ are assumed to be sea salt particles. The composition of sea salt aerosol in the model differs somewhat from the sea water composition in Table 1.1. In the model only Na^+ is considered as cation because the cations are chemically unreactive in the atmospheric aerosol. The anions considered are Cl^- , Br^- , HCO_3^- and for the iodine run also I^- and IO_3^- . According to these assumptions, the molar ratio of Br^- to Na^+ (used as the sum of cations in sea water) is about $1.8 \cdot 10^{-3}$ and $\text{HCO}_3^- : \text{Na}^+ = 4.2 \cdot 10^{-3}$ (see also *Sander and Crutzen*, 1996).

Upon model initialisation “fresh” sea salt with a pH of about 8 is present everywhere in the MBL (this is also the pH of freshly emitted sea salt). Bicarbonate, HCO_3^- , is an efficient buffer (see also *Chameides and Stelson* (1992)). It is strongly supersaturated in sea salt aerosol compared to air ($H^* \approx 1.6$, the equivalent total equilibrium concentration at pH=8 is about 0.5 mM whereas the initial concentration in sea salt is about 20 - 30 mM (see *Seinfeld and Pandis* (1998), section 6.3.2)) so it degasses as soon as enough acidity is present to allow the backward reaction of : $\text{CO}_2 + \text{H}_2\text{O} \longleftrightarrow \text{HCO}_3^- + \text{H}^+$. In fresh sea salt aerosol this acidity is mainly derived from the uptake of SO_2 and subsequent oxidation at high pH's by O_3 to S(VI) which is mainly in the form of SO_4^{2-} . Therefore 2 moles of CO_2 are effectively replaced by 1 mole of SO_2 leading to a net mass loss of the aerosol. The same happens when the acidity is derived from the uptake of

Table 2.2: Initial mixing ratios of gas phase species (in nmol/mol).

species	remote (MBL)	remote (FT)	cont. infl. (MBL)	cont. infl. (FT)
CO	70.0		150.0	
NO ₂	0.02	0.03	0.5	
HNO ₃	0.01	0.05	0.1	
NH ₃	0.08		0.2	
SO ₂	0.09		1.0	
O ₃	20.0	50.0	50.0	70.0
CH ₄	1800.0		1800.0	
C ₂ H ₆	0.5		5.0	
HCHO	0.3		0.3	
H ₂ O ₂	0.6		0.8	
PAN	0.01	0.1	0.1	1.0
HCL	0.04		0.04	
DMS	0.06		0.06	
CH ₃ I	0.002			
C ₃ H ₇ I	0.001			

Values are for the 2 scenarios “remote” and “continentally influenced”. A value for the free troposphere (FT) is given only when it is different from the MBL value. CH₃I and C₃H₇I are accounted for only in the “iodine” run.

Table 2.3: Initial size distribution of the aerosol.

mode i	$N_{tot,i}$ (1/cm ³)	$R_{N,i}$ (μm)	σ_i
1	100	0.027	1.778
2	120	0.105	1.294
3	6	0.12	2.818

The data is after *Hoppel and Frick* (1990). The particle size distribution is calculated according to $\frac{dN(r)}{dlgr} = \sum_{i=1}^3 \frac{N_{tot,i}}{\lg\sigma_i\sqrt{2\pi}} \times \exp\left(-\frac{(\lg r - \lg R_{N,i})^2}{2(\lg\sigma_i)^2}\right)$. $\lg x = \log_{10}x$.

HCl (which degassed from other, already acidified particles). The aerosol gains in mass if the acidity is derived from the uptake of HNO₃. When the aerosol loses mass because of this acid displacement, “negative aerosol processing” i.e. shrinking occurs which leads to the presence of sea salt aerosol in the “sulfate aerosol” bin.

In the model there is no difference between fresh and aged sea salt aerosol, all are lumped into the same aerosol bin, so the averaged pH is usually smaller than 6, so that species other than O₃ are responsible for the oxidation of S(IV). Furthermore, the uptake of acidic gases like HNO₃ from the gas phase rapidly acidifies the sea salt aerosol particles.

2.4 Model resolution and integration scheme

The atmosphere between the sea surface and 2000 m is divided into 150 layers. The lowest 100 layers have a constant layer height of 10 m, the layers above 1000 m are spaced logarithmically. These numbers are variable, however, for a run with a higher boundary layer the layer height could be increased to 20 m and the model domain could be extended to 3500 m.

Figures 2.3 and 2.4 show where the variables are actually defined on the model grid - some are defined in the middle of the layers others on the upper layer boundary (“wall”, which is why the respective variables usually have a “w” in their name). The latter is usually true for variables that are needed to calculate gradients between adjacent layers (e.g. turbulence variables). In models of radiative transfer model layer “zero” is usually the one that is most distant (i.e. ∞) from the Earth’s surface, whereas in dynamical models it is the other way round. This has always to be considered when exchanging variables between these submodels! The radiative transfer model that is used here is PIFM2 (see page 12), and several layers that define the optical properties between the top of the model and ∞ are added on top of the MISTRAL layers. The data for these layers is based on climatologies. For details see the PIFM references.

The usual operator splitting approach is used with a timestep of 10 s. Radiative fluxes and photolysis frequencies are calculated every 60 s and depending on the solar zenith angle, respectively.

The very stiff chemical differential equation system is solved with a third order Rosenbrock method (ROS3). A box model version of the model (using ROS2) was compared to results from the commercial integration system FACSIMILE (*Curtis and Sweetenham, 1987*) that uses a computationally more expensive Gear solver. Using the complete set of reactions we yielded good agreement between the different solvers. All chemical reactions in gas and aqueous phases, equilibria and phase transfer reactions are calculated as one coupled system using the kinetic preprocessor KPP (*Damian-Iordache, 1996; Damian et al., 2002; Sandu and Sander, 2006*) which allows rapid change of the chemical mechanism without major changes in the source code.

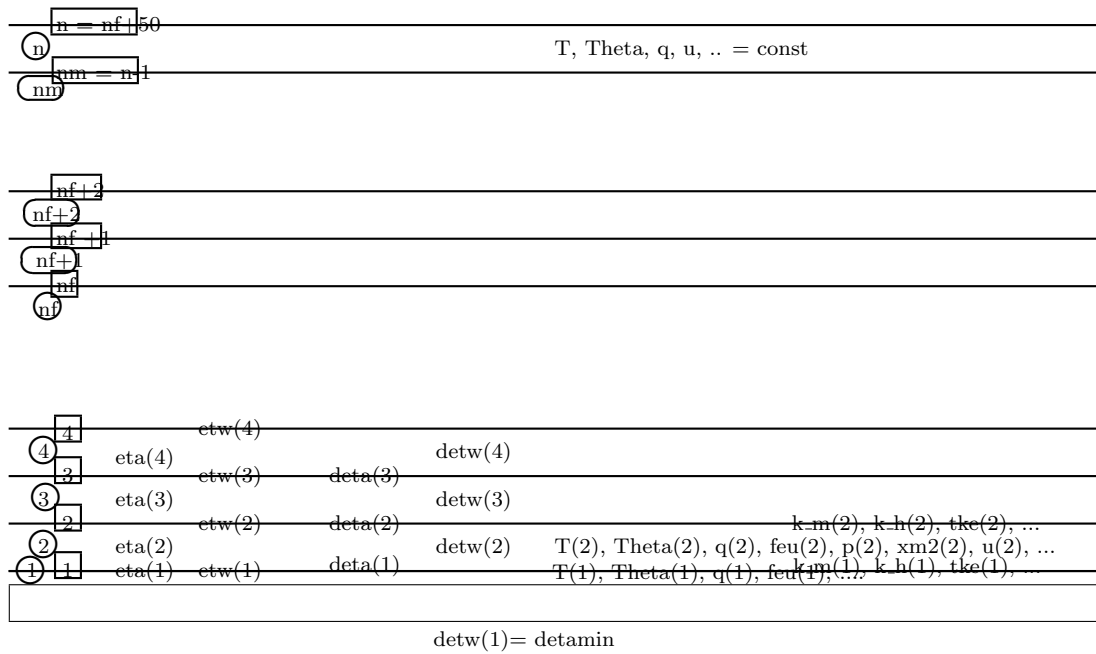


Figure 2.3: Model grid: meteorology

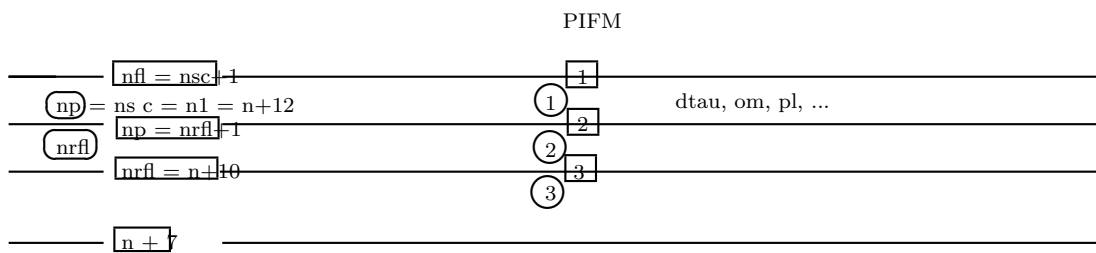


Figure 2.4: Model grid: radiation

Chapter 3

Model structure

This chapter explains the technical details of MISTRA. Figures 3.1 and 3.2 are flow diagrams of the model initialization and time integration, respectively. Table 3.1 gives a brief description of the files that MISTRA consist of. The more important files are explained in greater detail in sections 3.1, 3.2, and 3.3. In section 3.5 the main steps to run MISTRA are explained. Section 3.6 deals with changing the code, whereas in section 3.4 the chemistry submodule is explained in detail.

The in- and output files including unit number and a brief decription are listed in the appendix in table E.1.

file	description
*.f files	
activity.f	Calculation of activity coefficients according to the Pitzer theory including bromine salts. By Beiping Luo.
aer.f	Routines for integration of the chemistry mechanism for layers with gas and aerosol phase chemistry. Automatically generated by <code>make_kpp.scr</code> .
bud_a.f ¹	Subroutine for output of the rates of chemical reactions for layers with gas phase and aerosol phase chemistry. Automatically generated by <code>make_kpp.scr</code> .
bud_g.f ¹	Subroutine for output of the rates of chemical reactions for layers with gas phase chemistry only. Automatically generated by <code>make_kpp.scr</code> .
bud_t.f ¹	Subroutine for output of the rates of chemical reactions for layers with gas phase, aerosol and droplet phase chemistry. Automatically generated by <code>make_kpp.scr</code> .
bud_s_a.f ¹	Subroutine for output of the rates of sulfur oxidation reactions for layers with aerosol phase chemistry. Automatically generated by <code>make_kpp.scr</code> .
bud_s_g.f ¹	Subroutine for output of the rates of sulfur oxidation reactions for layers with gas phase chemistry only. Automatically generated by <code>make_kpp.scr</code> .

file	description
bud_s_t.f ¹	Subroutine for output of the rates of sulfur oxidation reactions for layers with aerosol and droplet phase chemistry. Automatically generated by <code>make_kpp.scr</code> .
gas.f	Routines for integration of the chemistry mechanism for layers with gas phase chemistry only. Automatically generated by <code>make_kpp.scr</code> .
jrate.f	Routines of the photolysis module.
kpp.f	Routines of the chemistry module. Definition and calculation of properties like Henry's law constants, uptake coefficients, liquid water content of chemistry bins, call to chemistry integration routines, call to activity coefficients subroutines
nrad.f	Routines of the radiation module PIFM2.
outp.f	Output subroutines ascii and binary output.
out_netCDF.f	Output subroutines for netCDF output.
radinit.f	Initialization of radiation variables.
str.f	Main program and dynamical and microphysical subroutines.
tot.f	Routines for integration of the chemistry mechanism for layers with gas, aerosol and droplet phase chemistry. Automatically generated by <code>make_kpp.scr</code> .
*.h files	
aer.h	Common blocks and definitions for the gas and aerosol phase chemical mechanism.
aer_s.h	dito, different data
gas.h	Common blocks and definitions for the gas phase only chemical mechanism.
gas_s.h	dito, different data
tot.h	Common blocks and definitions for the gas, aerosol and droplet phase chemical mechanism.
tot_s.h	dito, different data
additional files	
euler_in.dat	Definition of advection of species.
namelist.name	User defined switches for model options.
gas_species.csv	Definition of initial gas phase mixing ratios and emission fluxes.
Makefile	For use with <code>make</code> to generate *.o files and executable.
data files	
clark.dat	data needed for calculation of surface fluxes in SR claf
initr.dat	optical parameters for PIFM2
ozeankw.dat	aerosol optical parameters, shortwave, ocean aerosol mode
ozeanlw.dat	aerosol optical parameters, longwave, ocean aerosol mode
ruralkw.dat	aerosol optical parameters, shortwave, rural aerosol mode
rurallw.dat	aerosol optical parameters, longwave, rural aerosol mode
urbankw.dat	aerosol optical parameters, shortwave, urban aerosol mode

file	description
urbanlw.dat	aerosol optical parameters, longwave, urban aerosol mode

Table 3.1: Brief description of the files.¹ The routines in **bud_***.f are for output of the rates in 8 predefined levels only, whereas **bud_s_***.f ensure output of the sulfur rates for all model layers.

3.1 *.f90 and *.f files

3.1.1 str.f90

This file contains the main program and the dynamical and microphysical subroutines. The main program is divided into two parts, model initialization and time integration.

First the **mistra_cfg** namelist is read, and the initialization routines are called. This includes initial output (the actual plot routines are in **outp.f** or **out_netCDF**, respectively). If the restart option is selected, the output from a previous run is used as input. This is especially useful to avoid lengthy model spin-up if several sensitivity runs are made with the same dynamical setup. In routine **initm** the meteorological initial conditions are defined. Several different versions are included which yield different cases, e.g. cloudy run, cloud-free run, tropical conditions, or mid-latitude conditions (Figure 3.1 is a flow chart of the model initialization).

After the initialization the time integration starts. This is within the **do 1000 it=it0+1, itmax** loop. Operator splitting is used for the different dynamical, microphysical, and chemical processes, i.e. they are not calculated simultaneously but sequentially. To assure that all processes are solved with an appropriate timestep, different timesteps are used. Radiation is calculated with a 60 sec timestep, whereas the dynamics, microphysics, surface fluxes and chemical reactions are calculated with a fractional timestep of 10 sec (note that in version u6 the timestep of dynamics was 10 sec whereas that of the chemistry was 60 sec). The timestep for calculation of the chemical reaction system is split into smaller sub-timesteps within **SR kpp_driver**. At the end of the loop the chosen output is made and the loop is repeated. MISTRA was written based on a fog model (MIFOG, *Bott et al. (1990)*, *Bott and Carmichael (1993)*, *von Glasow and Bott (1999)*) where a soil module was needed. This is of course not used for the MBL but is still part of the source code (**SR soil**, **SR surf1**). See Figure 3.2 for a flow chart of the order of the different routines in integration.

MISTRA can also be run in box model mode by using the appropriate switch in the namelist. For this an additional routine is called during initialization and the time integration is completely different (see Figure 3.4). The main idea is to use the complete radiation model to get accurate photolysis rates but to not use the meteorological routines at all. Chemistry is calculated in layer 2 (the

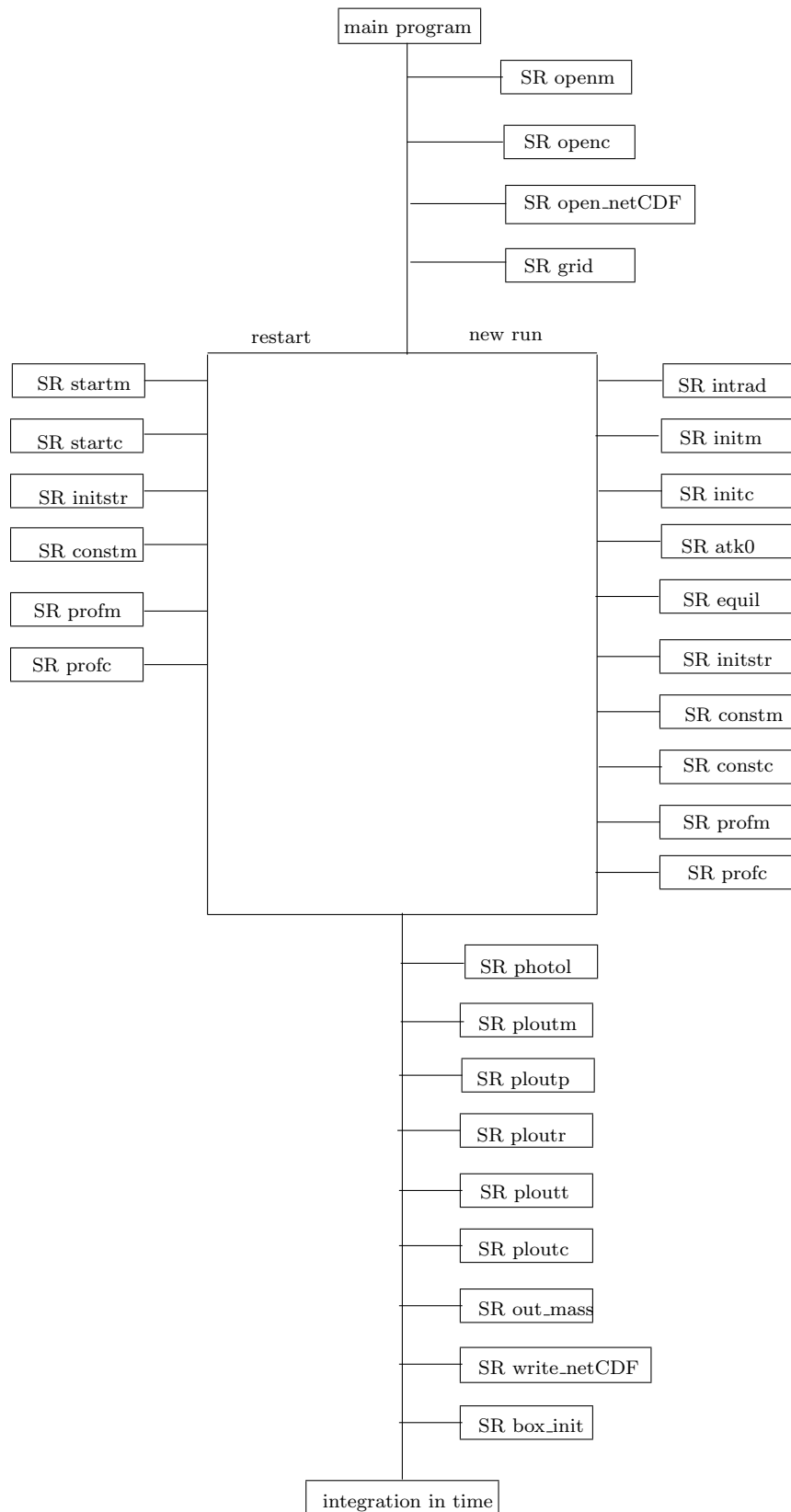


Figure 3.1: Model initialization

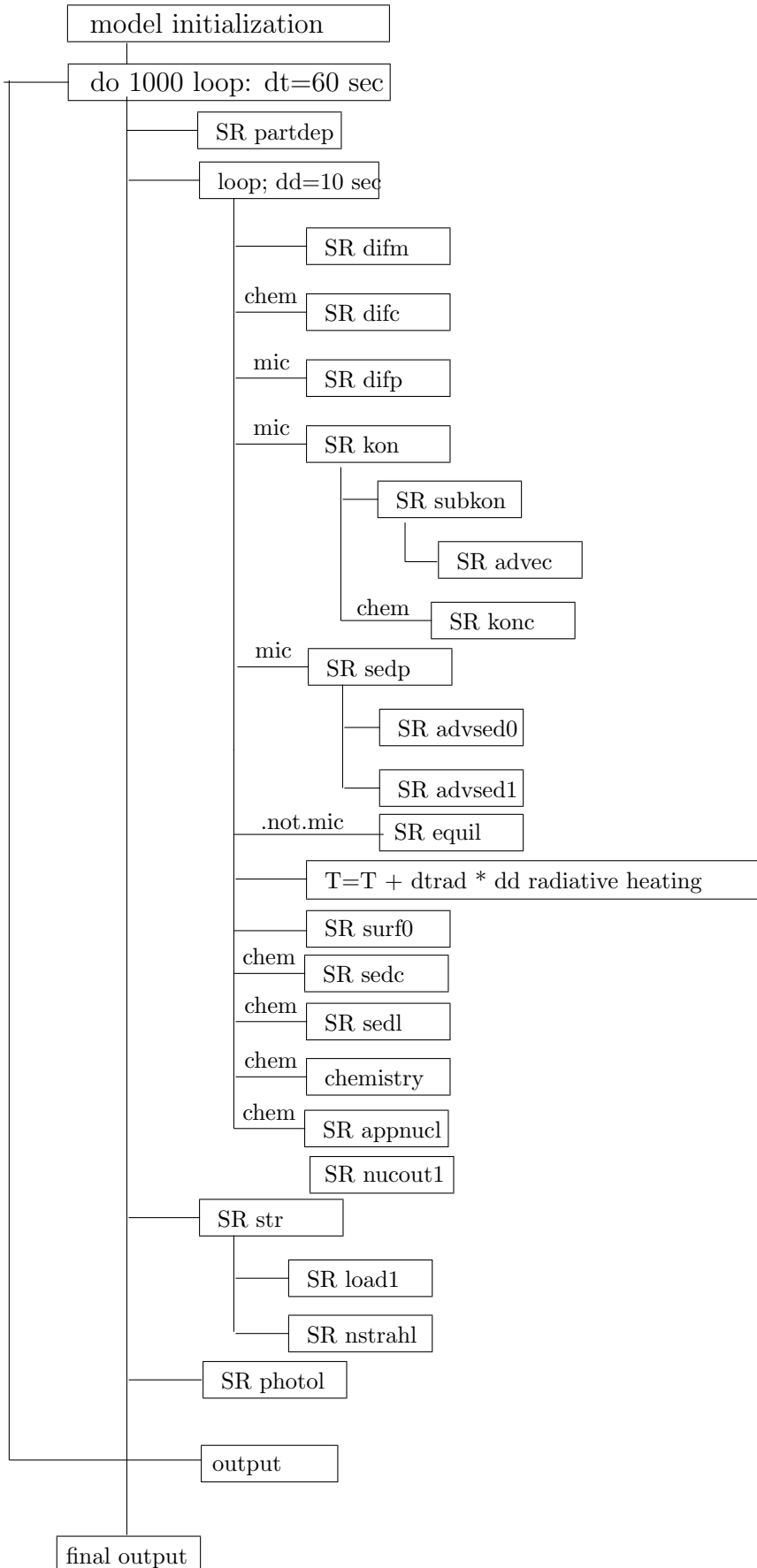
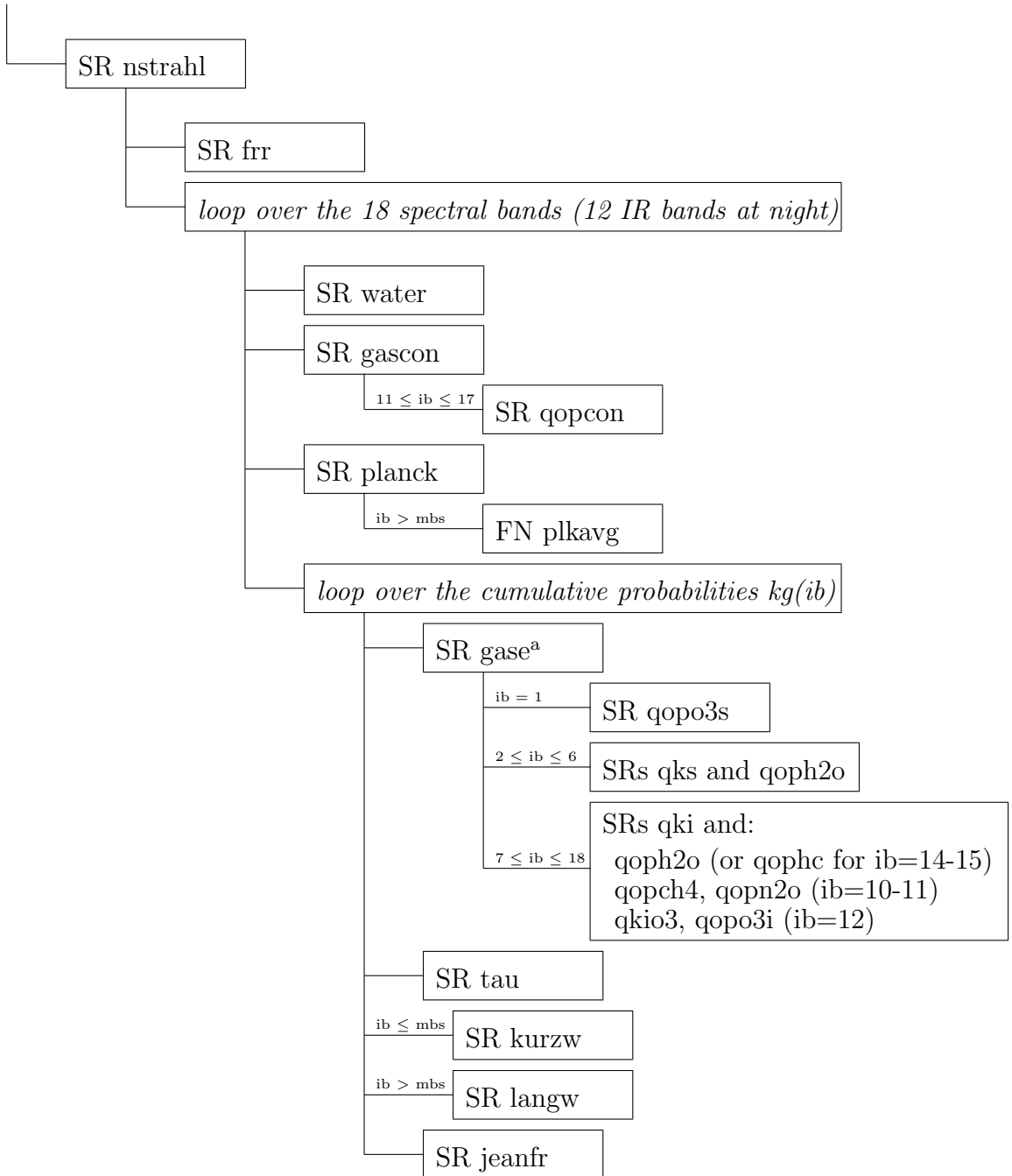


Figure 3.2: Model integration



a. The subroutines called by **SR gase** depend on the gases that absorb in each spectral band. See Table 2 in *Loughlin et al. (1997)* for more details.

Figure 3.3: Radiation code

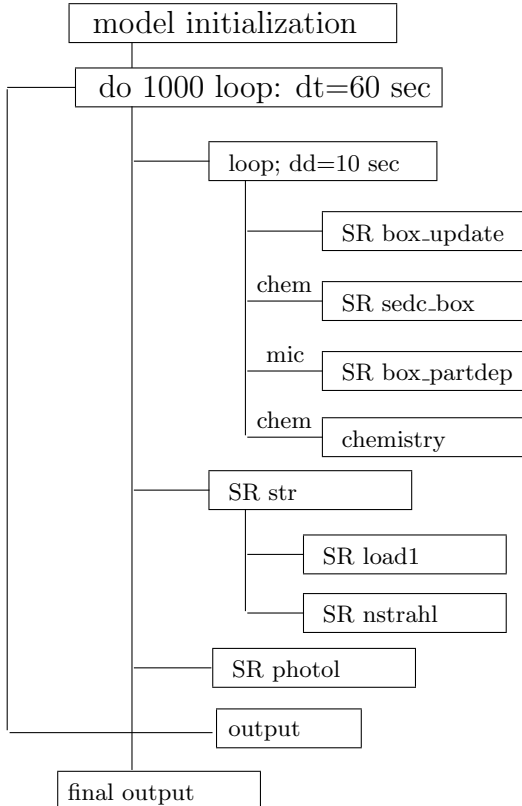


Figure 3.4: Model integration in box model mode

first “real” layer above the infinitesimally thin 1st layer). So far only cloud-free scenarios can be run, but this should be changed in future versions where also aerosol processing has to be improved. All relevant routines are included in **SR str** and **SR kpp**. Output is controlled with a switch. Note: Some elements of the box model might need updating.

The grid of the vertical layers, the two-dimensional partical grid (and the soil, see above) is set up in routine **SR grid**. The vertical grid includes an infinitesimally thin 1st layer. Θ , u , v , q are defined in the middle of the model layers whereas the turbulent exchange coefficients K_m , K_h and K_e are defined on the grid boundaries (see Figure 2.3). On top of the n layers of the MBL model are 12 layers ($n1 = n + 12$) that extend up to “infinity” to have additional layers for the calculation of the radiation transfer. Note, that the numbering for the atmospheric grid starts with 1 at the surface, but the numbering for the radiation layers start with 1 at “infinity”, i.e. the uppermost layer (see Figure 2.4).

The two-dimensional particle grid is depicted in Figure 2.2. For every of the nka dry aerosol radius interval there are nkt total particle radius intervals, which are different according to the water load of the particle. For dry particles, the total radius r (`rq(nka,nkt)` and `rw(nka,nkt)` in the code) equals the dry particle radius a (`rn(nka)` in the code), for humidified particles the total radius r increases on a logarithmic grid. In the code the variables `rq(nka,nkt)` and `rw(nka,nkt)` are used, which are the total radius in the middle and on the upper

“wall” of the bin, respectively.

3.1.2 kpp.f

This file contains most of the routines that are needed for the chemical submodule. Only turbulent transport, deposition, output, cloud processing, and the call to the chemical routines are in `str.f` and `outp(_b).f`.

A routine that is central for the determination of the parameters for aqueous phase chemistry is `liq_parm`. From here, routines that calculate the following properties are called: the liquid water content of the 2/4 aqueous phases, time dependent variables as the Henry’s or equilibrium constants, the transfer coefficients between gas and aqueous phase, and the activity coefficients. The subroutine `kpp_driver` calls the routines that are provided by KPP and which do the integration of the stiff ODE system. For more details see section 3.4.

3.2 *.h files

These files are auxilliary files for KPP. They contain the common blocks, data blocks, and global variables for KPP. They are included in the code using the `include` statement.

3.3 Additional files

3.3.1 euler_in.dat

Defines the values of the advection terms of gas phase chemical species if the switch `neula` is set to 0 in the namelist.

3.3.2 namelist mistra_cfg

Defines switches (logicals) how to run the model, i.e. inclusion of microphysics, chemistry, halogen chemistry, iodine chemistry. Further the option restart can be chosen, then the dynamics and chemistry of a previous run can be used as input for this run.

Furthermore, the integration time in hours (variable `lstmax`) is defined and the number of chemical liquid bins for the output can be chosen (2 or 4) to reduce the output size of a model run (variable `nkc_l`). The variable `fogtype` cannot be changed, it is a suffix for the output files and only has “historic relevance”.

The ozone column in Dobson units is needed for the calculation of the photolysis rates.

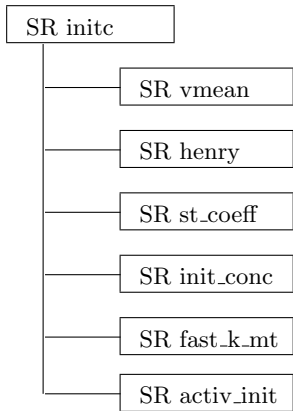


Figure 3.5: Initialization of the chemistry. The routines `vmean`, `henry`, `st_coeff`, and `fast_k_mt` are called for the aerosol-only and the aerosol plus droplet reaction sets.

3.3.3 gas_species.csv

Initialization mixing ratios of gas phase species in nmol/mol (ppb). Note that CO is now a variable and has to be included at the bottom a second time, this will be changed in future versions. The emission fluxes from the sea surface are given in molec cm⁻² sec⁻¹.

3.4 Integration of chemical reaction scheme with KPP

The chemical reaction mechanism is a stiff set of ordinary differential equations. It is solved with the subroutines produced by the kinetic preprocessor KPP, that was written by Adrian Sandu and Valeriu Damian-Iordache (*Damian-Iordache*, 1996; *Damian et al.*, 2002; *Sandu and Sander*, 2006). Check these publications for general informations. As of June 2016, the version of KPP used in Mistra was updated to the latest distributed KPP version (v2.2.3). Note that several corrections have been further implemented in KPP. This modified version based on v2.2.3 is thus provided in Mistra distribution.

Note that two parameters of KPP might have to be increased if one want to use very large reaction mechanisms: in file `gdata.h` of KPP distribution, increase the maximum number of equations and species, `MAX_EQN` and `MAX_SPECIES`.

Currently, the solver ROS3 is being used which is part of the family of Rosenbrock solvers. Previously (up to v7.3.3) the solver ROS 2 (*Verwer et al.*, 1997), which is not part of the standard KPP distribution, was used. ROS3 was introduced in v7.3.3_ROS3. The advantage of ROS3 is that the timestep is automatically adjusted, which typically leads to drastic CPU time savings compared to the manual timestep “control” used in ROS2.

The reaction set is solved completely coupled, which would mean that in a layer without aerosol (and droplet) chemistry, most reaction rates would be zero,

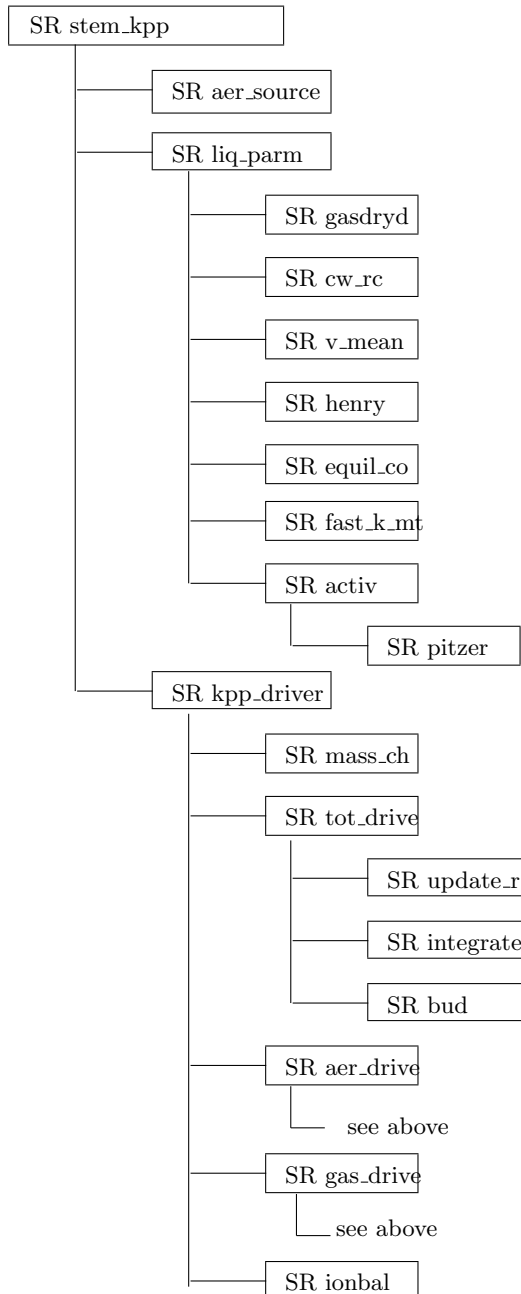


Figure 3.6: Chemistry integration. The routines `vmean`, `henry`, `equil_co`, and `fast_k_mt` are called for the aerosol-only and the aerosol plus droplet reaction sets.

leading to excessive computing times and unnecessary stiff reaction sets. To avoid this problem, three reaction mechanisms are used:

- one for layers with gas phase chemistry only: “gas”
- one for layers with gas and aerosol phase chemistry: “aer”
- and the third for the complete reaction mechanism including gas, aerosol and droplet phase chemistry: “tot”

To ensure that these three submechanisms use the same reaction files, so-called `master_*` files are used: `master_aqueous.eqn`, `master_gas.eqn`, and `master.spc`. If a reaction is changed in one of these “master” files, it will be used in all mechanisms, which is especially important for the aqueous phase, where otherwise errors are easily made.

As KPP uses common blocks and data blocks, the names of these blocks have to be changed to assure unambiguous names. This is done with a script (`mult_ch.scr`) that uses the programs `awk` and `sed` that are standard under UNIX. It is executed automatically when the KPP subroutines are made with the script `make_kpp.scr`. Then the routines containing the output files for the reaction rates are also produced. These scripts are “hand made” and if large scale changes are made in the equation files (*.eqn) they might have to be adjusted. To ease the generation of the chemical mechanism files used in Mistra, a specific Makefile has been implemented in the mech subdirectory. To generate the files for the first time, or after any change in the chemical mechanism, run `make` to generate the files. For each mechanism, the user has to validate the copy of the new files into the main source directory.

3.5 How to run the model

So far the model was successfully run on DEC-Alpha machines and on a number of Linux workstations (RedHat, SuSE, Debian). Currently the Intel fortran compiler `ifort` is generally used, but the model has also been extensively tested with `gfortran`. A 5-day model run where no cloud forms usually takes about 10 h on the Linux cluster `Mafalda`. If a cloud is present the CPU time is roughly doubled, depending on cloud depth.

All files listed in Table 3.1 should be in the same directory. By using the `make` program (just type `make`) the executable `mistra` is made.

During run time, the namelist, the files `gas_species.csv`, `euler_in.dat` and the files `clark.dat`, `initr.dat`, `ozeankw.dat`, `oceanlw.dat`, `ruralkw.dat`, `rurallw.dat`, `urbankw.dat`, and `urbanlw.dat` are read. To save disk space, the latter files - that are not changed between runs because they contain mainly lookup tables - are stored in a separate directory ('`input_files/`').

If sensitivity runs with different chemical initial conditions are planned, file `gas_species.csv` has to be changed, if the dynamical and microphysical properties are to be changed this has to be done in routine `initm` in file `str.f`.

The model configuration is defined in the namelist. As of now, the namelist contains only the main switches (box or 1D, with or without chemistry, with or without 2D microphysical description, etc.), while several tuning options are still hard-coded in the relevant routines. In future versions, these tuning options will be included in specific namelists to allow more flexibility, and avoid recompiling the code frequently.

3.6 How to change the model

New reactions can be included very easily in the model. The `*.eqn` files that contain the kinetic information have to be changed and then KPP has to be run and the new set of KPP-files has to be used for the next model run. After editing the mechanism files, type `make` in the mechanism subdirectory, then re-compile the model. See also section 3.4.

For “historic reasons” not all species that are transported in the model are included in the chemistry scheme, because some organic reactions (from *Lurmann et al.*, 1986b) have been deleted from the mechanism. To ensure easy re-use of these reactions, the species have not been deleted but some are overwritten. If in doubt check the comments in file `outp.f` that contain an up-to-date list of the species. To insert new chemical species, the parameters `j1`, `j2`, `j3`, `j5`, `j6` have to be changed in the `global_params.f` module.

If new variables are introduced be sure to chose names with at least 3 characters to facilitate the search after if with the “search” function of your text editor. When adding new species, please add them to the comments in `SR ploutc*` in `outp.f` which serve as reference for what index is allocated to what species. Additionally, the species have to be added in `SR open_chem_gas` and/or `SR open_chem_aq`. Make sure to add the correct index, name and to adjust the length of the character variables in the variable definition. Possibly slight adjustments of the output in `SR write_chem_gas` and/or `SR write_chem_aq` have to made as well. All gases undergo dry deposition. For new species therefore the molecular mass has to be defined in `gas_species.csv` and indexes adjusted in `gasdrydep`.

For soluble species, i.e. species that are being exchanged between the gas and aqueous phase, the Henry’s law coefficient and accommodation coefficients have to be defined (`SR henry_a/t` and `SR st_coeff_a/t`) and they have to be included in `SR fast_k_mt_a/t`, where the exchange coefficients are being calculated, and in `gas_mk/km.dat`, `aer_mk/km.dat` and `drive_tot.f`, where the hand-over between MISTRA and KPP happens. To avoid potential future mistakes, please *always* add new species in all these subroutines/files (i.e., `SR open_chem_gas`, `SR open_chem_aq`, `SR henry_a/t`, `SR st_coeff_a/t`, `gasdrydep`, `gas_mk/km.dat`, `aer_mk/km.dat` and `drive_tot.f`), but comment them if they are not currently taking part in phase exchange, possibly due to a lack of data.

The subroutine that probably has to be changed quite frequently is `SR initm`. It defines the initial conditions of the MBL. See pages 25 and 33. Old versions that were used in previous studies are no longer part of the source code (as of

v7.4.0) but can be provided upon request to the authors.

To change the chemical mechanism change the appropriate `master_*.eqn` file and check if a new specie has to be added to `master.spc` or even as a new tracer. In that case the number of tracers in *all* subroutines has to be changed and input as well as output routines have to be changed. Then run `make` in the `./mech` subdirectory and confirm the copy of all relevant files to the working directory. Then the executable for MISTRA has to be remade by running `make`.

Chapter 4

Description of the nucleation module

This chapter refers to the version that was developed for (MISTRAL_v7.3.3.ROS3.S). The module and text are written by Susanne Pechtl (b. Marquart), with updates by Josué Bock.

4.1 Physical concept

The nucleation module developed for MISTRAL consists of a two-step parameterisation: in the first step, the “real” is calculated, being the nucleation rate of thermodynamic stable clusters about 1 nm in diameter. The second step is the “apparent” nucleation, which describes the growth of the nuclei by condensable vapors up to the size of the model’s lowest size bin. In the following, the “apparent” nucleation scheme is described first.

The nucleation module is also documented in *Pechtl et al. (2006)*, where additionally the results of model sensitivity studies are discussed. The module was originally set up for MISTRAL v7.3.3a.S, but is adopted principally unchanged up to the present version (v7.3.3.ROS3.S).

4.1.1 Apparent nucleation

The apparent nucleation module is based on a paper by *Kerminen and Kulmala (2002)*, which connects the “real” nucleation rate of thermodynamic stable clusters (TSC) to an “apparent” nucleation rate of larger particles by means of an analytical formula. The motivation for this procedure is that the “real” nucleation rate cannot be measured (since the smallest aerosol size which can presently be measured is 3 nm diameter, whereas TSCs are around 1 nm in diameter). From the model point of view, the nucleation process itself often cannot be modelled explicitly as it is computationally expensive. E.g., if nucleation should be treated in a model whose smallest aerosol size bin is larger than the TSC size (such as in MISTRAL), the “apparent” nucleation rate can be used to calculate particle numbers appearing in the smallest aerosol size bin of the respective model.

The “apparent” nucleation rate is calculated from the “real” using information about the size of the nuclei (TSC), the background particle size distribution, as well as sink and growth processes. The nuclei are assumed to grow by condensation of non- (or very low-) volatile vapors (which can be chosen in the model, but which is designed for OIO in the present version) onto the nuclei (growth rate gr). Gas-phase diffusion and the transitional correction for the condensational mass flux (*Fuchs and Sutugin (1970)*) is implicitly accounted for. Sink processes are mainly the condensation of the condensable vapors onto background particles (CS, accounting for the transitional correction for the condensational mass flux, *Fuchs and Sutugin (1970)*), as well as coagulation with background particles (gamma, semi-empirical formula depending on temperature and sizes of background particles and nuclei).

The main assumptions of *Kerminen and Kulmala (2002)* are:

- (1) The total nuclei number concentration must remain sufficiently low to prevent effective self-coagulation ($< 10^5 - 10^6$ nuclei/cm³), because coagulation among nuclei is not accounted for. In the model, the total nuclei concentration (conc_{nuc}) is diagnosed (for checking purpose) using eq. (19) in *Kerminen and Kulmala (2002)* (see below). Not including self-coagulation tends to lead to an underestimation of apparent nuclei (*Kerminen et al. (2004)*).
- (2) The growth rate is constant during the growth process from the “real” to the “apparent” size, i.e., the concentration of the condensable vapors remains constant.
- (3) The pre-existing background particle population remains unchanged during nuclei growth.
- (4) The vapors are non-volatile, i.e. the saturation vapor pressure over a particle surface approaches zero. That means that, in principle, the condensable vapor can completely be removed from the gas phase by condensation. Since in reality, some condensable vapors are presumably semi-volatile, the “apparent” nucleation rate is probably overestimated.

Kerminen et al. (2004) extended the parameterisation of *Kerminen and Kulmala (2002)* for semi-volatile (esp. organic) vapors by introducing a critical diameter (dcrit): For cluster sizes below dcrit, the nuclei only grow by non-volatile vapors (with growth rate gr); for sizes above dcrit, the nuclei grow by non-volatile and semi-volatile vapors (with the higher total growth rate gr+grs). The critical cluster size decreases with increasing actual supersaturation of the semi-volatile vapor. This amendment of *Kerminen et al. (2004)* is also included in the parameterisation for MISTRAL. Note that presently only one dcrit is implemented. I.e., if there is more than one semi-volatile vapor, a mean saturation vapor pressure is calculated and used as approximation (see below).

Note that in reality there can be a non-negligible time lag between the “real” nucleation and the “apparent” nucleation depending on the growth rate, which is not accounted for in the present model version (where the timestep is 10 seconds). According to *Dal Maso et al. (2002)*, typical growth rates for the coastal environment is 15-180 nm/h, i.e. 0.3-3 nm/min, which is considerably higher than e.g. in the boreal forest. *O'Dowd et al. (2002)* even gives 0.1-0.35 nm/s,

i.e. 6-21 nm/min as initial growth rate for Mace Head. Hence, growth from 1 to 10 nm would take roughly 0.5-30 minutes. This time lag has to be kept in mind when interpreting the model results (see also below)! Because the growth rate (gr) is calculated by the nucleation module, the exact time lag can be determined for a model run.

The nucleation module is designed and tested for the 1D column version of MISTRAL. There is no principal problem to use it in the box model mode, but this has not been tested up to now.

4.1.2 Real nucleation

The “real” nucleation rate and the diameter of the TSCs (nuclei), which are needed as input for the “apparent” nucleation routine, can either be prescribed or calculated by two different “real” nucleation routines. First, a ternary H₂SO₄-NH₃-H₂O nucleation routine (relying on a paper by Napari *et al.* (2002)); second, by a homogeneous OIO nucleation routine which was set up relying on data provided by Lovejoy/Burkholder. In the model, both or only one ternary nucleation processed can be switched on.

4.1.2.1 Ternary H₂SO₄-H₂O-NH₃ nucleation

In this routine, the “real” nucleation rate is explicitly calculated as a function of NH₃ and H₂SO₄ concentrations, relative humidity, and temperature (Napari *et al.* (2002)). The nuclei diameter is a function of temperature and the “real” nucleation rate. The ternary nucleation rate increases with increasing H₂SO₄, increasing NH₃, decreasing humidity and decreasing temperature.

After ternary nucleation, the gas phase concentrations of H₂SO₄ and NH₃ are updated in the model. In contrast to the changes in the gas phase, the changes in liquid phase H₂SO₄ and NH₃ are neglected (see also below). Hence, ternary nucleation is considered as a sink for total H₂SO₄ and NH₃.

In the atmosphere, H₂SO₄ mixing ratios are normally smaller than NH₃ mixing ratios, i.e., nucleation decreases gas-phase H₂SO₄ relatively stronger than NH₃. Due to the daily cycle of H₂SO₄, ternary nucleation only occurs during day (max around noon). In the model, the H₂SO₄ gas phase concentration is significantly smaller with ternary nucleation than without nucleation.

4.1.2.2 Homogeneous OIO nucleation

Here, the “real” nucleation rate is explicitly calculated as a function of OIO mixing ratios and temperature. The function was set up by me as statistical fit to data I received from Ned Lovejoy. The data were computed with the nucleation model described in Burkholder *et al.* (2004). The cluster diameter is 2 nm, the cluster density 2 g/cm³, i.e., the cluster contained 34 OIO molecules.

The work of Burkholder *et al.* (2004) is (to my knowledge) presently the only one providing information about a (quantitative) nucleation rate depending on the presence of iodine oxides in the gas phase. Several thermodynamic parameters

of their nucleation model depend on lab studies (e.g., OIO uptake coefficient = 1). However, it should be noted that neither the OIO concentration nor the cluster concentration (or even nucleation rates) were directly measured: The OIO production mechanism is via photolysis of CH_2I_2 or CF_3I (forming I radicals), subsequent reaction with ozone and self-reaction of the produced IO to OIO (suggested by Hoffmann *et al.* (2001)). Total particle concentration and size distribution ($d > 3 \text{ nm}$) were measured dependent on time with UCPC and DMA.

In the homogeneous OIO nucleation modul for MISTRA, the gas-phase OIO mixing ratios are updated in the model. As above, changes in liquid phase OIO is neglected, i.e., “real” nucleation is a sink for total OIO (in contrast to the apparent nucleation, which is a much stronger sink for OIO).

4.2 Treatment in MISTRA

All three nucleation subroutines (ternary, homogeneous OIO and apparent nucleation) are contained in the FORTRAN77 program nuc.f90, which is presently used in MISTRA Version 7.3.3_ROS3.S. There are a lot of comments in the program, so have a look there, too. If nucleation should be calculated in MISTRA, set NUC=TRUE in istart.

The ternary nucleation routine (“ternucl”) and the homogeneous OIO nucleation routine (“oionucl”) do not have to be changed. They are always called if NUC=TRUE in istart (for output reasons), but “felt” by the model only if the following switches are set .true.: If “Napari”=true (in nuc.f90), ternary nucleation provides the input for the apparent nucleation routine, if “Lovejoy”=true, homogeneous OIO nucleation provides the necessary input. If both switches are set true, both “real” nucleation routines contribute to the nucleation rate of clusters. This is technically implemented as time-split process, i.e., the subroutine “appnucl” is called twice, calling “ternucl” the first and “oionucl” the second time. This of course is not completely exact since both nucleation processes occur simultaneous in reality – so if the importance of the two “real” nucleation processes should be compared, it is better to do two different model runs with only one “real” nucleation process each.

The “apparent” nucleation routine can (and has to be) changed according to the scenario which shall be computed. There are some options to chose and parameters to adjust (most of them are commented with “adjust” in the program, so the places where changes have to be made can easily be identified). If not noted otherwise, the following changes have to be done in nuc.f90:

1. the number of condensable gases (nvap). One or more gases from MISTRA can be used. In addition, there is one “vapor” called NUCV (species 75), newly introduced in MISTRA, which does not participate in chemistry. NUCV should therefore be used for “fictive” or unknown condensable gases. In that case, NUCV has to be initialised or emitted (gas_species.csv).

2. the name of condensable gases (which must be identical to the name provided in `gas_species.csv`); and their type in MISTRA, i.e. “normal” gas phase species (`s1`) or radical (`s3`) (`ical=0` or `ical=1`, respectively)).
3. from Mistra v9.0 onwards, the molar masses of the condensable vapors (m_{vap}) is automatically imported from the values specified in `gas_species.csv`, and has thus no longer to be duplicated in `nuc.f90`.
4. the concentrations of the condensable vapors (`conc`).
5. the saturation concentration of the condensable vapors, representing their vapor pressure directly above the particle surface (`concsat`). For non-volatile vapors, `concsat=0`. Non-zero `concsat` (which is the extension of *Kerminen et al.* (2004)) should not be too different in magnitude, otherwise the present restriction to only one critical cluster-size may be too inexact. Since saturation vapor pressures are quite rarely known exactly, this is not a serious limitation.
6. feedback of particles formed by “apparent” nucleation to background particle distribution and chemistry 0/1/2 (`ifeed` in `str.f`). If `ifeed=0`, the nucleation is not felt by the microphysics, i.e., the background particle distribution is not updated (hence, further nucleation is not restricted by enhanced particle concentrations). If `ifeed=1`, the background particle distribution is updated by adding the “(apparent nucleation rate * time step)” to $f(k,1,its)$. Automatically, the chemistry feels the enhanced particle concentration via exchange gas-liquid phase (which is not completely realistic because the chemistry bins are much coarser than the microphysics bins!). For that reason, the option `ifeed=2` allows that the nucleation is felt by the microphysics (i.e., the background particle distribution is updated), but not by the chemistry. I.e., the chemistry “sees” a hypothetical background particle distribution without nucleation. This is done technically by not letting the apparent nucleated particles grow out of the 1st dry microphysical bin and not including this 1st bin into the chemical “sulfate” bins (1 and 3).
7. coupling to ternary H2SO4-H2O-NH3 nucleation yes/no (`Napari` in `str.f`).
8. coupling to homogeneous OIO nucleation yes/no (`Lovejoy` in `str.f`). If both (7) and (8) are set true, both “real” nucleation processes are used as input for “apparent” nucleation (automatically set switch “both” in `str.f`).
9. If no coupling to a “real” nucleation routine, prescribe a “real” nucleation rate (J_{real}) and the TSC radius (d_{nucini}).
10. the lowest aerosol size bin in MISTRA (`rnw0` and `rw0` in `str.f`). Up to now, most (dry, i.e. cloudless) runs have been performed with `rnw0=rw0=5 nm`, i.e., the apparent nuleation rate is for a dry diameter of about 10 nm (and a wet equilibrium diameter of about 13 nm, see below). Much larger size bins should not be used, because this would not really be only nucleation any

more. $rnw0=rw0=3$ nm is not stable after a while (error “aersol growth”), $rnw0=rw0=10$ nm is not stable either (error $IER < 0$). In the latter case, the condensable vapor tends to be gone in the 1st nucleation time step. $rnw0=rw0=7$ nm is (at least technically) possible.

11. the accommodation coefficient for the condensable vapor (α_{phaa}). Up to now, α_{phaa} was always set to 1. Note that α_{phaa} is only needed for the calculation of the condensation sink (condensation to background particles). Therefore, large α_{phaa} yields a large condensation sink and, hence, a low(!) nucleation rate (not tested, but this is straightforward).
12. other possibilities to adjust (not tested up to now): fraction of soluble species (fcs), number of ions ($xnue$), the uppest nucleation level. Up to now, the first two values are set to 1, the uppest nucleation level is the model top.

For the treatment according to *Kerminen and Kulmala* (2002), a 1D background particle distribution is required. This is calculated from the 2D particle distribution in MISTRA using all possible wet (droplet) classes attributed to the 1st dry (aerosol) class as size bins for the 1D distribution, in which all other particles are classified. The 1D background particle distribution is included into the .nc output. Note that from version v7.3.3 on there exists a better subroutine (oneD-dist) for setting up the 1D particle size distribution (for output reasons) largely getting rid of artificial spikes by using a finer 1D size bin resolution (max. $nka+nkt$).

It is assumed that the freshly “apparent” nucleated particles are in equilibrium with ambient water vapor. Therefore, the equilibrium wet particle diameter is calculated in analogy to the general procedure in MISTRA. The dry and the wet particle diameters determine the position of the new particles in the 2D MISTRA particle grid. The ratio wet/dry diameter is used as factor to enhance the growth rate (gr). This procedure was chosen after personal communication with Veli-Matti Kerminen (2004).

The relative contributions of the condensable vapors (if more than one is applied) to nuclei growth is calculated depending on their concentrations, molar masses, and molecular speeds. They are used to update the gas-phase MISTRA species. For that purpose, the increase in (dry) diameter from the “real” (TSC) to the “apparent” particle is calculated. Regarding the liquid phase, it should obviously be assumed that all condensable vapor goes into the small (1st) chemical aerosol class. However, this is only realised for OIO up to now, which goes as unreactive OIO into the liquid phase (for mass conserving reasons only). If other gases than OIO are used for “apparent” nucleation it should be considered how treat the respective condensing vapor: It can either be assumed to vanish as soon as it condenses onto nuclei (not mass-conserving!), it can be treated unreactive in liquid phase (similar to OIO) or as reactive (in that case note the problem that in MISTRA it will be “smeared out” over the whole sulfate bin in chemistry). In contrast to the gas phase, the liquid phase is not updated (see below).

The total nuclei concentration (conc_{nuc}) is diagnosed in order to check if the nuclei concentration (which comprises all particle sizes between the “real” and the “apparent” diameter) is within the allowed range ($< 10^5 - 10^6$ nuclei/cm³).

A short description of all runs which were performed up to now can be found on guille: /data2/Susanne/MISTRA/runs_mistra.txt.

Output of the nucleation routine is in 4 .asc files (also used for gnu-plotting), the file nuc.nc (used for ferret-plotting), the file nuc.out (which provides some additional information mainly for consistency checks, and which is overwritten every time step).

A Ferret plot program for quicklooks can be found (as for other variables in MISTRA) in plot_progs/plot_nuc_v733.sc. There are two additional plot scripts (mainly for historical reasons) which may have to modified slightly : gnu_nuc.sc and ferret_nuc.sc in the run subdirectories plot_progs/NUCLEATION.

4.3 Drawbacks, limitations, and unsolved problems

The time lag between “real” nucleation and “apparent” nucleation (i.e., the time needed for the growth from the TSC diameter to the diameter of the smallest aerosol size bin in the model) is not accounted for. Since the “apparent” nucleation rate is calculated every time step (10 s) and the MISTRA variables (gas and liquid phase concentrations and background particle distribution) are updated accordingly, the temporal evolution is probably somewhat unrealistic.

If feedback of the “apparent” nucleation on the background distribution is allowed, the number of small particles increases drastically. This is not completely realistic, because (1) MISTRA has no coagulation, and (2) the time lag of “apparent” nucleation is not accounted for.

The loss of condensable vapor due to the condensation to background particles are not (and cannot easily be) considered in the model within the same nucleation timestep. However, if feedback with background particles is allowed, vapors are taken up by aerosols anyway in the following time steps. Hence, the respective error should be negligible.

Probably the most serious limitation of the present nucleation parameterisation is that self-coagulation amoung nuclei is not taken into account (which may become important for low background particle, high nuclei concentration and little available condensable vapor). Accoring to Kerminen *et al.* (2004), this may lead to an underestimation of the “apparent” nucleation rate already for “real” nucleation rates > 100 particles/cm³. Kerminen *et al.* are presently working on parameterizing the effect of self-coagulation (Kerminen, pers. comm.). In the model runs, the total nuclei concentration (conc_{nuc}) diagnosed by nuc.f90 is often at the upper end of the allowed range (especially if the condensable vapor concentration is low, leading to small growth rates). Hence, neglecting self-coagulation amoung nuclei might indeed induce an error.

New particles do grow out of the smalles microphysical bin, but it was not

checked yet whether the growth is realistic. It was not tested up to now if the “apparent” nucleated particles are able to grow to climatically active (cloud droplet) sizes in the model when the humidity is large enough. A “cloudy” MISTRA run should be performed. This could not be done up to now (with ROS2) since MISTRA+clouds seems to have problems with iodine halogen chemistry (run crashes after less than one model hour; total chemistry mechanism might be too large?). ROS3 has not yet been tested on that.

Chapter 5

Photolysis

5.1 Theory

Parts of the text of this section are taken from *Landgraf and Crutzen* (1998).

Many important chemical reactions in the atmosphere are photochemical reactions where molecules undergo photodissociation. The rates of these reactions, called photolysis rates, depend on the actual atmospheric shortwave radiation field and are therefore not constant in time, but have to be reevaluated with changing solar zenith angle, aerosol load, or cloud cover.

The photolysis rate coefficient (J_x) for a gas X can be calculated from the spectral actinic flux $F(\lambda)$ via the integral

$$J_x = \int_I \sigma_x(\lambda) \phi_x(\lambda) F(\lambda) d\lambda \quad (5.1)$$

where λ is the wavelength, σ_x the absorption cross section, ϕ_x the quantum yield and I the photochemically active spectral interval $178.6 \text{ nm} \leq \lambda \leq 752.5 \text{ nm}$.

Landgraf and Crutzen (1998) (abbreviated as LC98) propose a model which does not calculate the photolysis rates by approximating the integral (5.1) by the sum

$$J_x \approx \sum_{i=1}^N \sigma_x(\lambda_i) \phi_x(\lambda_i) F(\lambda_i) \Delta \lambda_i, \quad (5.2)$$

as this would lead to excessive computing times, because for accurate results N had to be in the order of 100. LC98 suggested a method using only 8 spectral bins (see table 5.1) approximating (5.1) by:

$$J_x \approx J_{1,x}^a + \sum_{i=2}^8 J_{i,x}^a \cdot \delta_i \quad (5.3)$$

where $J_{i,x}^a$ is the photolysis rate for a purely absorbing atmosphere. In the spectral bin 1, the Schumann-Runge band, the effect of scattering by air molecules,

aerosol and cloud particles can be neglected, so $J_x \approx J_{1,x}^a$. In the spectral range $202.0 \text{ nm} \leq \lambda \leq 752.5 \text{ nm}$ the influence of scattering is significant, so the factor δ_i :

$$\delta_i := \frac{F(\lambda_i)}{F^a(\lambda_i)}, \quad (5.4)$$

with the actinic flux of a purely absorbing atmosphere $F^a(\lambda_i)$, is introduced. δ_i is calculated online for one wavelength for each interval (λ_i in table 5.1). The $J_{i,x}^a$ are precalculated with a fine spectral resolution and are approximated during runtime from lookup tables or by using polynomials. The advantage of this procedure is, that the fine absorption structures that are present in σ_x and ϕ_x in integral (5.1) are considered and only Rayleigh and cloud scattering, included in $F(\lambda_i)$, are treated with a coarse spectral resolution which is justified. Further processes with only small wavelength dependencies can be treated this way too.

The spectral regions listed in table 5.1 are chosen such that errors introduced by this approximation are small.

Table 5.1: Subdivision of the spectral range $178.6 \text{ nm} \leq \lambda \leq 752.5 \text{ nm}$ in eight intervals; λ_a and λ_b are the initial and the final, and λ_i the fixed wavelength in interval I_i . σ_{O_2} and σ_{O_3} are the oxygen and ozone cross section for the wavelengths λ_i .

interval	λ_a [nm]	λ_b [nm]	λ_i [nm]	$\sigma_{O_2}(\lambda_i)$ [cm^2]	$\sigma_{O_3}(\lambda_i)$ [cm^2]
1	178.6	202.0	see text		
2	202.0	241.0	205.1	$7.63 \cdot 10^{-24}$	$3.51 \cdot 10^{-19}$
3	241.0	289.9	287.9	0.	$1.71 \cdot 10^{-18}$
4	289.9	305.5	302.0	0.	$2.82 \cdot 10^{-19}$
5	305.5	313.5	309.0	0.	$1.11 \cdot 10^{-19}$
6	313.5	337.5	320.0	0.	$2.81 \cdot 10^{-20}$
7	337.5	422.5	370.0	0.	$1.90 \cdot 10^{-23}$
8	422.5	752.5	580.0	0.	$4.55 \cdot 10^{-21}$

$J_{i,x}^a$ is calculated as a function of the slant column of O_3 , V_{O_3} , because absorption by aerosol and cloud particles and other gases play only a minor role for most chemical applications in the determination of the actinic fluxes. For the spectral intervals 1 and 2 absorption by O_2 has to be accounted for additionally. $J_{i,x}^a$ can be written as (see LC98 for details of the derivation):

$$J_{i,x}^a = \overline{\phi\sigma}_{i,x}(V_{O_3}) \overline{F}_{i,o} \exp\{-\tau_i(V_{O_3})\} \quad (5.5)$$

As the $J_{i,x}^a$ depend only on the slant column O_3 V_{O_3} it is important to find a good approximation for V_{O_3} . $\overline{F}_{i,o}$ is the integrated solar irradiance per interval calculated from the spectral solar irradiance at the top of the atmosphere, $F_o(\lambda)$:

$$\overline{F}_{i,o} = \int_{I_i} F_o(\lambda) d\lambda. \quad (5.6)$$

Using the averaged optical cross section $\bar{\sigma}_{i,x}(V_{O_3})$, $\tau_i(V_{O_3})$ can be calculated as:

$$\tau_i(V_{O_3}) = \int_0^{V_{O_3}} \bar{\sigma}_{i,O_3}(V'_{O_3}) dV'_{O_3} \quad (5.7)$$

and the optical depth of an optically thin model layer can be approximated by

$$\Delta\tau_i(V_{O_3}; V'_{O_3}) \approx \frac{1}{2} \{ \bar{\sigma}_{i,O_3}(V_{O_3}) + \bar{\sigma}_{i,O_3}(V'_{O_3}) \} \Delta V_{O_3}, \quad (5.8)$$

where V_{O_3} is the ozone column at the top of the layer, V'_{O_3} at the bottom of the layer and $\Delta V_{O_3} = V'_{O_3} - V_{O_3}$.

The remaining terms $\overline{\phi\sigma}_{i,x}$ and $\overline{\sigma}_{i,O_3}$ can be handled with a lookup table for intervals 3 and 4 and can be described by polynomials for intervals 5 – 8.

$$\overline{\phi\sigma}_{i,x} = \sum_{j=0}^{n_i} A_{i,j,x} V_{O_3}^j \quad (5.9)$$

$$\overline{\sigma}_{i,O_3} = \sum_{j=0}^{n_i} B_{i,j,O_3} V_{O_3}^j \quad (5.10)$$

with $n_i \leq 4$ and appropriate, species dependent coefficients $A_{i,j,x}$ and B_{i,j,O_3} .

As already stated above, O_2 is an important absorber in the spectral intervals 1 and 2, so in these two spectral regions, $\overline{\phi\sigma}_{i,x}$ and $\overline{\sigma}_{i,O_3}$ have to be calculated as functions of $V(O_2)$ and $V(O_3)$. See LC98 for details.

So far the photolysis rates are calculated for an isothermal atmosphere of temperature T_0 . To account for the atmospheric temperature profile a correction function

$$f_{i,x}(\delta T) := \frac{\overline{\phi\sigma}_{i,x}(T)}{\overline{\phi\sigma}_{i,x}(T_0)} \quad (5.11)$$

is introduced, where T is the real temperature and $\delta T = T - T_0$. $f_{i,x}(\delta T)$ can be approximated with polynomials with constant coefficients except for the spectral region 1.

As shown in LC98 the errors of their approximation for photolysis rates in the lower troposphere are less than 10 % for solar zenith angles below 80° . For greater SZA the error may exceed 50 % for some species. Therefore no problems should arise in situations where high SZA are present only a short while.

5.2 Calculation of the effective values

As stated in section 5.1, the basic idea of the model of LC98 is not to calculate the photolysis rate with a fine spectral resolution but to work with only 8 spectral intervals in which the averaged product of cross section and quantumyield $\overline{\phi\sigma}_{i,x}$

and the effective optical depths τ_i are used. In section (5.2.1) the structure of the programs that calculate these effective values will be explained.

The first two spectral intervals often comprise a special case because of additional oxygen absorption. For the troposphere only intervals 4-8 are important. For “historical reasons” in the source code interval no. 1 is called 0 or explicitly Schumann - Runge band.

Warning: Although similar, the files `sig.f`, `sig_eff.f` and `main.f` in `..photo/band_param/sig_cal` and `~/photolys` (or the files concatenated in `jrate.f`) are not the same! This holds also for the corresponding data files `sig.dat/sig2.new` and `lookt.dat`, as the order of the species (and also some data) differs. Use only the appropriate `sig.dat/sig2.new` file.
 To avoid even greater confusion all updates of the files `sig.dat` and `lookt.dat` are named differently, e.g. `lookt0900.dat` for the September version of 2000.

When changing the code for inclusion of a new species, the easiest way to do and check this, is to implement an already existing species with a new name (e.g. *dummy*) and check if the results are the same for the old and the “new” species. Then just add as many dummy species as needed which later can easily be replaced with real species using the “search and replace” function of your text editor.

5.2.1 Structure of the programs to calculate the effective values for the band model

A variety of programs exists to calculate the effective values. They have to be executed for each of the 8 spectral intervals. The program `run` (compiled from `main.f`, `deltatm.f`, `sig.f` and `sig_eff.f`) in directory `/band_param/sig_cal` calculates the effective values $\bar{\phi}\sigma_{i,x}$, τ_i for all species with a `write` statement in `sig_eff.f` for 2000 slant columns of ozone (difference 1 DU each). Remember that $\bar{\phi}\sigma_{i,x}$ and τ_i are only dependent on $V(O_3)$ and for the first two intervals also on $V(O_2)$.

The script `look_basic.exe` runs `run` for all 8 spectral intervals. The results are written to `/result/sig_eff.1-8` and `/result/tau_eff.1-8`. To use these values in the on-line photolysis model, they have to be processed. For intervals 1 – 4 lookup tables are generated. The data in these tables will be interpolated during execution of the band model to the actual values. For intervals 5 – 8 the data is fitted to polynomials of n-th degree as a function of the slant column of ozone, because in `band` the effective values are calculated with polynomials of the slant column of ozone. For each spectral interval and each species specific parameters have to be found. In the subdirectory `/fit` there are PV-WAVE/IDL plotroutines for the individual spectral intervals to fit polynomials of n-th degree to the data. The quality of the fit can be estimated with the plotted relative error (in percent) of the fit. As a rule of thumb for an interval with a significant contribution to the total photolysis rate these errors should not be greater than 1 – 2 % (J. Landgraf,

pers. comm. 1998). The fit parameters from `sig1-8.pro` are saved in `coeff.dat` (**for one species for one interval!**). This file is overwritten each time, `sig1-8.pro` is executed. They have to be written manually, again for each species for each spectral interval, to the file `~/photolys/data/lokt.dat`. While inserting new data in `lokt.dat` be sure that the order of the species and intervals is correct.

For many species the photolysis rates depend on temperature. In eq. (5.11) (eq. (24) in LC98) $f_{i,X}(\delta T)$ comprises a relation between the cross section $\overline{\phi\sigma}_{i,x}$ for the actual and for a reference temperature $T_0 = 250\text{K}$. The script `look_temp.exe` runs `run` for *one* spectral interval for 15 temperature values T_i , $i = 1..15$ ($T=180\text{-}320\text{ K}$).

The function $f_{i,X}(\delta T)$ has to be found with a PV-WAVE/IDL plotprogram for each wavelength bin. The effective cross section is then evaluated as a function of the deviation δT from T_0 . The function $f_{i,X}(\delta T)$ has to be evaluated in addition to $\overline{\phi\sigma}_{i,x}$. For interval 1 a lookup table is generated by `temp1.pro`, while for intervals 2-8 parameters for polynamials are calculated with `temp2.pro` and `temp3_8.pro`. The parameters for intervals 2-8 have to be written *manually* to the corresponding data block (e.g. DATA `TJ_dummy`) in `jrate.f` (common block `T_COEFF` in subroutine `LOOKUP`). The lookup table for interval 1 has to be written to `lokt.dat` in addition to the non-temperature dependent lookup table for this species. In `lokt.dat` the order of data blocks is: non-temperature dependent data, temperature dependent data, and data for calculation of heating rates.

In `jrate.f` subroutine `PHOTO_CAL` all these values have to be inserted for each spectral bin. See section (5.2.3).

5.2.2 Introducing a new species in the programs for the effective values

For the introduction of a new species in `/band_param/sig_cal` changes have to be made in the routines `main.f`, `sig.f`, and `sig_eff.f`.

- In `main.f` the new species has to be added to the variable definition for the call of `cross_atm` and `sig_eff`.

The variable `CRS_XX` is defined as `CS_XX` or `CST_XX` if `XX` is temperature dependent (`CS` stands for cross section). For the actinic flux the variable `FACT` is used, it is calculated with a four-stream model.

- In `sig_eff.f` variables have to be defined (`CRS_XX` and `RJ_XX`) and the photolysis rates have to be calculated:

$$\begin{aligned} \text{RJ}_\text{XX}(K3, K2) &= \text{RJ}_\text{XX}(K3, K2) + \text{CRS}_\text{XX}(L) * \\ &\$ \quad \text{FACT}(K3, K2, L) \end{aligned}$$

and the respective data has to be written to the output file `/result/sig_eff.dat`:

```

      write(3,*) 'XX'
      DO K2=1,MAX
        WRITE(3,'(1P,6E12.4)')
$          (RJ_XX(K3,K2)/FINT(K2,K3), K3=1,MAXV3)
      ENDDO

```

- In `sig.f` in subroutine `cross_init` a read statement has to be introduced, for a not-temperature dependent species:

```

open (7,file='sig2.new')

READ(7,*)
READ(7,101)CS_XX

```

and

```

READ(7,*)
READ(7,201)T_XX
DO I=1,3
  READ(7,101)(CS_XX(L,I),L=1,MAXWAV)
ENDDO

```

for a temperature dependent species. The corresponding variable has to be defined in the common block `/cross_sec/` or `/cross_sec_T/`, respectively .

Don't forget to insert the new cross sections into `sig2.new` at the correct place! Run the scripts and plot the data as described in section 5.2.1. Now all data for the introduction of a new species in the band model is available.

5.2.3 Introducing a new species in the band model

After all the data for the calculation of the effective parameters $\overline{\phi\sigma}_{i,x}$ and τ_i have been made available for a new species, the species also has to be included in the band model itself. The following is a list of subroutines in which changes have to be made for the inclusion of the photolysis of a species which is not dependent on temperature.

Table 5.2: What to change for a new NOT temperature dependent species in the band model (`jrate.f`)

subroutine	what to include	what for
SR photol	double precision RJdummy(0:MAXLAY,MJ) call band (..,RJdummy,..) photol_j(..,k)=RJdummy(k,1)	photolysis rate save to MISTRAL variables

continued on next page

<i>continued from previous page</i>		
subroutine	what to include	what for
SR band	in call: RJ_dummy double precision RJ_dummy(0:MAXLAY,MJ) double precision TJ_dummy(MJ,0:MAXLAY) call photo_cal (...TJ_dummy,...) RJ_dummy(K,J) = TJ_dummy(J,K)	photolysis rate photolysis rate photolysis rate photolysis rate photolysis rate
SR photo_cal	in call: RJ_dummy cb/F_O2/ CS_dummy(58,2,2) cb/LOOK/ A1_dummy(55,2), B1_dummy(55,2) cb/LOOK/ A2_dummy(55), B2_dummy(55) cb/LOOK/ A3_dummy(55), B3_dummy(55) cb/C_POLY/C4_dummy(..),C5_dummy(..), C6_dummy(..),C7_dummy(..) double precision RJ_dummy(MJ,0:MAXLAY) double precision SIG_DUMMY(0:7) calculation of SIG_DUMMY, RJ_DUMMY	photolysis rate unchanged cross section lookup tables for interval 2 interval 3 interval 4 polynomial parameters for intervals 5-8 photolysis rate effective cross section the calculation of effective cross section and photolysis rate
SR lookup	cb/F_O2/ CS_dummy(58,2,2) cb/LOOK/ A1_dummy(55,2), B1_dummy(55,2) cb/LOOK/ A2_dummy(55), B2_dummy(55) cb/LOOK/ A3_dummy(55), B3_dummy(55) cb/C_POLY/C4_dummy(..),C5_dummy(..), C6_dummy(..),C7_dummy(..) read CS_dummy read A1_dummy B1_dummy read A2_dummy B2_dummy read A3_dummy B3_dummy read C4-7_dummy	unchanged cross section lookup tables for interval 2 interval 3 interval 4 polynomial parameters for intervals 5-8 read cross section read lookup tables read lookup tables read lookup tables read polynomial parameters

When including a new species that has a temperature dependency for the quantum yield the additional changes have to be made (compare with e.g. NO_3^- in the code):

Table 5.3: What to change additionally for a new temperature dependent species in the band model (jrate.f)

subroutine	what to include	what for
SR cross_init	cb/cross_sec/ CS_dummy(MAXWAV) read CS_dummy	cross section (only necessary for T dependent photolysis rates)
SR cross_atm	cb/cross_sec/ CS_dummy(MAXWAV)	photolysis rate (only necessary for T dependent photolysis rates)
SR photo_cal	calculation of SIG_DUMMY, RJ_DUMMY multiply with TJ_dummy(*,7)	apply eq. (5.11)
SR lookup	in cb /T_COEFF/: TJ_dummy(*,7) DATA statement for TJ_dummy(*,7)	define coefficients for calculation of $f_{i,x}$ (eq. (5.11))

Below an example of the calculation of $\overline{\phi\sigma}_{i,x}$ is shown for the temperature dependent photolysis of HCHO:

```
C-----
C CH2O -> COH + H
C-----

      SIG_CHOH(3)=P1(TJ_CHOH(1,3),TJ_CHOH(2,3),TEMP2(J,K))*$          P1(B3_CHOH(I3(J)),A3_CHOH(I3(J)),V3_DU2(J))
      SIG_CHOH(4)=P3(C4_CHOH(1),C4_CHOH(2),C4_CHOH(3),$          C4_CHOH(4),V3_DU2(J))
      SIG_CHOH(5)=P1(TJ_CHOH(1,5),TJ_CHOH(2,5),TEMP2(J,K))*$          P2(C5_CHOH(1),C5_CHOH(2),C5_CHOH(3),V3_DU2(J))
      SIG_CHOH(6)=P1(TJ_CHOH(1,6),TJ_CHOH(2,6),TEMP2(J,K))*$          P1(C6_CHOH(1),C6_CHOH(2),V3_DU2(J))

      RJ_CHOH(J,K)=
      $          SIG_CHOH(3)    * FINT(J,3) +
      $          SIG_CHOH(4)    * FINT(J,4) +
      $          SIG_CHOH(5)    * FINT(J,5) +
      $          SIG_CHOH(6)    * FINT(J,6)
```

Only the 4 wavelength bins 4 – 7 (note: bin 1 in code is “0”) contribute to the photolysis rate of HCHO. The spectral contributions are calculated in the variables **SIG_CHOH(..)**. In wavelength bin 4 (in code bin 3) lookup tables are used. The variable **I3(J)** determines which part of the table has to be extracted. This variable is determined in the code further up. According to eqs. (5.3) and

(5.5) ((7) and (14) in LC98) RJ_{CHOH} is calculated which is the quantity we are looking for.

When changing the code for a temperature dependent species it is always advantageous to do this in 2 steps. First, change the code without inclusion of a temperature dependence and compare the results with a reference run where the high spectral resolution should be used. If the results are encouraging proceed with the second step, the inclusion of the temperature dependence.

To assess the importance of a spectral interval in relation to total photolysis rate, the plot program *J.pro* may be used, which plots a vertical profile of the photolysis rate of the 8 intervals in comparison to a tabulated value for the total photolysis rate.

Warning: During inclusion of new species it was not clear how important the absolute number of the maximum error in interval 2 is. If this band-model version should be used for the stratosphere check this again (species IBr, C₃H₇I, CH₂ClI, Cl₂; interval3: CH₃I)!

5.3 Multiple scattering and photolysis rates

Photolysis of O₃ produces O(¹D) which reacts with H₂O to OH. The vertical profile of O(¹D) shows an enhancement above the cloud and in higher cloud layers (Figure 5.1) compared to the base cloud-free run. Only below 550 m O(¹D) is smaller in the cloudy run than in the cloud-free run. The cause for this is the increase of the actinic flux in the higher layers of the cloud and above the cloud due to multiple scattering of photons by the cloud droplets (for a detailed explanation see *Landgraf* (1998) and *Trautmann et al.* (1999)). The effect is an enhancement of OH concentrations in a cloudy atmosphere. In the model OH is greater in all levels in the cloudy run than in the cloud-free run and not only where O(¹D) is greater, because water vapour is more abundant than in the cloud-free run. In this run, cloud base is around 550 m and cloud top around 800 m.

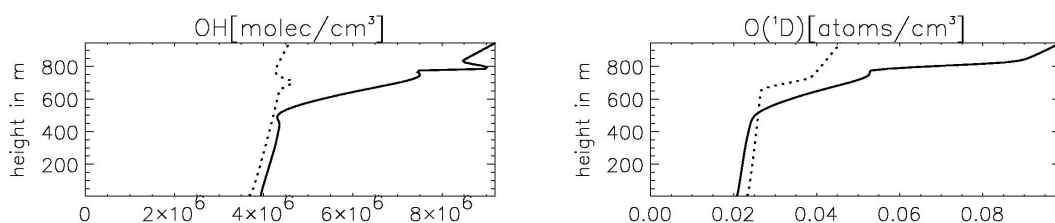


Figure 5.1: Vertical profile of OH and O(¹D) at noon on the second model day for the base cloudy run (solid line) and the base cloud-free run (dotted line). The time is given in hours since model start. Cloud top is at 800 m.

Plots of the cross sections that are used plus typical photolysis rates (“J-values”) can be found in sections F and G, respectively.

Appendix A

Treatment of turbulent transport

The exact description of turbulence remains one of the unsolved problems of classical physics. This is due to the non-linear characteristic of turbulence. *Stull* (1988) describes in detail the different concepts and equations that are briefly discussed here.

Turbulent fluxes appear in the prognostic equations of fluids. They can be derived by the so-called Reynold's averaging of the conservation equations, e.g. Newton's second law for the conservation of momentum. A fundamental problem in the description of turbulent flows is known as "the closure problem". As the number of unknowns in the set of equations for turbulent flow is larger than the number of equations, the set of equations is not closed. Therefore parameterizations have to be made that maintain the fundamental properties of turbulent flow, e.g. that gradients of the conserved variables disappear when the fluid is well-mixed. A property that is invariant for individual fluid elements is said to be conserved. Applied to the atmosphere this means that no gradients exist in a well mixed part of it (e.g. the MBL) for the absolute humidity or the mass mixing ratios or molar fraction of chemical species or particles (see e.g. *Pielke* (2002), p. 8).¹

The frequently used gradient transport theory parameterizes the turbulent fluxes with the help of a turbulent exchange coefficient that is abbreviated as K (this is the reason for the often used term "K - theory"). The turbulent flux is parameterized as (here only written for the vertical turbulent flux):

$$\overline{w' \Phi'} = -K \frac{\partial \bar{\Phi}}{\partial z}, \quad (\text{A.1})$$

w' is the turbulent fluctuation of the vertical velocity w and Φ' is the turbulent fluctuation for a variable Φ . The prognostic variables for particle concentrations ($f(a, r)$) and concentrations of chemical species (c_g and $c_{a,i}$) as they are used in the model are no conserved variables because they are not independent on the density of air. This is due to the choice to define them in particles per volume of

¹Note that positive tracers are transported in mass concentrations in *Stull* (1988) i.e. in kg m⁻³ - this should be wrong..

air and in mol of a substance per volume of air, respectively. As only mass mixing ratios or molar fractions would be conserved variables that have no gradient in a well mixed fluid the mean density of the air, ρ , has to be used as a factor. Therefore the turbulent fluxes are parameterized in the model as:

$$\overline{w'f(a,r)'} = -K \frac{\rho}{m(a,r)} \frac{\partial f(a,r)m(a,r)/\rho}{\partial z} \quad (\text{A.2})$$

$$\overline{w'c'} = -K\rho \frac{\partial c/\rho}{\partial z}. \quad (\text{A.3})$$

where c stands for gas phase as well as aqueous phase concentrations and $m(a,r)$ is the mass of one particle with dry radius a and total radius r . Now the turbulent fluxes are proportional to the gradients of the conserved variables $f(a,r)m(a,r)/\rho$ and c/ρ and they are therefore in agreement with the gradient transport theory. To transform the conserved variables back to the prognostic variables that are used in the model, they have to be multiplied again with ρ . This ensures also that the unit of the turbulent flux $\overline{w'\Phi'}$ is correct.

In the prognostic equations (equation 2.1 to 2.6, 2.10 and 2.13) changes due to turbulent movements are by the divergence of the turbulent fluxes, so there the derivation of the turbulent fluxes with respect to height appears. In equation 2.6 the mass of a single particle $m(a,r)$ is omitted because it is a constant and cancels out.

Appendix B

Calculation of the aqueous fraction

The distribution ratio of a species between gas and aqueous phase is defined as the ratio of gas phase concentration and aqueous concentration (see e.g. *Seinfeld and Pandis* (1998), chapter 6.2.1):

$$f_A = \frac{c_a}{c_g}, \quad (\text{B.1})$$

where both c_g and c_a are given in mol/m³_{air}. If Henry's equilibrium is assumed, equation B.1 can be written as

$$f_A = k_H^{cc*} w_l \quad (\text{B.2})$$

with the effective Henry's constant k_H^{cc*} that takes dissociation effects in the aqueous phase into account. The aqueous fraction is defined as the ratio of the concentration in the aqueous phase and the total concentration:

$$X_{aq} = \frac{c_a}{c_a + c_g} = \frac{f_A}{1 + f_A} = \frac{k_H^{cc*} w_l}{1 + k_H^{cc*} w_l}. \quad (\text{B.3})$$

Figure B.1 shows the aqueous fraction for different liquid water contents as a function of the effective Henry's constant. As unit for the Henry's constant the most commonly used one was taken: mol/(l atm) = M/atm.

The Figure shows that for typical cloud liquid water contents (0.1 to 1 g/m³) an effective Henry's constant of 10⁷ M/atm is sufficient to have an aqueous fraction of nearly unity. This is the case for e.g. HNO₃. The Henry's constant for NO₂ is only 4 · 10⁻³ M/atm, so it is nearly completely partitioned towards the gas phase.

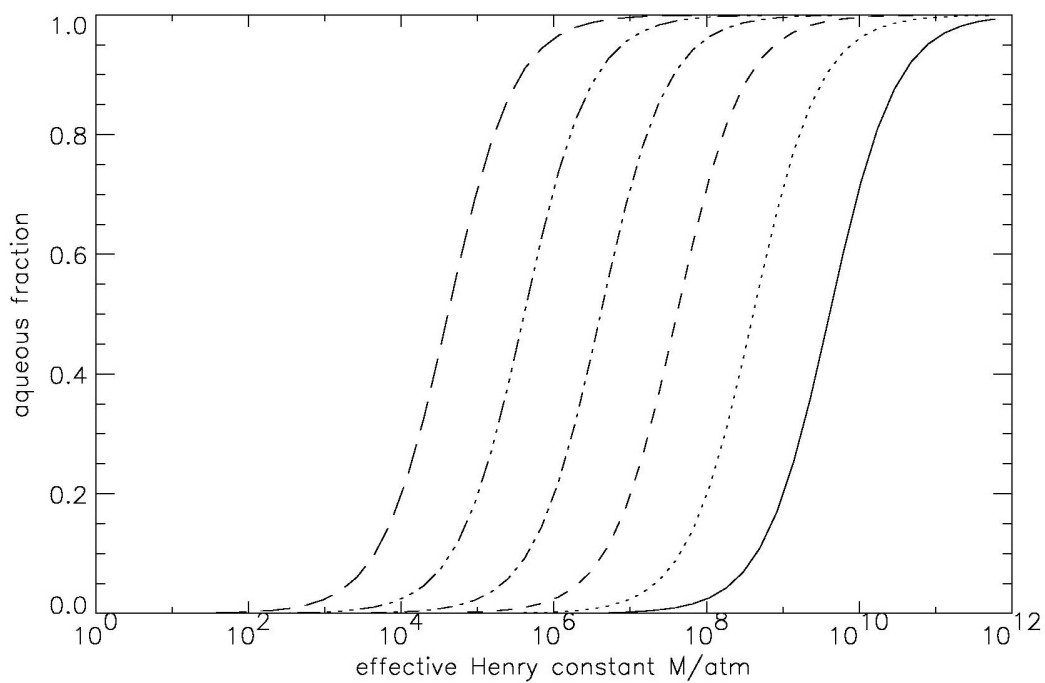


Figure B.1: Aqueous fraction as function of the Henry's constant for different liquid water contents. Long-dashed line: $w_l = 1 \text{ g/m}^3$, dash-dot-dot-dotted line: $w_l = 0.1 \text{ g/m}^3$, dash-dotted line: $w_l = 0.01 \text{ g/m}^3$, dashed line: $w_l = 10^{-3} \text{ g/m}^3$, dotted line: $w_l = 10^{-4} \text{ g/m}^3$, solid line: $w_l = 10^{-5} \text{ g/m}^3$

Appendix C

List of symbols

C.1 Variable names

variable	description	unit
A_{pl}	cross section of the ship plume	m^2
a	dry aerosol radius	m
\bar{v}	mean molecular speed	m/s
C	condensation rate	$\text{kg}/(\text{m}^3 \text{s})$
$c_{a,i}$	concentration of aqueous phase species in bin i	$\text{mol}/\text{m}_\text{air}^3$
c_{bg}	background concentration	$\text{mol}/\text{m}_\text{air}^3$
c_g	concentration of gas phase species	$\text{mol}/\text{m}_\text{air}^3$
c_p	specific heat of dry air at constant pressure	$\text{J}/(\text{kg K})$
c_w	specific heat of water	$\text{J}/(\text{kg K})$
D	dry deposition (gases and aerosols)	$\text{mol}/(\text{m}^3 \text{s})$
D_a	aerosol diffusion coefficient	m^2/s
D_g	gas phase diffusion coefficient	m^2/s
D'_v	water vapor diffusion coefficient	m^2/s
E	surface gas phase emission	$\text{mol}/(\text{m}^3 \text{s})$
E_n	net radiative flux density	W/m^2
e	turbulence kinetic energy	$1/(\text{m}^2 \text{s})$
$F(\lambda)$	spectral actinic flux	$\text{W}/(\text{m}^2 \text{m})$
F	flux of sea salt particles from the ocean	$1/(\text{m}^2 \text{s})$
$F_d(a, r)$	net radiative flux at the particle's surface	W
F_{dep}	dry deposition flux	$\text{mol}/(\text{m}^2 \text{s})$
$f(a, r)$	two-dimensional particle size distribution function	$1/\text{m}^3$
f	Coriolis parameter	$1/\text{s}$
h_0	reference height of the ship plume	m
H^*	effective Henry constant	$\text{mol}/(\text{m}^3 \text{Pa})$
h_{pl}	height of the ship plume	m
J_x	photolysis rate (or photo dissociation coefficient)	$1/\text{s}$
$J_{i,x}^a$	photolysis rate for a purely absorbing atmosphere	$1/\text{s}$
K_e	exchange coefficient for e	m^2/s

variable	description	unit
K_h	turbulent exchange coefficients for heat	m^2/s
K_m	turbulent exchange coefficients for momentum	m^2/s
k_H^{cc}	dimensionless Henry constant	1
k_H	Henry constant	$\text{mol}/(\text{m}^3 \text{ Pa})$
k'	thermal conductivity of moist air	$\text{W}/(\text{m K})$
k_t	mass transfer coefficient	$\text{m}_{\text{air}}^3/(\text{m}_{\text{aq}}^3 \text{ s})$
$k_{t,i}$	mass transfer coefficient for aqueous bin i	$\text{m}_{\text{air}}^3/(\text{m}_{\text{aq}}^3 \text{ s})$
\bar{k}_t	mean transfer coefficient for a particle population	$\text{m}_{\text{air}}^3/(\text{m}_{\text{aq}}^3 \text{ s})$
l	mixing length	m
L	chemical destruction	1/s
L	latent heat of condensation	J/kg
L	Monin-Obukhov length	m
M	molar mass	g/mol
$m_w(a, r)$	liquid water mass of the particle	kg
n_{kc}	number of the aqueous classes	1
p_0	air pressure at the surface	Pa
p	air pressure	Pa
P	chemical production	$\text{mol}/(\text{m}^3 \text{ s})$
P_{pc}	transport of chemical species from the aerosol to the cloud droplet regimes	$\text{mol}/(\text{m}^3 \text{ s})$
q	specific humidity	kg/kg
r_a	aerodynamic resistance	s/m
r_b	quasi-laminar layer resistance	s/m
r_c	surface resistance	s/m
R	gas constant for dry air	$\text{J}/(\text{mol K})$
R_v	specific gas constant for water vapor	$\text{J}/(\text{kg K})$
r	total particle radius	m
Sc	Schmidt number	1
S_h	stability function	
S_∞	ambient supersaturation	1
S_m	stability function	
S_r	supersaturation at the droplet's surface	1
St	Stokes number	1
T	temperature	K
t	time	s
u	wind speed in x-direction	m/s
u_{10}	wind speed in 10 m height	m/s
u_*	friction velocity	m/s
u_g	geostrophic wind	m/s
v	wind speed in y-direction	m/s
$v_{a,i}^{dry}$	dry deposition velocity of particles	m/s
v_g^{dry}	dry deposition velocity of gases	m/s
v_g	geostrophic wind	m/s
\bar{v}	mean molecular speed	m/s

variable	description	unit
w	vertical/subsidence velocity	m/s
w_0	reference width of the ship plume	m
$w_{l,i}$	liquid water content of aqueous bin i	kg/m ³
w_{pl}	width of the ship plume	m
w_t	particle sedimentation velocity	m/s
z_0	roughness length	m
α	accommodation coefficient	1
α	horizontal plume expansion rate	1
β	vertical plume expansion rate	1
δ_i	describes the effect of scattering by air molecules, aerosol and cloud particles	1
κ	von Kármán constant	1
λ	mean free path length	m
λ	wavelength	m
ν	dynamic viscosity of air	kg/(m s)
Φ	generic meteorological variable	-
Φ_s	stability function	1
ϕ_x	quantum yield	1
ρ	air density	kg/m ³
ρ_s	saturation vapor density	kg/m ³
ρ_w	density of water	kg/m ³
σ_x	absorption cross section	m ²
Θ	potential temperature	K

C.2 Names in the source code

name	description	unit
parameter		
n	total number of gridlayers	e.g. nf + 50
nb	number of soil layers, not used	e.g. 20
nf	number of equidistant gridlayers	e.g. 100
nka	number of aerosol classes	e.g. 50
nkt	number of droplet classes	e.g. 40
nrlay	number of gridlayers used in the radiative code PIFM2 and in the photolysis code	e.g. n -1 + 11
nrlev	number of levels (= layer boundaries) used in the radiative code PIFM2	e.g. n -1 + 12
grid		
eta(n)	height of layer (middle of layer)	m
etw(n)	height of layer (w="wall")	m
deta(n)	deta(k)=eta(k+1)-eta(k)	m
detw(n)	detw(k)=etw(k)-etw(k-1)	m

name	description	unit
meteorology		
t(n)	temperature	K
theta(n)	pot. temp.	K
thetl(n)	liq. wat. pot. temp.	K
p(n)	pressure	Pa
rho(n)	air density	kg/m ³
u(n)	wind	m/s
v(n)	wind	m/s
w(n)	wind	m/s
xm1(n)	spec. humidity	kg/kg
xm2(n)	LWC	kg/m ³
feu(n)	relative humidity	1
turbulence		
atke(n)	exchange coeff. TKE	m ² /s
atk _h (n)	exchange coeff. heat	m ² /s
atk _m (n)	exchange coeff. momentum	m ² /s
buoy(n)	buoyancy term	K/m
gh(n)	stability function heat	1
gm(n)	stability function momentum	1
sm(n)	see mellor + yamada	K/m
sh(n)	"	K/m
tke(n)	turbulence kinetic energy	m ² /s ²
tkep(n)	production of TKE	m ² /s ³
xl(n)	mixing length	m
microphysics		
dew(nkt)	dew(jt)=ew(jt)-ew(jt-1)	mg
e(nkt)	water mass (middle of bin)	mg
en(nka)	aerosol mass (middle of bin)	mg
enw(nka)	aerosol mass (max of bin)	mg
ew(nkt)	water mass (max of bin)	mg
ff(nkt,nka,n)	2 dim. particle spectrum	1/cm ³
fcs(nka)	fraction of soluble material in dry aerosol	1
fsum(n)	number of particles	1/cm ³
nar(n)	aerosol type	1
rn(nka)	radius of aerosol	μm
rq(nkt,nka)	radius of particle (middle of bin)	μm
rw(nkt,nka)	radius of particle (max, w="wall")	μm
sr(nka,nkt)	saturation at r=rc (Köhler curve)	1
xmol2(nka)	mol masses of water	g/mol
xmol3(nka)	mol masses of aerosol	g/mol
xnue	number of ions per dissociating compound	1
soil		
ak(nb)		

name	description	unit
aks	K_{η_s} - saturation hydraulic conductivity	m s^{-1}
anu0	reference for thermal conductivity	
anu	ν , thermal conductivity of the soil	
bs	dimensionless coefficient for hydraulic properties of soil	1
bs0	reference for exponent bs	
d(nb)		
dzb(nb)	$dzb(k) = zb(k+1) - zb(k)$	m
dzbw(nb)	$dzbw(k) = zbw(k+1) - zbw(k)$	m
eb(nb)	vol. moisture content	m^3/m^3
ebc	reference value for soil moisture	
ebs	η_s - soil porosity = saturation moisture potential	$\text{cm}^3 \text{ cm}^{-3}$
psi1	moisture potential	m
psi2	moisture potential	m
psis	saturation moisture potential	m
rhoc	density * specific heat capacity, soil	$\text{J m}^{-3} \text{ K}^{-1}$
rhocw	density * specific heat capacity, water	$\text{J m}^{-3} \text{ K}^{-1}$
tb(nb)	temperature	K
zb(nb)	depth of layer (middle of layer)	m
surface fluxes		
ajb	heatflux from ground	
ajd	dew flux	
ajl	latent microturbulent enthalpy flux	
ajm	ground moisture flux	
ajq	microturbulent flux of water vapor	
ajs	water flux due to droplet sedimentation	
ajt	sensible microturbulent enthalpy flux	
ds1		
ds2		
reif	rime	
sk	short wave radiative flux	
sl	long wave radiative flux	
tau	dew	
trdep		
radiation		
nrlev	number of levels in the radiation code	$n+11$
nrlay	number of layers (= half level)	$nrlev-1$
mb	number of spectral bands	18
mbs	number of solar spectral bands	6
mbir	number of IR spectral bands	12
dtrad(n)	heating rate radiation	K/s
dtcon(n)	heating rate condensation	K/s

name	description	unit
radiation coefficients for liquid water:		
ncw	number of tabulated effective radius	
ret(ncw)	tabulated effective droplet radius	m
r2wt(ncw)	tabulated LWC	kg/m ³
b2wt(ncw,mb)	extinction coefficient	1/m
w2wt(ncw,mb)	single scattering albedo	
g2wt(ncw,mb)	asymmetry factor	
radiation coefficients for diagnostic aerosols:		
feux(8)	tabulated values of relative humidity	
seanew(8,mb,4)	extinction cross-section	m ²
saanew(8,mb,4)	absorption cross-section	m ²
ganew(8,mb,4)	asymmetry factor	
xa0(11)	tabulated water volume fraction in aerosol	
radiation coefficients for prognostic aerosols:		
na0	number of tabulated water volume fraction in aerosol	11
nw0	number of tabulated aerosol radius	40
xa0(na0)	tabulated water volume fraction in aerosol	
xw0(nw0)	tabulated aerosol radius	μm
qabs0(mb,nw0,na0)	absorption coefficient	
qext0(mb,nw0,na0)	extinction coefficient	
asym0(mb,nw0,na0)	asymmetry factor	
qabs(mb,nkt,nka,)	interpolated absorption coefficient	
qext(mb,nkt,nka,)	interpolated extinction coefficient	
asym(mb,nkt,nka,)	interpolated asymmetry factor	
misc., constants		
alat	latitude	°
cp	specific heat of dry air	
dd	fractional timestep (10s)	s
declin	declination	°
dt	timestep (60s)	s
g	gravitational constant	m/s ²
itmax	max model time	min
lcl	lowest cloud layer	1
lct	top cloud layer	1
lday	model day	day
lst	hour	h
lmin	minute	min
pi	π	1
r0	specific gas constant of dry air	J/(kg × K)
r1	specific gas constant of water vapour	J/(kg × K)

name	description	unit
rad	water density	kg m^{-3}
rhow	water density	kg m^{-3}
time	total time of the run	s
tw	water temperature (SST)	K
ug	geostrophic wind u	m/s
vg	geostrophic wind v	m/s
wmax	subsidence max	m/s
wmin	subsidence min	m/s
z0	roughness length	m
zinv	inversion layer	1
chemistry		
j1	number of gas phase species w/o radicals	65
j2	number of liquid phase species w/o ions	j1 + j3
j3	species additionally in liquid phase, e.g. radicals, lumped sp	8
j5	number of radical gas species	30
j6	number of ions in liquid phase	40
ka	border between small and large aerosol	e.g. 34
kinv	inversion layer	e.g. 70
kw(nka)	border between aerosol and droplets	
neula	number of advected species	10
nkc	number of liquid phase classes	4
nspec	number of species in the actual chemistry scheme	
aircc	concentration of air molecules	molec/cm^3
alpha(nf, nspec)	accommodation coefficient	1
am3(n, 2)	air/CO concentration	mol/m^3
bg(2, 15, 1400)	(accumulated) reaction rates	$\text{molec}/(\text{cm}^3 \text{ s}) / \text{molec/cm}^3$
brsss	bromine concentration in particles (for mass balance only)	$\text{mol}/\text{m}_\text{air}^3$
cloud(n)	cloud present in layer	true/false
cloudt(n, nkc)	cloud present in layer at t-1	true/false
c1sss	chlorine concentration in particles (for mass balance only)	$\text{mol}/\text{m}_\text{air}^3$
cm(nf, nkc)	liquid water volume in particle class	$\text{m}_\text{aq}^3/\text{m}_\text{air}^3$
cm3(n, 2)	air/CO concentration	molec/cm^3
co1in	init concentration of CO2 at ground	nmol/mol
co2in	init concentration of CO2 at top	nmol/mol
conv1	conversion factor	$\text{m}_\text{air}^3/\text{mol} / \text{cm}_\text{air}^3/\text{molec}$
conv2(nf, nkc)	conversion factor	$1/(1000 \times \text{m}^3/\text{m}_\text{air}^3)$
cw(nf, nkc)	total particle volume in particle class	$\text{m}^3/\text{m}_\text{air}^3$

name	description	unit
cwm(n,nkc)	same as cw(nf,nkc) but in different common block	
den	change of particle mass in SR stem_kpp	mg (=en)
dtarr(6)	fractional timestep for KPP - longer selection	s
dtarr2(6)	fractional timestep for KPP - shorter selection	s
es1(j1)	emission rates of gaseous species	molec/(cm ² s)
fcs(nka)	fraction of soluble material in dry aerosol	1
freep(nf)	free path length	m
fs1(n,nka)	aerosol mass, small	mg/cm ³
fs2(n,nka)	aerosol mass, large	mg/cm ³
h20ppm	water vapor mixing ratio	μmol/mol
halo	halogen chemistry active	true/false
henry(nf,nspec)	inverse dimensionless Henry constants	mol _{gas} /m ³ _{air}
iod	iodine chemistry active	mol _{aq} /m ³ _{aq}
is4(n,3)	array for output of parameters 1 = am3(n,1) 3 = am3(n,2)	true/false
jend(6)	number of fractional timesteps for KPP	1
jend2(6)	number of fractional timesteps for KPP	1
part_n(n,nkc.nka)	new particle concentration for SR konc	1/cm ³
part_o(n,nkc,nka)	old particle concentration for SR konc	1/cm ³
ph_rat(38)	photolysis rates	1/s
photol_j(43,n)	photolysis rates	1/s
pntot(n,nkc)	particle concentration per aqueous bin	1/cm ³
rc(nf,nkc)	mean radius of particle	m
rcm(n,nkc)	same as rc(nf,nkc) but in different common block	
s1(n,j1)	concentration gas phase species	mol/m ³
s1in(j1)	init concentration at surface	nmol/mol
s2in(j1)	init concentration at top of model	nmol/mol
s3(n,j5)	concentration of radicals (gas)	mol/m ³
sa1(nka,j2)	initial loading of aerosol with chemical species	mol/particle
sap1(n)	total number of aerosol particles, small	1/cm ³
sap2(n)	total number of aerosol particles, large	1/cm ³
sion1(n,j6,nkc)	concentration of ions	mol/m ³ (air)
s11(n,j2,nkc)	concentration of liquid phase species	mol/m ³ (air)
slp1	concentration per aerosol, small	mol/m ³ / (particle/cm ³) = μmol/part

name	description	unit
slp2	concentration per aerosol, large	mol/m ³ / (particle/cm ³) =μmol/part
smp1(n)	total aerosol mass, small	mg/cm ³
smp2(n)	total aerosol mass, large	mg/cm ³
te	= t(n)	K
vd(nka,nkt)	particle dry deposition velocity	m/s
vdm(nkc)	liquid class dry deposition velocity	m/s
vg(j1)	dry deposition velocity for gases	m/s
vmean(nf,nspec)	mean molecular speed	m/s
vol1(n,nkc,nka)	particle volume integrated over jt	μm ³ /cm ³
vol2(n,nkc)	particle volume integrated over ia and jt	μm ³ /cm ³
vt(nf,nkc)	particle sedimentation velocity	m/s
xadv(10)	advection strength	mol/(mol day)
xdeliss	deliquescence relative humidity for sea salt	1
xdelisulf	deliquescence relative humidity for sulfate	1
xgamma(nf,j6,nkc)	γ coefficients from Pitzer	1
xkmt(nf,nkc,nspec)	mass transfer coefficient	m _{air} ³ /m _{aq} ³ s
xkef(nf,nkc,nspec)	forward rate constant for equilibria	mol/l
xkeb(nf,nkc,nspec)	forward rate constant for equilibria	mol/l
xnasss	sodium concentration in particles (for mass balance only)	mol/m _{air} ³

Table C.2: The variables of KPP are not listed here.

Appendix D

Tables of reaction rate coefficients

This collection comprises a complete listing of all gas and aqueous phase species (Table D.1), gas phase (Table D.2) and aqueous phase (Table D.3) reaction rates, as well as rates for the heterogeneous (particle surface) reactions (Table D.4), aqueous phase equilibrium constants (Table D.5), Henry constants and accommodations coefficients (Table D.6).

The major reaction cycles involving halogens are depicted in Figure D.1

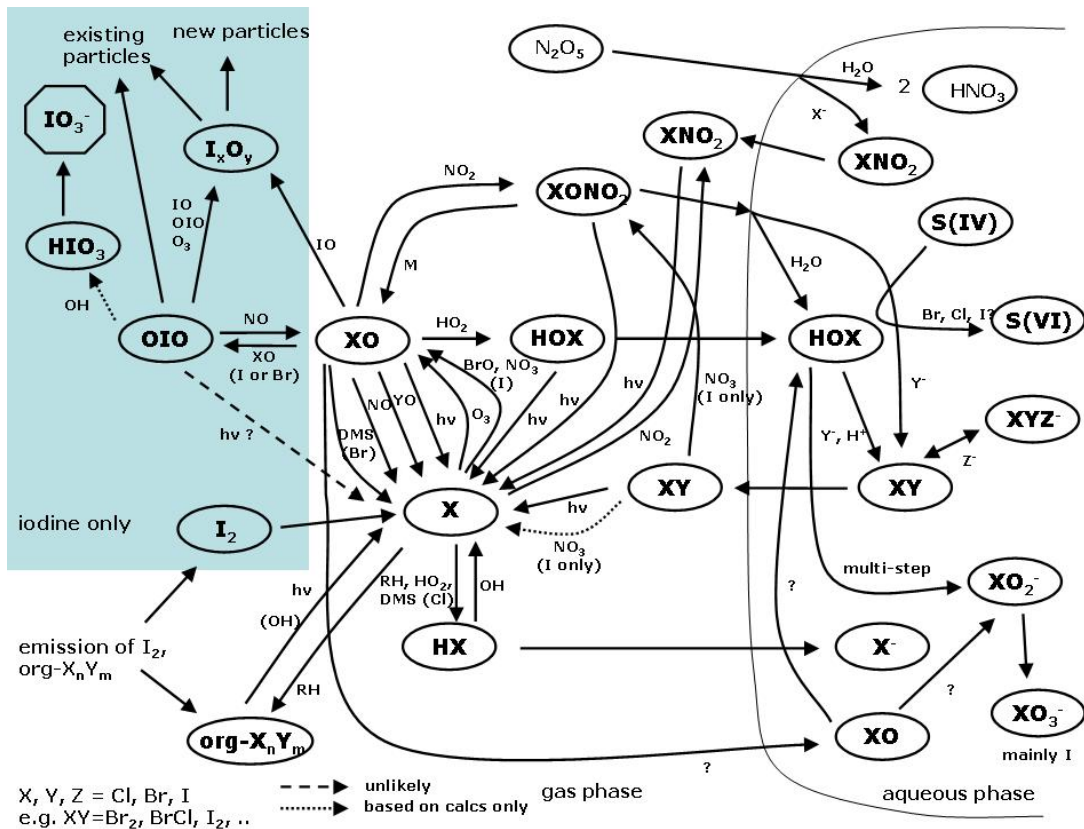


Figure D.1: Schematic diagram of the major bromine, chlorine, and sulfur related reactions in the gas and aqueous phase (from *von Glasow and Crutzen, 2007*).

Table D.1: Species

Gas phase
O ¹ D, O ₂ , O ₃ , OH, HO ₂ , H ₂ O ₂ , H ₂ O
NO, NO ₂ , NO ₃ , N ₂ O ₅ , HONO, HNO ₃ , HNO ₄ , PAN, NH ₃
CO, CO ₂ , CH ₄ , C ₂ H ₆ , C ₂ H ₄ , HCHO, HCOOH, ALD, CH ₂ O ₂ , HOCH ₂ O ₂ , CH ₃ CO ₃ , CH ₃ O ₂ , C ₂ H ₅ O ₂ , EO ₂ , CH ₂ O ₂ , ROOH
Cl, ClO, OCLO, HCl, HOCl, Cl ₂ , Cl ₂ O ₂ , ClNO ₂ , ClNO ₃
Br, BrO, HBr, HOBr, Br ₂ , BrNO ₂ , BrNO ₃ , BrCl
SO ₂ , H ₂ SO ₄ , DMS, CH ₃ SCH ₂ OO, DMSO, DMSO ₂ , CH ₃ S, CH ₃ SO, CH ₃ SO ₂ , CH ₃ SO ₃ , CH ₃ SO ₂ H, CH ₃ SO ₃ H
Liquid phase (non-charged)
O ₂ , O ₃ , OH, HO ₂ , H ₂ O ₂ , H ₂ O
NO, NO ₂ , NO ₃ , HONO, HNO ₃ , HNO ₄ , NH ₃
CO ₂ , HCHO, HCOOH, CH ₃ OH, CH ₃ OO, CH ₃ OOH
Cl, HCl, HOCl, Cl ₂
Br, HBr, HOBr, Br ₂ , BrCl
SO ₂ , H ₂ SO ₄ , DMSO, DMSO ₂ , CH ₃ SO ₂ H, CH ₃ SO ₃ H
Liquid phase (ions)
H ⁺ , OH ⁻ , O ₂ ⁻
NO ₂ ⁻ , NO ₃ ⁻ , NO ₄ ⁻ , NH ₄ ⁺
HCO ₃ ⁻ , CO ₃ ⁻ , HCOO ⁻
Cl ⁻ , Cl ₂ ⁻ , ClO ⁻ , ClOH ⁻
Br ⁻ , Br ₂ ⁻ , BrO ⁻ , BrCl ₂ ⁻ , Br ₂ Cl ⁻ , BrOH ⁻
HSO ₃ ⁻ , SO ₃ ²⁻ , HSO ₄ ⁻ , SO ₄ ²⁻ , HSO ₅ ⁻ , SO ₃ ⁻ , SO ₄ ⁻ , SO ₅ ⁻ , CH ₃ SO ₃ ⁻ , CH ₂ OHSO ₂ ⁻ , CH ₂ OHSO ₃ ⁻

Table D.2: Gas phase reactions.

no	reaction	n	$A [(\text{cm}^{-3})^{1-n} \text{s}^{-1}]$	$-E_a / R [\text{K}]$	reference
O 1	$\text{O}^1\text{D} + \text{O}_2 \rightarrow \text{O}_3$	2	3.2×10^{-11}	70	DeMore <i>et al.</i> (1997)
O 2	$\text{O}^1\text{D} + \text{N}_2 \rightarrow \text{O}_3$	2	1.8×10^{-11}	110	DeMore <i>et al.</i> (1997)
O 3	$\text{O}^1\text{D} + \text{H}_2\text{O} \rightarrow 2 \text{OH}$	2	2.2×10^{-10}		DeMore <i>et al.</i> (1997)
O 4	$\text{O}_3 + \text{OH} \rightarrow \text{HO}_2 + \text{O}_2$	2	1.5×10^{-12}	-880	Sander <i>et al.</i> (2000)
O 5	$\text{O}_3 + \text{HO}_2 \rightarrow \text{OH} + 2\text{O}_2$	2	2.0×10^{-14}	-680	Sander <i>et al.</i> (2000)
O 6	$\text{O}_3 + h\nu \rightarrow \text{O}_2 + \text{O}^1\text{D}$	1			DeMore <i>et al.</i> (1997)
O 7	$\text{HO}_2 + \text{OH} \rightarrow \text{H}_2\text{O} + \text{O}_2$	2	4.8×10^{-11}	250	DeMore <i>et al.</i> (1997)
O 8	$\text{HO}_2 + \text{HO}_2 \rightarrow \text{H}_2\text{O}_2 + \text{O}_2$	2			DeMore <i>et al.</i> (1997)
O 9	$\text{H}_2\text{O}_2 + h\nu \rightarrow 2\text{OH}$	1			DeMore <i>et al.</i> (1997)
O 10	$\text{H}_2\text{O}_2 + \text{OH} \rightarrow \text{HO}_2 + \text{H}_2\text{O}$	2	2.9×10^{-12}	-160	DeMore <i>et al.</i> (1997)
N 1	$\text{NO} + \text{OH} \xrightarrow{M} \text{HONO}$	2			DeMore <i>et al.</i> (1997)
N 2	$\text{NO} + \text{HO}_2 \rightarrow \text{NO}_2 + \text{OH}$	2	3.5×10^{-12}	250	DeMore <i>et al.</i> (1997)
N 3	$\text{NO} + \text{O}_3 \rightarrow \text{NO}_2 + \text{O}_2$	2	3.0×10^{-12}	-1500	Sander <i>et al.</i> (2000)
N 4	$\text{NO} + \text{NO}_3 \rightarrow 2\text{NO}_2$	2	1.5×10^{-11}	170	DeMore <i>et al.</i> (1997)
N 5	$\text{NO}_2 + \text{OH} \xrightarrow{M} \text{HNO}_3$	2			Sander <i>et al.</i> (2000)
N 6	$\text{NO}_2 + \text{HO}_2 \xrightarrow{M} \text{HNO}_4$	2			Atkinson <i>et al.</i> (1997)
N 7	$\text{NO}_2 + \text{O}_3 \rightarrow \text{NO}_3 + \text{O}_2$	2			DeMore <i>et al.</i> (1997)
N 8	$\text{NO}_2 + h\nu \rightarrow \text{NO} + \text{O}_3$	1			DeMore <i>et al.</i> (1997)
N 9	$\text{NO}_2 + \text{NO}_3 \xrightarrow{M} \text{N}_2\text{O}_5$	3			Sander <i>et al.</i> (2000)
N 10	$\text{NO}_3 + h\nu \rightarrow \text{NO} + \text{O}_2$	1			Wayne <i>et al.</i> (1991)
N 11	$\text{NO}_3 + h\nu \rightarrow \text{NO}_2 + \text{O}_3$	1			Wayne <i>et al.</i> (1991)
N 12	$\text{NO}_3 + \text{HO}_2 \rightarrow 0.3 \text{HNO}_3 + 0.7 \text{OH} + 0.7 \text{NO}_2 + \text{O}_2$	2	4.40×10^{-12}		Atkinson <i>et al.</i> (Dec. 2002)
N 13	$\text{N}_2\text{O}_5 \xrightarrow{M} \text{NO}_2 + \text{NO}_3$	1			Sander <i>et al.</i> (2000)
N 14	$\text{N}_2\text{O}_5 + \text{H}_2\text{O} \rightarrow 2\text{HNO}_3$	2	2.6×10^{-22}		Mentel <i>et al.</i> (1996)
N 15	$\text{N}_2\text{O}_5 + h\nu \rightarrow \text{NO}_2 + \text{NO}_3$	1			DeMore <i>et al.</i> (1997)
N 16	$\text{HONO} + \text{OH} \rightarrow \text{NO}_2$	2	1.8×10^{-11}	-390	DeMore <i>et al.</i> (1997)
N 17	$\text{HONO} + h\nu \rightarrow \text{NO} + \text{OH}$	1			DeMore <i>et al.</i> (1997)
N 18	$\text{HNO}_3 + h\nu \rightarrow \text{NO}_2 + \text{OH}$	1			DeMore <i>et al.</i> (1997)

Table D.2: Continued.

no	reaction	n	$A [(\text{cm}^{-3})^{1-n} \text{s}^{-1}]$	$-E_a / R [\text{K}]$	reference
N 19	$\text{HNO}_3 + \text{OH} \rightarrow \text{NO}_3 + \text{H}_2\text{O}$	2	2		Atkinson <i>et al.</i> (1997)
N 20	$\text{HNO}_4 \xrightarrow{M} \text{NO}_2 + \text{HO}_2$	1	2		Atkinson <i>et al.</i> (1997)
N 21	$\text{HNO}_4 + \text{OH} \rightarrow \text{NO}_2 + \text{H}_2\text{O} + \text{O}_2$	2	1.3×10^{-12}	380	DeMore <i>et al.</i> (1997)
N 22	$\text{HNO}_4 + h\nu \rightarrow \text{NO}_2 + \text{HO}_2$	1	1		DeMore <i>et al.</i> (1997)
N 23	$\text{HNO}_4 + h\nu \rightarrow \text{OH} + \text{NO}_3$	1	1		DeMore <i>et al.</i> (1997)
C 1	$\text{CO} + \text{OH} \xrightarrow{\text{O}_2} \text{HO}_2 + \text{CO}_2$	2	2		DeMore <i>et al.</i> (1997)
C 2	$\text{CH}_4 + \text{OH} \xrightarrow{\text{O}_2} \text{CH}_3\text{OO} + \text{H}_2\text{O}$	2	2.4×10^{-12}	-1710	Lurmann <i>et al.</i> (1986a)
C 3	$\text{C}_2\text{H}_6 + \text{OH} \rightarrow \text{C}_2\text{H}_5\text{O}_2 + \text{H}_2\text{O}$	2	1.7×10^{-11}	-1232	Lurmann <i>et al.</i> (1986a)
C 4	$\text{C}_2\text{H}_4 + \text{OH} \rightarrow \text{EO}_2$	2	1.66×10^{-12}	474	Lurmann <i>et al.</i> (1986a)
C 5	$\text{C}_2\text{H}_4 + \text{O}_3 \rightarrow \text{HCHO} + 0.4\text{CH}_2\text{O}_2 + 0.12\text{HO}_2 + 0.42\text{CO}$ + 0.06CH_4	2	1.2×10^{-14}	-2633	Lurmann <i>et al.</i> (1986a)
C 6	$\text{HO}_2 + \text{CH}_3\text{OO} \rightarrow \text{ROOH} + \text{O}_2$	2	3.8×10^{-13}	800	DeMore <i>et al.</i> (1997)
C 7	$\text{HO}_2 + \text{C}_2\text{H}_5\text{O}_2 \rightarrow \text{ROOH} + \text{O}_2$	2	7.5×10^{-13}	700	DeMore <i>et al.</i> (1997)
C 8	$\text{HO}_2 + \text{CH}_3\text{CO}_3 \rightarrow \text{ROOH} + \text{O}_2$	2	4.5×10^{-13}	1000	DeMore <i>et al.</i> (1997)
C 9	$\text{CH}_3\text{OO} + \text{CH}_3\text{OO} \rightarrow 1.4\text{HCHO} + 0.8\text{HO}_2 + \text{O}_2$	2	1.5×10^{-13}	220	Lurmann <i>et al.</i> (1986a)
C 10	$\text{C}_2\text{H}_5\text{O}_2 + \text{NO} \rightarrow \text{ALD} + \text{HO}_2 + \text{NO}_2$	2	4.2×10^{-12}	180	Lurmann <i>et al.</i> (1986a)
C 11	$2\text{C}_2\text{H}_5\text{O}_2 \rightarrow 1.6\text{ALD} + 1.2\text{HO}_2$	2	5.00×10^{-14}		Lurmann <i>et al.</i> (1986a)
C 12	$\text{EO}_2 + \text{NO} \rightarrow \text{NO}_2 + 2.0\text{HCHO} + \text{HO}_2$	2	4.2×10^{-12}	180	Lurmann <i>et al.</i> (1986a)
C 13	$\text{EO}_2 + \text{EO}_2 \rightarrow 2.4\text{HCHO} + 1.2\text{HO}_2 + 0.4\text{ALD}$	2	5.00×10^{-14}		Lurmann <i>et al.</i> (1986a)
C 14	$\text{HO}_2 + \text{EO}_2 \rightarrow \text{ROOH} + \text{O}_2$	2	3.00×10^{-12}		Lurmann <i>et al.</i> (1986a)
C 15	$\text{HCHO} + h\nu \rightarrow 2\text{HO}_2 + \text{CO}$	1	1		DeMore <i>et al.</i> (1997)
C 16	$\text{HCHO} + h\nu \rightarrow \text{CO} + \text{H}_2$	1	1		DeMore <i>et al.</i> (1997)
C 17	$\text{HCHO} + \text{OH} \xrightarrow{\text{O}_2} \text{HO}_2 + \text{CO} + \text{H}_2\text{O}$	2	1.00×10^{-11}		DeMore <i>et al.</i> (1997)
C 18	$\text{HCHO} + \text{HO}_2 \rightarrow \text{HOCH}_2\text{O}_2$	2	6.7×10^{-15}	600	DeMore <i>et al.</i> (1997)
C 19	$\text{HCHO} + \text{NO}_3 \xrightarrow{\text{O}_2} \text{HNO}_3 + \text{HO}_2 + \text{CO}$	2	5.8×10^{-16}		DeMore <i>et al.</i> (1997)
C 20	$\text{ALD} + \text{OH} \rightarrow \text{CH}_3\text{CO}_3 + \text{H}_2\text{O}$	2	6.9×10^{-12}	250	Lurmann <i>et al.</i> (1986a)
C 21	$\text{ALD} + \text{NO}_3 \rightarrow \text{HNO}_3 + \text{CH}_3\text{CO}_3$	2	1.40×10^{-15}		DeMore <i>et al.</i> (1997)
C 22	$\text{ALD} + h\nu \rightarrow \text{CH}_3\text{OO} + \text{HO}_2 + \text{CO}$	1	1		Lurmann <i>et al.</i> (1986a)
C 23	$\text{ALD} + h\nu \rightarrow \text{CH}_4 + \text{CO}$	1	1		Lurmann <i>et al.</i> (1986a)

Table D.2: Continued.

no	reaction	n	$A \text{ [(cm}^{-3}\text{)}^{1-n} \text{s}^{-1}]$	$-E_a / R \text{ [K]}$	reference
C 24	$\text{HOCH}_2\text{O}_2 + \text{NO} \longrightarrow \text{HCOOH} + \text{HO}_2 + \text{NO}_2$	2	4.2×10^{-12}	180	Lurmann <i>et al.</i> (1986a)
C 25	$\text{HOCH}_2\text{O}_2 + \text{HO}_2 \longrightarrow \text{HCOOH} + \text{H}_2\text{O} + \text{O}_2$	2	2.00×10^{-12}		Lurmann <i>et al.</i> (1986a)
C 26	$2 \text{ HOCH}_2\text{O}_2 \longrightarrow 2 \text{ HCOOH} + 2 \text{ HO}_2 + 2 \text{ O}_2$	2	1.00×10^{-13}		
C 27	$\text{HCOOH} + \text{OH} \xrightarrow{\text{O}_2} \text{HO}_2 + \text{H}_2\text{O} + \text{CO}_2$	2	4.0×10^{-13}		DeMore <i>et al.</i> (1997)
C 28	$\text{CH}_3\text{CO}_3 + \text{NO}_2 \longrightarrow \text{PAN}$	2	4.70×10^{-12}		Lurmann <i>et al.</i> (1986a)
C 29	$\text{PAN} \longrightarrow \text{CH}_3\text{CO}_3 + \text{NO}_2$	1	1.9×10^{16}		DeMore <i>et al.</i> (1997)
C 30	$\text{CH}_3\text{CO}_3 + \text{NO} \longrightarrow \text{CH}_3\text{OO} + \text{NO}_2 + \text{CO}_2$	2	4.2×10^{-12}	180	Lurmann <i>et al.</i> (1986a)
C 31	$\text{CH}_3\text{OO} + \text{NO} \xrightarrow{\text{O}_2} \text{HCHO} + \text{NO}_2 + \text{HO}_2$	2	3.0×10^{-12}	280	DeMore <i>et al.</i> (1997)
C 32	$\text{ROOH} + \text{OH} \longrightarrow 0.7 \text{ CH}_3\text{OO} + 0.3 \text{ HCHO} + 0.3 \text{ OH}$	2	3.8×10^{-12}	200	DeMore <i>et al.</i> (1997), see note
C 33	$\text{ROOH} + h\nu \longrightarrow \text{HCHO} + \text{OH} + \text{HO}_2$	1	1		DeMore <i>et al.</i> (1997), see note
S 1	$\text{SO}_2 + \text{OH} \longrightarrow \text{H}_2\text{SO}_4 + \text{HO}_2$	2	2		Lurmann <i>et al.</i> (1986a)
S 2	$\text{CH}_3\text{SCH}_3 + \text{OH} \longrightarrow \text{CH}_3\text{SCH}_2\text{OO} + \text{H}_2\text{O}$	2	2		Atkinson <i>et al.</i> (1997)
S 3	$\text{CH}_3\text{SCH}_3 + \text{OH} \xrightarrow{\text{O}_2} \text{CH}_3\text{SOCH}_3 + \text{HO}_2$	2	2		Atkinson <i>et al.</i> (1997)
S 4	$\text{CH}_3\text{SCH}_3 + \text{NO}_3 \xrightarrow{\text{O}_2} \text{CH}_3\text{SCH}_2\text{OO} + \text{HNO}_3$	2	1.9×10^{-13}	520	Atkinson <i>et al.</i> (1999)
S 5	$\text{CH}_3\text{SCH}_3 + \text{Cl} \xrightarrow{\text{O}_2} \text{CH}_3\text{SCH}_2\text{OO} + \text{HCl}$	2	3.3×10^{-10}		Atkinson <i>et al.</i> (1999)
S 6	$\text{CH}_3\text{SCH}_3 + \text{Br} \xrightarrow{\text{O}_2} \text{CH}_3\text{SCH}_2\text{OO} + \text{HBr}$	2	9.0×10^{-11}		Jefferson <i>et al.</i> (1994)
S 7	$\text{CH}_3\text{SCH}_3 + \text{BrO} \longrightarrow \text{CH}_3\text{SOCH}_3 + \text{Br}$	2	2.54×10^{-14}	850	Ingham <i>et al.</i> (1999)
S 8	$\text{CH}_3\text{SCH}_2\text{OO} + \text{NO} \longrightarrow \text{HCHO} + \text{CH}_3\text{S} + \text{NO}_2$	2	4.9×10^{-12}	263	Urbanski <i>et al.</i> (1997)
S 9	$\text{CH}_3\text{SCH}_2\text{OO} + \text{CH}_3\text{SCH}_2\text{OO} \xrightarrow{\text{O}_2} 2 \text{ HCHO} + 2 \text{ CH}_3\text{S}$	2	1.0×10^{-11}		Urbanski <i>et al.</i> (1997); Atkinson <i>et al.</i> (Dec. 2000), product ratios from van Dingen <i>et al.</i> (1994)
S 10	$\text{CH}_3\text{S} + \text{O}_3 \longrightarrow \text{CH}_3\text{SO} + \text{O}_2$	2	1.15×10^{-12}	432	Atkinson <i>et al.</i> (Dec. 2002)
S 11	$\text{CH}_3\text{S} + \text{NO}_2 \longrightarrow \text{CH}_3\text{SO} + \text{NO}$	2	3.0×10^{-11}	210	Atkinson <i>et al.</i> (Dec. 2002); Kukui <i>et al.</i> (2000), product ratios from van Dingen <i>et al.</i> (1994)
S 12	$\text{CH}_3\text{SO} + \text{NO}_2 \xrightarrow{\text{O}_2} 0.82 \text{ CH}_3\text{SO}_2 + 0.18 \text{ SO}_2 + 0.18 \text{ MO}_2 + \text{NO}$	2	1.2×10^{-11}		
S 13	$\text{CH}_3\text{SO} + \text{O}_3 \xrightarrow{\text{O}_2} \text{CH}_3\text{SO}_2$	2	6.0×10^{-13}		Atkinson <i>et al.</i> (Dec. 2002)
S 14	$\text{CH}_3\text{SO}_2 \longrightarrow \text{SO}_2 + \text{CH}_3\text{OO}$	1	1.9×10^{13}	-8661	Barone <i>et al.</i> (1995)
S 15	$\text{CH}_3\text{SO}_2 + \text{NO}_2 \longrightarrow \text{CH}_3\text{SO}_3 + \text{NO}$	2	2.2×10^{-12}		Ray <i>et al.</i> (1996)
S 16	$\text{CH}_3\text{SO}_2 + \text{O}_3 \longrightarrow \text{CH}_3\text{SO}_3$	2	$3. \times 10^{-13}$		Barone <i>et al.</i> (1995)
S 17	$\text{CH}_3\text{SO}_3 + \text{HO}_2 \longrightarrow \text{CH}_3\text{SO}_3\text{H}$	2	$5. \times 10^{-11}$		Barone <i>et al.</i> (1995)
S 18	$\text{CH}_3\text{SO}_3 \xrightarrow{\text{H}_2\text{O}, \text{O}_2} \text{CH}_3\text{OO} + \text{H}_2\text{SO}_4$	1	1.36×10^{14}	-11071	Barone <i>et al.</i> (1995)

Table D.2: Continued.

no	reaction	n	$A [(\text{cm}^{-3})^{1-n} \text{s}^{-1}]$	$-E_a / R [\text{K}]$	reference
S 19	$\text{CH}_3\text{SOCH}_3 + \text{OH} \rightarrow 0.95 \text{CH}_3\text{SO}_2\text{H} + 0.95 \text{CH}_3\text{OO} + 0.05 \text{DMSO}_2$	2	8.7×10^{-11}		<i>Urbanski et al. (1998)</i>
S 20	$\text{CH}_3\text{SO}_2\text{H} + \text{OH} \rightarrow 0.95 \text{CH}_3\text{SO}_2 + 0.05 \text{CH}_3\text{SO}_3\text{H} + 0.05 \text{HO}_2 + \text{H}_2\text{O}$	2	$9. \times 10^{-11}$		<i>Kukui et al. (2003)</i> ³
S 21	$\text{CH}_3\text{SO}_2\text{H} + \text{NO}_3 \rightarrow \text{CH}_3\text{SO}_2 + \text{HNO}_3$	2	1.0×10^{-13}		<i>Yin et al. (1990)</i>
S 22	$\text{CH}_3\text{SCH}_3 + \text{OH} \xrightarrow{\text{NO}_2\text{O}_3} \text{CH}_3\text{SO}_2 + \text{HCHO} + \text{NO}_2$	2	1.12×10^{-11}	-253	<i>Atkinson et al. (1999)</i>
Cl 1	$\text{Cl} + \text{O}_3 \rightarrow \text{ClO} + \text{O}_2$	2	2.3×10^{-11}	-200	<i>Sander et al. (2000)</i>
Cl 2	$\text{Cl} + \text{H}_2\text{O}_2 \rightarrow \text{HCl} + \text{HO}_2$	2	1.1×10^{-11}	-980	<i>DeMore et al. (1997)</i>
Cl 3	$\text{Cl} + \text{CH}_4 \xrightarrow{\text{O}_2} \text{HCl} + \text{CH}_3\text{OO}$	2	9.6×10^{-12}	-1360	<i>Sander et al. (2000)</i>
Cl 4	$\text{Cl} + \text{C}_2\text{H}_6 \xrightarrow{\text{O}_2} \text{HCl} + \text{C}_2\text{H}_5\text{O}_2$	2	7.7×10^{-11}	-90	<i>DeMore et al. (1997)</i>
Cl 5	$\text{Cl} + \text{C}_2\text{H}_4 \xrightarrow{\text{O}_2} \text{HCl} + \text{C}_2\text{H}_5\text{O}_2$	2	$1. \times 10^{-10}$		<i>Mallard et al. (1993)</i>
Cl 6	$\text{Cl} + \text{HCHO} \xrightarrow{\text{O}_2} \text{HCl} + \text{HO}_2 + \text{CO}$	2	8.1×10^{-11}	-30	<i>DeMore et al. (1997)</i>
Cl 7	$\text{Cl} + \text{ROOH} \rightarrow \text{CH}_3\text{OO} + \text{HCl}$	2	5.7×10^{-11}		<i>Wallington et al. (1990), see note</i>
Cl 8	$\text{Cl} + \text{ClNO}_3 \rightarrow \text{Cl}_2 + \text{NO}_3$	2	9.6×10^{-12}	140	<i>Yokelson et al. (1995)</i>
Cl 9	$\text{ClO} + \text{HO}_2 \rightarrow \text{HOCl} + \text{O}_2$	2	4.8×10^{-13}	700	<i>DeMore et al. (1997)</i>
Cl 10	$\text{ClO} + \text{NO} \rightarrow \text{Cl} + \text{NO}_2$	2	6.4×10^{-12}	290	<i>DeMore et al. (1997)</i>
Cl 11	$\text{ClO} + \text{NO}_2 \xrightarrow{\text{M}} \text{ClNO}_3$	2			<i>Sander et al. (2000)</i>
Cl 12	$\text{ClO} + \text{CH}_3\text{OO} \rightarrow \text{Cl} + \text{HCHO} + \text{HO}_2$	2	3.3×10^{-12}	-115	<i>DeMore et al. (1997)</i>
Cl 13	$\text{ClO} + \text{ClO} \rightarrow \text{Cl}_2\text{O}_2$	2			<i>Sander et al. (2000)</i>
Cl 14	$\text{Cl}_2\text{O}_2 \rightarrow \text{ClO} + \text{ClO}$	1			<i>DeMore et al. (1997)</i>
Cl 15	$\text{HCl} + \text{OH} \rightarrow \text{H}_2\text{O} + \text{Cl}$	2	2.6×10^{-12}	-350	<i>DeMore et al. (1997)</i>
Cl 16	$\text{ClNO}_3 \rightarrow \text{ClO} + \text{NO}_2$	1			<i>Anderson and Fahey (1990)</i>
Cl 17	$\text{OCIO} + h\nu \xrightarrow{\text{O}_2, \text{O}_3} \text{O}_3 + \text{ClO}$	1			<i>DeMore et al. (1997)</i>
Cl 18	$\text{Cl}_2\text{O}_2 + h\nu \rightarrow \text{Cl} + \text{Cl} + \text{O}_2$	1			<i>DeMore et al. (1997)</i>
Cl 19	$\text{Cl}_2 + h\nu \rightarrow 2 \text{Cl}$	1			<i>DeMore et al. (1997)</i>
Cl 20	$\text{HOCl} + h\nu \rightarrow \text{Cl} + \text{OH}$	1			<i>DeMore et al. (1997)</i>
Cl 21	$\text{ClNO}_2 + h\nu \rightarrow \text{Cl} + \text{NO}_2$	1			<i>DeMore et al. (1997)</i>
Cl 22	$\text{ClNO}_3 + h\nu \rightarrow \text{Cl} + \text{NO}_3$	1			<i>DeMore et al. (1997)</i>

Table D.2: Continued.

no	reaction	n	$A [(\text{cm}^{-3})^{1-n} \text{s}^{-1}]$	$-E_a / R [\text{K}]$	reference
Br 1	$\text{Br} + \text{O}_3 \rightarrow \text{BrO} + \text{O}_2$	2	1.7×10^{-11}	-800	DeMore <i>et al.</i> (1997)
Br 2	$\text{Br} + \text{HO}_2 \rightarrow \text{HBr} + \text{O}_2$	2	1.5×10^{-11}	-600	DeMore <i>et al.</i> (1997)
Br 3	$\text{Br} + \text{C}_2\text{H}_4 \xrightarrow{\text{O}_2} \text{HBr} + \text{C}_2\text{H}_5\text{O}_2$	2	5×10^{-14}		Singh and Zimmerman (1992)
Br 4	$\text{Br} + \text{HCHO} \xrightarrow{\text{O}_2} \text{HBr} + \text{CO} + \text{HO}_2$	2	1.7×10^{-11}	-800	DeMore <i>et al.</i> (1997)
Br 5	$\text{Br} + \text{ROOH} \rightarrow \text{CH}_3\text{OO} + \text{HBr}$	2	2.66×10^{-12}	-1610	Mallard <i>et al.</i> (1993)
Br 6	$\text{Br} + \text{BrNO}_3 \rightarrow \text{Br}_2 + \text{NO}_3$	2	4.9×10^{-11}		Orlando and Tyndall (1996)
Br 7	$\text{BrO} + \text{HO}_2 \rightarrow \text{HOBr} + \text{O}_2$	2	3.4×10^{-12}	540	DeMore <i>et al.</i> (1997)
Br 8	$\text{BrO} + \text{CH}_3\text{OO} \rightarrow \text{HOBr} + \text{HCHO}$	2	4.1×10^{-12}		Aranda <i>et al.</i> (1997)
Br 9	$\text{BrO} + \text{CH}_3\text{OO} \rightarrow \text{Br} + \text{HCHO} + \text{HO}_2$	2	1.6×10^{-12}		Aranda <i>et al.</i> (1997)
Br 10	$\text{BrO} + \text{NO} \rightarrow \text{Br} + \text{NO}_2$	2	8.8×10^{-12}	260	DeMore <i>et al.</i> (1997)
Br 11	$\text{BrO} + \text{NO}_2 \xrightarrow{M} \text{BrNO}_3$	2	2		Sander <i>et al.</i> (2000)
Br 12	$\text{BrO} + \text{BrO} \rightarrow 2 \text{Br} + \text{O}_2$	2	2.36×10^{-12}	40	DeMore <i>et al.</i> (1997)
Br 13	$\text{BrO} + \text{BrO} \rightarrow \text{Br}_2 + \text{O}_2$	2	2.79×10^{-14}	860	DeMore <i>et al.</i> (1997)
Br 14	$\text{HBr} + \text{OH} \rightarrow \text{Br} + \text{H}_2\text{O}$	2	1.1×10^{-11}		DeMore <i>et al.</i> (1997)
Br 15	$\text{BrNO}_3 \rightarrow \text{BrO} + \text{NO}_2$	1	2		Orlando and Tyndall (1996)
Br 16	$\text{BrO} + h\nu \xrightarrow{\text{O}_2} \text{Br} + \text{O}_3$	1	1		DeMore <i>et al.</i> (1997)
Br 17	$\text{Br}_2 + h\nu \rightarrow 2 \text{Br}$	1	1		Hubinger and Nee (1995)
Br 18	$\text{HOBr} + h\nu \rightarrow \text{Br} + \text{OH}$	1	1		Ingham <i>et al.</i> (1999)
Br 19	$\text{BrNO}_2 + h\nu \rightarrow \text{Br} + \text{NO}_2$	1	1		Scheffler <i>et al.</i> (1997)
Br 20	$\text{BrNO}_3 + h\nu \rightarrow \text{Br} + \text{NO}_3$	1	1		DeMore <i>et al.</i> (1997)
Hx 1	$\text{BrO} + \text{ClO} \rightarrow \text{Br} + \text{OCIO}$	2	9.5×10^{-13}	550	Sander <i>et al.</i> (2000)
Hx 2	$\text{BrO} + \text{ClO} \rightarrow \text{Br} + \text{Cl} + \text{O}_2$	2	2.3×10^{-12}	260	Sander <i>et al.</i> (2000)
Hx 3	$\text{BrO} + \text{ClO} \rightarrow \text{BrCl} + \text{O}_2$	2	4.1×10^{-13}	290	Mallard <i>et al.</i> (1993)
Hx 4	$\text{Br}_2 + \text{Cl} \rightarrow \text{BrCl} + \text{Br}$	2	1.2×10^{-10}		Mallard <i>et al.</i> (1993)
Hx 5	$\text{BrCl} + \text{Br} \rightarrow \text{Br}_2 + \text{Cl}$	2	3.3×10^{-15}		Mallard <i>et al.</i> (1993)
Hx 6	$\text{Br} + \text{Cl}_2 \rightarrow \text{BrCl} + \text{Cl}$	2	1.1×10^{-15}		Mallard <i>et al.</i> (1993)
Hx 7	$\text{BrCl} + \text{Cl} \rightarrow \text{Br} + \text{Cl}_2$	2	1.5×10^{-11}		Mallard <i>et al.</i> (1993)
Hx 8	$\text{BrCl} + h\nu \rightarrow \text{Br} + \text{Cl}$	1	1		DeMore <i>et al.</i> (1997)

n is the order of the reaction.¹ photolysis rates calculated online,² special rate functions (pressure dependent and/or humidity dependent),³ see text for sensitivity studies,⁴ only in “Luc” scenario. Notes: ALD is a generic aldehyde (see Lurmann *et al.* (1986a)), the rates for ROOH (reactions C32, C33, Cl7, Br5) were assumed as that of CH_3OOH , in reactions C4 and C5 C_2H_4 is used as generic alkene as in the Lurmann *et al.* (1986a) mechanism. The rate coefficients are calculated with $k = A \times \exp(-\frac{E_a}{RT})$.

Table D.3: Aqueous phase reactions.

no	reaction	$k_0 \text{ [} (\text{M}^{1-n})\text{s}^{-1} \text{]}$	$-E_a / R \text{ [K]}$	reference
O 1	$\text{O}_3 + \text{OH} \rightarrow \text{HO}_2$	1.1×10^8		<i>Søhested et al. (1984)</i>
O 2	$\text{O}_3 + \text{O}_2^- \rightarrow \text{OH} + \text{OH}^-$	1.5×10^9		<i>Søhested et al. (1983)</i>
O 3	$\text{OH} + \text{OH} \rightarrow \text{H}_2\text{O}_2$	5.5×10^9		<i>Buxton et al. (1988)</i>
O 4	$\text{OH} + \text{HO}_2 \rightarrow \text{H}_2\text{O}$	7.1×10^9		<i>Søhested et al. (1968)</i>
O 5	$\text{OH} + \text{O}_2^- \rightarrow \text{OH}^-$	1.0×10^{10}		<i>Søhested et al. (1968)</i>
O 6	$\text{OH} + \text{H}_2\text{O}_2 \rightarrow \text{HO}_2$	2.7×10^7	-1684	<i>Christensen et al. (1982)</i>
O 7	$\text{HO}_2 + \text{HO}_2 \rightarrow \text{H}_2\text{O}_2$	9.7×10^5	-2500	<i>Christensen and Søhested (1988)</i>
O 8	$\text{HO}_2 + \text{O}_2^- \xrightarrow{\text{H}^+} \text{H}_2\text{O}_2$	1.0×10^8	-900	<i>Christensen and Søhested (1988)</i>
N 1	$\text{HONO} + \text{OH} \rightarrow \text{NO}_2$	1.0×10^{10}		assumed = N7 <i>Barker et al. (1970)</i>
N 2	$\text{HONO} + \text{H}_2\text{O}_2 \xrightarrow{\text{H}^+} \text{HNO}_3$	4.6×10^3		<i>Damschen and Martin (1983)</i>
N 3	$\text{NO}_3^- + \text{OH}^- \rightarrow \text{NO}_3^- + \text{OH}$	8.2×10^7	-6800	<i>Eaxner et al. (1992)</i>
N 4	$\text{NO}_2 + \text{NO}_2 \rightarrow \text{HNO}_3 + \text{HONO}$	1.0×10^8	-2700	<i>Lee and Schwartz (1981)</i>
N 5	$\text{NO}_2 + \text{HO}_2 \rightarrow \text{HNO}_4$	1.8×10^9		<i>Warneck (1999)</i>
N 6	$\text{NO}_2^- + \text{O}_3 \rightarrow \text{NO}_3^- + \text{O}_2$	5.0×10^5	-6950	<i>Damschen and Martin (1983)</i>
N 7	$\text{NO}_2^- + \text{OH} \rightarrow \text{NO}_2 + \text{OH}^-$	1.0×10^{10}		<i>Barker et al. (1970)</i>
N 8	$\text{NO}_4^- \rightarrow \text{NO}_2^- + \text{O}_2$	8.0×10^{-1}		<i>Warneck (1999)</i>
C 1	$\text{HCHO} + \text{OH} \rightarrow \text{HCOOH} + \text{HO}_2$	7.7×10^8	-1020	<i>Chin and Wine (1994)</i>
C 2	$\text{HCOOH} + \text{OH} \rightarrow \text{HO}_2 + \text{CO}_2$	1.1×10^8	-991	<i>Chin and Wine (1994)</i>
C 3	$\text{HCOO}^- + \text{OH} \rightarrow \text{OH}^- + \text{HO}_2 + \text{CO}_2$	3.1×10^9	-1240	<i>Chin and Wine (1994)</i>
C 4	$\text{CH}_3\text{OO} + \text{HO}_2 \rightarrow \text{CH}_3\text{OOH}$	4.3×10^5		estimated by <i>Jacob (1986)</i>
C 5	$\text{CH}_3\text{OO} + \text{O}_2^- \rightarrow \text{CH}_3\text{OOH} + \text{OH}^-$	5.0×10^7		estimated by <i>Jacob (1986)</i>
C 6	$\text{CH}_3\text{OH} + \text{OH} \rightarrow \text{HCHO} + \text{HO}_2$	9.7×10^8		<i>Buxton et al. (1988)</i>
C 7	$\text{CH}_3\text{OOH} + \text{OH} \rightarrow \text{CH}_3\text{OO}$	2.7×10^7	-1715	estimated by <i>Jacob (1986)</i>
C 8	$\text{CH}_3\text{OOH} + \text{OH} \rightarrow \text{HCHO} + \text{OH}$	1.1×10^7	-1715	estimated by <i>Jacob (1986)</i>
C 9	$\text{CO}_3^- + \text{O}_2^- \rightarrow \text{HCO}_3^- + \text{OH}^-$	6.5×10^8		<i>Ross et al. (1992)</i>
C 10	$\text{CO}_3^- + \text{H}_2\text{O}_2 \rightarrow \text{HCO}_3^- + \text{HO}_2$	4.3×10^5		<i>Ross et al. (1992)</i>
C 11	$\text{CO}_3^- + \text{HCOO}^- \rightarrow \text{HCO}_3^- + \text{HCO}_3^- + \text{HO}_2$	1.5×10^5		<i>Ross et al. (1992)</i>
C 12	$\text{HCO}_3^- + \text{OH} \rightarrow \text{CO}_3^-$	8.5×10^6		<i>Ross et al. (1992)</i>
C 13	$\text{DOM} + \text{OH} \rightarrow \text{HO}_2$	5.0×10^9		estimated by <i>Anastasio et al. (2003)</i> from <i>Ross et al. (1998)</i>

Table D.3: Continued.

no	reaction	$k_0 [(\text{M}^{1-n})\text{s}^{-1}]$	$-E_a / R [\text{K}]$	reference
S 1	$\text{SO}_3^- + \text{O}_2 \rightarrow \text{SO}_5^-$	1.5×10^9		<i>Huij and Neta (1987)</i>
S 2	$\text{HSO}_3^- + \text{O}_3 \rightarrow \text{SO}_4^{2-} + \text{H}^+ + \text{O}_2$	3.7×10^5	-5500	<i>Hoffmann (1986)</i>
S 3	$\text{SO}_3^{2-} + \text{O}_3 \rightarrow \text{SO}_4^{2-} + \text{O}_2$	1.5×10^9	-5300	<i>Hoffmann (1986)</i>
S 4	$\text{HSO}_3^- + \text{OH} \rightarrow \text{SO}_3^-$	4.5×10^9		<i>Buxton et al. (1988)</i>
S 5	$\text{SO}_3^{2-} + \text{OH} \rightarrow \text{SO}_3^- + \text{OH}^-$	5.5×10^9		<i>Buxton et al. (1988)</i>
S 6	$\text{HSO}_3^- + \text{HO}_2 \rightarrow \text{SO}_4^{2-} + \text{OH} + \text{H}^+$	3.0×10^3		upper limit D. Sedlak pers. comm. with R. Sander
S 7	$\text{HSO}_3^- + \text{O}_2^- \rightarrow \text{SO}_4^{2-} + \text{OH}$	3.0×10^3		upper limit D. Sedlak pers. comm. with R. Sander
S 8	$\text{HSO}_3^- + \text{H}_2\text{O}_2 \rightarrow \text{SO}_4^{2-} + \text{H}^+$	$5.2 \times 10^6 \times \frac{[\text{H}^+]}{[\text{H}^+] + 0.1\text{M}}$	-3650	<i>Damschen and Martin (1983)</i>
S 9	$\text{HSO}_3^- + \text{NO}_2 \xrightarrow{\text{NO}_2} \text{HSO}_4^- + \text{HONO} + \text{HONO}$	2.0×10^7		<i>Clifton et al. (1988)</i>
S 10	$\text{SO}_3^{2-} + \text{NO}_2 \xrightarrow{\text{NO}_2} \text{SO}_4^{2-} + \text{HONO} + \text{HONO}$	2.0×10^7		<i>Clifton et al. (1988)</i>
S 11	$\text{HSO}_3^- + \text{NO}_3 \rightarrow \text{SO}_3^- + \text{NO}_3^- + \text{H}^+$	1.4×10^9	-2000	<i>Exner et al. (1992)</i>
S 12	$\text{HSO}_3^- + \text{HNO}_4 \rightarrow \text{HSO}_4^- + \text{NO}_3^- + \text{H}^+$	3.1×10^5		<i>Warneck (1999)</i>
S 13	$\text{HSO}_3^- + \text{CH}_3\text{OOH} \xrightarrow{\text{H}^+} \text{SO}_4^{2-} + \text{H}^+ + \text{CH}_3\text{OH}$	1.6×10^7	-3800	<i>Lind et al. (1987)</i>
S 14	$\text{SO}_3^{2-} + \text{CH}_3\text{OOH} \xrightarrow{\text{H}^+} \text{SO}_4^{2-} + \text{CH}_3\text{OH}$	1.6×10^7	-3800	<i>Lind et al. (1987)</i>
S 15	$\text{HSO}_3^- + \text{HCHO} \rightarrow \text{CH}_2\text{OHHSO}_3^-$	4.3×10^{-1}		<i>Boyce and Hoffmann (1984)</i>
S 16	$\text{SO}_3^{2-} + \text{HCHO} \xrightarrow{\text{H}^+} \text{CH}_2\text{OHHSO}_3^-$	1.4×10^4		<i>Boyce and Hoffmann (1984)</i>
S 17	$\text{CH}_2\text{OHHSO}_3^- + \text{OH}^- \rightarrow \text{SO}_3^{2-} + \text{HCHO}$	3.6×10^3		<i>Seinfeld and Pandis (1998)</i>
S 18	$\text{HSO}_3^- + \text{HSO}_5^- \xrightarrow{\text{H}^+} \text{SO}_4^{2-} + \text{SO}_4^{2-} + \text{H}^+ + \text{H}^+$	7.1×10^6		<i>Betterton and Hoffmann (1988)</i>
S 19	$\text{SO}_4^- + \text{OH} \rightarrow \text{HSO}_5^-$	1.0×10^9		<i>Jiang et al. (1992)</i>
S 20	$\text{SO}_4^- + \text{HO}_2 \rightarrow \text{SO}_4^{2-} + \text{H}^+$	3.5×10^9		<i>Jiang et al. (1992)</i>
S 21	$\text{SO}_4^- + \text{O}_2^- \rightarrow \text{SO}_4^{2-}$	3.5×10^9		assumed =S20
S 22	$\text{SO}_4^- + \text{H}_2\text{O} \rightarrow \text{SO}_4^{2-} + \text{H}^+ + \text{OH}$	1.1×10^1	-1110	<i>Herrmann et al. (1995)</i>
S 23	$\text{SO}_4^- + \text{H}_2\text{O}_2 \rightarrow \text{SO}_4^{2-} + \text{H}^+ + \text{HO}_2$	1.2×10^7		<i>Wine et al. (1989)</i>
S 24	$\text{SO}_4^- + \text{NO}_3^- \rightarrow \text{SO}_4^{2-} + \text{NO}_3^- + \text{NO}_3^- + \text{H}^+$	5.0×10^4		<i>Exner et al. (1992)</i>
S 25	$\text{SO}_4^- + \text{HSO}_3^- \rightarrow \text{SO}_3^- + \text{SO}_4^{2-} + \text{H}^+$	8.0×10^8		<i>Huij and Neta (1987)</i>
S 26	$\text{SO}_4^- + \text{SO}_3^- \rightarrow \text{SO}_3^- + \text{SO}_4^{2-}$	4.6×10^8		<i>Huij and Neta (1987)</i>

Table D.3: Continued.

no	reaction	k_0 [$(\text{M}^{1-n})\text{s}^{-1}$]	$-E_a / R$ [K]	reference
S 27	$\text{SO}_4^{2-} + \text{NO}_3^- \rightarrow \text{NO}_3^- + \text{SO}_4^-$	1.0×10^5		<i>Logager et al.</i> (1993)
S 28	$\text{SO}_5^- + \text{HSO}_3^- \rightarrow \text{SO}_4^- + \text{SO}_4^{2-} + \text{H}^+$	7.5×10^4		<i>Huie and Neta</i> (1987)
S 29	$\text{SO}_5^- + \text{SO}_3^{2-} \rightarrow \text{SO}_4^- + \text{SO}_4^{2-}$	9.4×10^6		<i>Huie and Neta</i> (1987); <i>Deister and Warneck</i> (1990)
S 30	$\text{SO}_5^- + \text{HSO}_3^- \rightarrow \text{SO}_3^- + \text{HSO}_5^-$	2.5×10^4		<i>Huie and Neta</i> (1987); <i>Deister and Warneck</i> (1990)
S 31	$\text{SO}_5^- + \text{SO}_3^{2-} \xrightarrow{\text{H}^+} \text{SO}_3^- + \text{HSO}_5^-$	3.6×10^6		<i>Buxton et al.</i> (1996)
S 32	$\text{SO}_5^- + \text{O}_2^- \xrightarrow{\text{H}^+} \text{HSO}_5^- + \text{O}_2$	2.3×10^8		<i>Ross et al.</i> (1992)
S 33	$\text{SO}_5^- + \text{SO}_5^- \rightarrow \text{H}_2\text{O}$	1.0×10^8		<i>Gershenson et al.</i> (2001)
S 34	$\text{DMS} + \text{O}_3 \rightarrow \text{O}_2 + \text{DMSO}$	8.6×10^8		<i>Ross et al.</i> (1998)
S 35	$\text{DMS} + \text{OH} \rightarrow 0.5 \text{ CH}_3\text{SO}_3^- + 0.5 \text{ CH}_3\text{OO} + 0.5 \text{ HSO}_4^- + \text{HCHO} + \text{H}^+$	1.9×10^{10}		<i>Bardouki et al.</i> (2002)
S 36	$\text{DMSO} + \text{OH} \rightarrow \text{CH}_3\text{SO}_2^- + \text{CH}_3\text{OO} + \text{H}^+$	4.5×10^9		<i>Bardouki et al.</i> (2002)
S 37	$\text{CH}_3\text{SO}_2^- + \text{OH} \rightarrow \text{CH}_3\text{SO}_3^- + \text{H}_2\text{O} - \text{O}_2$	1.2×10^{10}		<i>Bardouki et al.</i> (2002)
S 38	$\text{CH}_3\text{SO}_3^- + \text{OH} \rightarrow \text{SO}_4^{2-} + \text{H}^+ + \text{CH}_3\text{OO}$	1.2×10^7		<i>Bonsang et al.</i> (1991)
Cl 1	$\text{Cl} + \text{H}_2\text{O}_2 \rightarrow \text{HO}_2 + \text{Cl}^- + \text{H}^+$	2.0×10^9		<i>Yu</i> (2001)
Cl 2	$\text{Cl} + \text{H}_2\text{O} \rightarrow \text{H}^+ + \text{ClOH}^-$	1.8×10^5		<i>Yu</i> (2001)
Cl 3	$\text{Cl} + \text{NO}_3^- \rightarrow \text{NO}_3 + \text{Cl}^-$	1.0×10^8		<i>Buxton et al.</i> (1999b)
Cl 4	$\text{Cl} + \text{DOM} \rightarrow \text{Cl}^- + \text{HO}_2$	5.0×10^9		estimated by <i>Anastasio et al.</i> (2003) from <i>Ross et al.</i> (1998)
Cl 5	$\text{Cl} + \text{SO}_4^{2-} \rightarrow \text{SO}_4^- + \text{Cl}^-$	2.1×10^8		<i>Buxton et al.</i> (1999a)
Cl 6	$\text{Cl} + \text{Cl} \rightarrow \text{Cl}_2$	8.8×10^7		<i>Wu et al.</i> (1980)
Cl 7	$\text{Cl}^- + \text{OH} \rightarrow \text{ClOH}^-$	4.2×10^9		<i>Yu</i> (2001)
Cl 8	$\text{Cl}^- + \text{O}_3 \rightarrow \text{ClO}^- + \text{O}_2$	3.0×10^{-3}		<i>Hoigné et al.</i> (1985)
Cl 9	$\text{Cl}^- + \text{NO}_3 \rightarrow \text{NO}_3^- + \text{Cl}$	9.3×10^6		<i>Exner et al.</i> (1992)
Cl 10	$\text{Cl}^- + \text{SO}_4^{2-} \rightarrow \text{SO}_4^{2-} + \text{Cl}$	2.5×10^8		<i>Buxton et al.</i> (1999a)
Cl 11	$\text{Cl}^- + \text{HSO}_5^- \rightarrow \text{HOCl} + \text{SO}_4^{2-}$	1.8×10^{-3}		<i>Forthnum et al.</i> (1960)
Cl 12	$\text{Cl}^- + \text{HOCl} + \text{H}^+ \rightarrow \text{Cl}_2$	2.2×10^4		<i>Ayers et al.</i> (1996)
Cl 13	$\text{Cl}_2 \rightarrow \text{Cl}^- + \text{HOCl} + \text{H}^+$	2.2×10^1		<i>Ayers et al.</i> (1996)
Cl 14	$\text{Cl}_2^- + \text{OH} \rightarrow \text{HOCl} + \text{Cl}^-$	1.0×10^9		<i>Ross et al.</i> (1998)
Cl 15	$\text{Cl}_2^- + \text{OH}^- \rightarrow \text{Cl}^- + \text{Cl}^- + \text{OH}$	4.0×10^6		<i>Jacobi</i> (1996)

Table D.3: Continued.

no	reaction	$k_0 [(\text{M}^{1-n})\text{s}^{-1}]$	$-E_a / R [\text{K}]$	reference
Cl 16	$\text{Cl}_2^- + \text{HO}_2 \rightarrow \text{Cl}^- + \text{H}^+ + \text{O}_2$	3.1×10^9 6.0×10^9		Yu (2001) $Jacobi$ (1996)
Cl 17	$\text{Cl}_2^- + \text{O}_2^- \rightarrow \text{Cl}^- + \text{Cl}^- + \text{O}_2$	7.0×10^5	-3340	$Jacobi$ (1996)
Cl 18	$\text{Cl}_2^- + \text{H}_2\text{O}_2 \rightarrow \text{Cl}^- + \text{Cl}^- + \text{H}^+ + \text{HO}_2$	6.0×10^7	-3340	$Jacobi$ (1996) assumed by $Jacobi$ (1996)
Cl 19	$\text{Cl}_2^- + \text{NO}_2^- \rightarrow \text{Cl}^- + \text{Cl}^- + \text{NO}_2$	7.0×10^5		estimated by $Anastasio$ et al. (2003) from $Ross$ et al. (1998)
Cl 20	$\text{Cl}_2^- + \text{CH}_3\text{OOH} \rightarrow \text{Cl}^- + \text{Cl}^- + \text{H}^+ + \text{CH}_3\text{OO}$	1.0×10^6		$Jacobi$ et al. (1996)
Cl 21	$\text{Cl}_2^- + \text{DOM} \rightarrow \text{Cl}^- + \text{Cl}^- + \text{HO}_2$		-1082	$Shoute$ et al. (1991)
Cl 22	$\text{Cl}_2^- + \text{HSO}_3^- \rightarrow \text{SO}_3^- + \text{Cl}^- + \text{Cl}^- + \text{H}^+$	4.7×10^8		$Jacobi$ et al. (1996)
Cl 23	$\text{Cl}_2^- + \text{SO}_3^{2-} \rightarrow \text{SO}_3^- + \text{Cl}^- + \text{Cl}^-$	6.2×10^7		Yu (2001)
Cl 24	$\text{Cl}_2^- + \text{Cl}_2^- \rightarrow \text{Cl}_2 + 2\text{Cl}^-$	6.2×10^9		Yu (2001)
Cl 25	$\text{Cl}_2^- + \text{Cl} \rightarrow \text{Cl}^- + \text{Cl}_2$	2.7×10^9		Yu (2001)
Cl 26	$\text{Cl}_2^- + \text{DMS} \rightarrow 0.5 \text{ CH}_3\text{SO}_3^- + 0.5 \text{ CH}_3\text{OO} + 0.5 \text{ HSO}_4^- + \text{HCHO} + 2\text{ Cl}^- + 2\text{ H}^+$	3.0×10^9		rate from $Ross$ et al. (1998)
Cl 27	$\text{ClOH}^- \rightarrow \text{Cl}^- + \text{OH}$	6.0×10^9		Yu (2001)
Cl 28	$\text{ClOH}^- + \text{H}^+ \rightarrow \text{Cl}$	4.0×10^{10}		Yu (2001)
Cl 29	$\text{HOCl} + \text{HO}_2 \rightarrow \text{Cl} + \text{O}_2$	7.5×10^6		assumed = Cl30 $Keppler$ et al. (2003)
Cl 30	$\text{HOCl} + \text{O}_2^- \rightarrow \text{Cl} + \text{OH}^- + \text{O}_2$	7.5×10^6		$Keppler$ et al. (2003)
Cl 31	$\text{HOCl} + \text{SO}_3^{2-} \rightarrow \text{Cl}^- + \text{HSO}_4^-$	7.6×10^8		$Fogelman$ et al. (1989)
Cl 32	$\text{HOCl} + \text{HSO}_3^- \rightarrow \text{Cl}^- + \text{HSO}_4^- + \text{H}^+$	7.6×10^8		assumed = Cl31 $Fogelman$ et al. (1989)
Cl 33	$\text{Cl}_2 + \text{HO}_2 \rightarrow \text{Cl}_2^- + \text{H}^+ + \text{O}_2$	1.0×10^9		$Bjergbakke$ et al. (1981)
Cl 34	$\text{Cl}_2 + \text{O}_2^- \rightarrow \text{Cl}_2^- + \text{O}_2$	1.0×10^9		assumed = Cl33 $Bjergbakke$ et al. (1981)
Br 1	$\text{Br} + \text{OH}^- \rightarrow \text{BrOH}^-$	1.3×10^{10}		$Zehavi$ and $Rabani$ (1972)
Br 2	$\text{Br} + \text{DOM} \rightarrow \text{Br}^- + \text{HO}_2$	2.0×10^8		estimated by $Anastasio$ et al. (2003) from $Ross$ et al. (1998)
Br 3	$\text{Br}^- + \text{OH} \rightarrow \text{BrOH}^-$	1.1×10^{10}		$Zehavi$ and $Rabani$ (1972)
Br 4	$\text{Br}^- + \text{O}_3 \rightarrow \text{BrO}^-$	2.1×10^2	-4450	$Haag$ and $Hoigné$ (1983)
Br 5	$\text{Br}^- + \text{NO}_3 \rightarrow \text{Br} + \text{NO}_3^-$	3.8×10^9		Zelner et al. 1996 in $Herrmann$ et al. (2000)
Br 6	$\text{Br}^- + \text{SO}_4^- \rightarrow \text{Br} + \text{SO}_4^{2-}$	2.1×10^9		$Jacobi$ (1996)
Br 7	$\text{Br}^- + \text{HSO}_5^- \rightarrow \text{HOBr} + \text{SO}_4^{2-}$	1.0		$Fortnum$ et al. (1960)
Br 8	$\text{Br}^- + \text{HOBr} + \text{H}^+ \rightarrow \text{Br}_2$	1.6×10^{10}		Liu and $Margerum$ (2001)

Table D.3: Continued.

no	reaction	k_0 [$(\text{M}^{1-n})\text{s}^{-1}$]	$-E_a / R$ [K]	reference
Br 9	$\text{Br}_2 \rightarrow \text{Br}^- + \text{HOBr} + \text{H}^+$	9.7×10^1	7457	<i>Liu and Margerum</i> (2001)
Br 10	$\text{Br}_2^- + \text{O}_2^- \rightarrow \text{Br}^- + \text{Br}^-$	1.7×10^8		<i>Wagner and Strehlow</i> (1987)
Br 11	$\text{Br}_2^- + \text{HO}_2 \rightarrow \text{Br}_2 + \text{H}_2\text{O}_2 - \text{H}^+$	4.4×10^9		<i>Matthew et al.</i> (2003)
Br 12	$\text{Br}_2^- + \text{H}_2\text{O}_2 \rightarrow \text{Br}^- + \text{Br}^- + \text{H}^+ + \text{HO}_2$	5.0×10^2		<i>Chameides and Stelson</i> (1992)
Br 13	$\text{Br}_2^- + \text{Br}_2^- \rightarrow \text{Br}^- + \text{Br}^- + \text{Br}_2$	1.9×10^9		<i>Ross et al.</i> (1992)
Br 14	$\text{Br}_2^- + \text{CH}_3\text{OOH} \rightarrow \text{Br}^- + \text{Br}^- + \text{H}^+ + \text{CH}_3\text{OO}$	1.0×10^5		assumed by <i>Jacobi</i> (1996)
Br 15	$\text{Br}_2^- + \text{DOM} \rightarrow \text{Br}^- + \text{Br}^- + \text{HO}_2$	1.0×10^5		estimated by <i>Anastasio et al.</i> (2003) from <i>Ross et al.</i> (1998)
Br 16	$\text{Br}_2^- + \text{NO}_2^- \rightarrow \text{Br}^- + \text{Br}^- + \text{NO}_2$	1.7×10^7	-1720	<i>Shoute et al.</i> (1991)
Br 17	$\text{Br}_2^- + \text{HSO}_3^- \rightarrow \text{Br}^- + \text{Br}^- + \text{H}^+ + \text{SO}_3^-$	6.3×10^7	-782	<i>Shoute et al.</i> (1991)
Br 18	$\text{Br}_2^- + \text{SO}_3^{2-} \rightarrow \text{Br}^- + \text{Br}^- + \text{SO}_3^-$	2.2×10^8	-650	<i>Shoute et al.</i> (1991)
Br 19	$\text{Br}_2^- + \text{DMS} \rightarrow 0.5 \text{ CH}_3\text{SO}_3^- + 0.5 \text{ CH}_3\text{OO} + 0.5 \text{ HSO}_4^- + \text{HCHO} + 2 \text{ Br}^- + 2 \text{ H}^+$	3.2×10^9		rate from <i>Ross et al.</i> (1998)
Br 20	$\text{BrOH}^- \rightarrow \text{Br}^- + \text{OH}^-$	3.3×10^7		<i>Zehavi and Rabani</i> (1972)
Br 21	$\text{BrOH}^- \rightarrow \text{Br} + \text{OH}^-$	4.2×10^6		<i>Zehavi and Rabani</i> (1972)
Br 22	$\text{BrOH}^- + \text{H}^+ \rightarrow \text{Br}$	4.4×10^{10}		<i>Zehavi and Rabani</i> (1972)
Br 23	$\text{BrOH}^- + \text{Br}^- \rightarrow \text{Br}_2^- + \text{OH}^-$	1.9×10^8		<i>Zehavi and Rabani</i> (1972)
Br 24	$\text{BrO}^- + \text{SO}_3^{2-} \rightarrow \text{Br}^- + \text{SO}_4^{2-}$	1.0×10^8		<i>Troy and Margerum</i> (1991)
Br 25	$\text{HOBr} + \text{HO}_2 \rightarrow \text{Br} + \text{O}_2$	1.0×10^9		<i>Herrmann et al.</i> (1999)
Br 26	$\text{HOBr} + \text{O}_2^- \rightarrow \text{Br} + \text{OH}^- + \text{O}_2$	3.5×10^9		<i>Schwarz and Bielski</i> (1986)
Br 27	$\text{HOBr} + \text{H}_2\text{O}_2 \rightarrow \text{Br}^- + \text{H}^+ + \text{O}_2$	1.2×10^6		<i>von Gunten and Oliveras</i> (1998)
Br 28	$\text{HOBr} + \text{SO}_3^{2-} \rightarrow \text{Br}^- + \text{HSO}_4^-$	5.0×10^9		<i>Troy and Margerum</i> (1991)
Br 29	$\text{HOBr} + \text{HSO}_3^- \rightarrow \text{Br}^- + \text{HSO}_4^- + \text{H}^+$	5.0×10^9		assumed = Br28
Br 30	$\text{Br}_2 + \text{HO}_2 \rightarrow \text{Br}_2^- + \text{H}^+ + \text{O}_2$	1.1×10^8		<i>Ross et al.</i> (1998)
Br 31	$\text{Br}_2 + \text{O}_2^- \rightarrow \text{Br}_2^- + \text{O}_2$	5.6×10^9		<i>Liu and Margerum</i> (2001)
Hx 1	$\text{Br}^- + \text{HOCl} + \text{H}^+ \rightarrow \text{BrCl}$	1.3×10^6		<i>Liu and Margerum</i> (2001)
Hx 2	$\text{Cl}^- + \text{HOBr} + \text{H}^+ \rightarrow \text{BrCl}$	2.3×10^{10}		<i>Liu and Margerum</i> (2001)
Hx 3	$\text{BrCl} \rightarrow \text{Cl}^- + \text{HOBr} + \text{H}^+$	3.0×10^6		<i>Liu and Margerum</i> (2001)
Hx 4	$\text{Br}^- + \text{ClO}^- + \text{H}^+ \rightarrow \text{BrCl} + \text{OH}^-$	3.7×10^{10}		<i>Kumar and Margerum</i> (1987)
Hx 5	$\text{Cl}_2 + \text{Br}^- \rightarrow \text{BrCl}_2^-$	7.7×10^9		<i>Liu and Margerum</i> (2001)
Hx 6	$\text{BrCl}_2^- \rightarrow \text{Cl}_2 + \text{Br}^-$	1.83×10^3		<i>Liu and Margerum</i> (2001)

Table D.3: Continued.

no	reaction	k_0 [$(\text{M}^{1-n})\text{s}^{-1}$]	$-E_a / R$ [K]	reference
hv 1	$\text{O}_3 + \text{hv} \rightarrow \text{OH} + \text{OH} + \text{O}_2$			assumed 2x gas phase
hv 2	$\text{H}_2\text{O}_2 + \text{hv} \rightarrow \text{OH} + \text{OH}$			assumed 2x gas phase
hv 3	$\text{NO}_3^- + \text{hv} \xrightarrow{\text{H}^+} \text{NO}_2 + \text{OH}$			Zellner <i>et al.</i> (1990)
hv 4	$\text{NO}_2^- + \text{hv} \xrightarrow{\text{H}^+} \text{NO} + \text{OH}$			Zellner <i>et al.</i> (1990); Burley and John-ston (1992)
hv 5	$\text{HOCl} + \text{hv} \rightarrow \text{OH} + \text{Cl}$			assumed 2x gas phase
hv 6	$\text{Cl}_2 + \text{hv} \rightarrow \text{Cl} + \text{Cl}$			assumed 2x gas phase
hv 7	$\text{HOBr} + \text{hv} \rightarrow \text{OH} + \text{Br}$			assumed 2x gas phase
hv 8	$\text{Br}_2 + \text{hv} \rightarrow \text{Br} + \text{Br}$			assumed 2x gas phase
hv 9	$\text{BrCl} + \text{hv} \rightarrow \text{Cl} + \text{Br}$			assumed 2x gas phase

n is the order of the reaction. 1 photolysis rates calculated online. The temperature dependence is $k = k_0 \times \exp(-E_a(\frac{1}{T} - \frac{1}{T_0}))$, $T_0 = 298$ K.

Table D.4: Heterogeneous reactions.

no	reaction	k	reference
H1	$\text{N}_2\text{O}_5 \xrightarrow{\text{H}_2\text{O}} \text{HNO}_{3aq} + \text{HNO}_{3aq}$	$\overline{k}_t(\text{N}_2\text{O}_5)w_{l,i}[\text{H}_2\text{O}]/\text{Het}_T$	Behnke <i>et al.</i> (1994), Behnke <i>et al.</i> (1997)
H2	$\text{N}_2\text{O}_5 \xrightarrow{\text{Cl}^-} \text{ClNO}_2 + \text{NO}_3^-$	$\overline{k}_t(\text{N}_2\text{O}_5)w_{l,i}f(\text{Cl}^-)/\text{Het}_T$	Behnke <i>et al.</i> (1994), Behnke <i>et al.</i> (1997)
H3	$\text{N}_2\text{O}_5 \xrightarrow{\text{Br}^-} \text{BrNO}_2 + \text{NO}_3^-$	$\overline{k}_t(\text{N}_2\text{O}_5)w_{l,i}f(\text{Br}^-)/\text{Het}_T$	Behnke <i>et al.</i> (1994), Behnke <i>et al.</i> (1997)
H4	$\text{ClNO}_3 \xrightarrow{\text{H}_2\text{O}} \text{HOCl}_{aq} + \text{HNO}_{3aq}$	$\overline{k}_t(\text{ClNO}_3)w_{l,i}[\text{H}_2\text{O}]/\text{Het}_T$	see note
H5	$\text{ClNO}_3 \xrightarrow{\text{Cl}^-} \text{Cl}_{2aq} + \text{NO}_3^-$	$\overline{k}_t(\text{ClNO}_3)w_{l,i}f(\text{Cl}^-)/\text{Het}_T$	see note
H6	$\text{ClNO}_3 \xrightarrow{\text{Br}^-} \text{BrCl}_{aq} + \text{NO}_3^-$	$\overline{k}_t(\text{ClNO}_3)w_{l,i}f(\text{Br}^-)/\text{Het}_T$	see note
H7	$\text{BrNO}_3 \xrightarrow{\text{H}_2\text{O}} \text{HOBr}_{aq} + \text{HNO}_{3aq}$	$\overline{k}_t(\text{BrNO}_3)w_{l,i}[\text{H}_2\text{O}]/\text{Het}_T$	see note
H8	$\text{BrNO}_3 \xrightarrow{\text{Cl}^-} \text{BrCl}_{aq} + \text{NO}_3^-$	$\overline{k}_t(\text{BrNO}_3)w_{l,i}f(\text{Cl}^-)/\text{Het}_T$	see note
H9	$\text{BrNO}_3 \xrightarrow{\text{Br}^-} \text{Br}_{2aq} + \text{NO}_3^-$	$\overline{k}_t(\text{BrNO}_3)w_{l,i}f(\text{Br}^-)/\text{Het}_T$	see note

For a definition of \overline{k}_t and $w_{l,i}$ see von Glasow *et al.* (2002a) or von Glasow (2001). $\text{Het}_T = [\text{H}_2\text{O} + f(\text{Cl}^-)[\text{Cl}^-] + f(\text{Br}^-)[\text{Br}^-]$, with $f(\text{Cl}^-) = 5.0 \times 10^2$ and $f(\text{Br}^-) = 3.0 \times 10^5$. H4 - H9: the total rate is determined by \overline{k}_t , the distribution among the different reaction paths was assumed to be the same as for reactions H1 - H3.

Table D.5: Aqueous phase equilibrium constants.

no	reaction	m	n	$K_0 [M^{n-m}]$	$-\Delta H/R [K]$	reference
EQ1	$\text{CO}_{2aq} \longleftrightarrow \text{H}^+ + \text{HCO}_3^-$	1	2	4.3×10^{-7}	-913	Chameides (1984)
EQ2	$\text{NH}_{3aq} \longleftrightarrow \text{OH}^- + \text{NH}_4^+$	1	2	1.7×10^{-5}	-4325	Chameides (1984)
EQ3	$\text{H}_2\text{O}_{aq} \longleftrightarrow \text{H}^+ + \text{OH}^-$	1	2	1.0×10^{-14}	-6716	Chameides (1984)
EQ4	$\text{HCOOH}_{aq} \longleftrightarrow \text{H}^+ + \text{HCOO}^-$	1	2	1.8×10^{-4}	Weast (1980)	
EQ5	$\text{HSO}_3^- \longleftrightarrow \text{H}^+ + \text{SO}_3^{2-}$	1	2	6.0×10^{-8}	1120	Chameides (1984)
EQ6	$\text{H}_2\text{SO}_{4aq} \longleftrightarrow \text{H}^+ + \text{HSO}_4^-$	1	2	1.0×10^3	Seinfeld and Pandis (1998)	
EQ7	$\text{HSO}_4^- \longleftrightarrow \text{H}^+ + \text{SO}_4^{2-}$	1	2	1.2×10^{-2}	Weast (1980)	
EQ8	$\text{HO}_{2aq} \longleftrightarrow \text{O}_2^- + \text{H}^+$	1	2	1.6×10^{-5}	Weinstein-Lloyd and Schwartz (1991)	
EQ9	$\text{SO}_{2aq} \longleftrightarrow \text{H}^+ + \text{HSO}_3^-$	1	2	1.7×10^{-2}	Chameides (1984)	
EQ10	$\text{Cl}_2^- \longleftrightarrow \text{Cl}_{aq} + \text{Cl}^-$	1	2	5.2×10^{-6}	Jayson et al. (1973)	
EQ11	$\text{HOCl}_{aq} \longleftrightarrow \text{H}^+ + \text{ClO}^-$	1	2	3.2×10^{-8}	Lax (1969)	
EQ12	$\text{HBr}_{aq} \longleftrightarrow \text{H}^+ + \text{Br}^-$	1	2	1.0×10^9	Lax (1969)	
EQ13	$\text{Br}_2^- \longleftrightarrow \text{Br}_{aq} + \text{Br}^-$	1	2	9.1×10^{-6}	Mamou et al. (1977)	
EQ14	$\text{HOBr}_{aq} \longleftrightarrow \text{H}^+ + \text{BrO}^-$	1	2	2.3×10^{-9}	Kelley and Tartar (1956)	
EQ15	$\text{BrCl}_{aq} + \text{Cl}^- \longleftrightarrow \text{BrCl}_2^-$	2	1	3.8	Wang et al. (1994)	
EQ16	$\text{BrCl}_{aq} + \text{Br}^- \longleftrightarrow \text{Br}_2\text{Cl}^-$	2	1	1.8×10^4	Wang et al. (1994)	
EQ17	$\text{Br}_2\text{aq} + \text{Cl}^- \longleftrightarrow \text{Br}_2\text{Cl}^-$	2	1	1.3	Wang et al. (1994)	
EQ18	$\text{HNO}_{3aq} \longleftrightarrow \text{H}^+ + \text{NO}_3^-$	1	2	1.5×10^1	Davis and de Bruin (1964)	
EQ19	$\text{HCl}_{aq} \longleftrightarrow \text{H}^+ + \text{Cl}^-$	1	2	1.7×10^6	Marsh and McElroy (1985)	
EQ20	$\text{HONO}_{aq} \longleftrightarrow \text{H}^+ + \text{NO}_2^-$	1	2	5.1×10^{-4}	Schwarz and White (1981)	
EQ21	$\text{HNO}_{4aq} \longleftrightarrow \text{NO}_4^- + \text{H}^+$	1	2	1.0×10^{-5}	Warneck (1999)	

The temperature dependence is $K = K_0 \times \exp(-\frac{\Delta H}{R}(\frac{1}{T} - \frac{1}{T_0}))$, $T_0 = 298$ K.

Table D.6: Henry constants and accommodation coefficients.

specie	K_H^0 [M/atm]	$-\Delta_{soln}H/R$ [K]	reference	α^0	$-\Delta_{obs}H/R$ [K]	reference
O ₃	1.2×10^{-2}	2560	Chameides (1984)	0.002	(at 292 K)	DeMore <i>et al.</i> (1997)
O ₂	1.3×10^{-3}	1500	Wilhelm <i>et al.</i> (1977)	0.01	2000	estimated
OH	3.0×10^1	4300	Hanson <i>et al.</i> (1992)	0.01	(at 293 K)	Takami <i>et al.</i> (1998)
HO ₂	3.9×10^3	5900	Hanson <i>et al.</i> (1992)	0.2	(at 293 K)	DeMore <i>et al.</i> (1997)
H ₂ O ₂	1.0×10^5	6338	Lind and Kok (1984)	0.077	2769	Worsnop <i>et al.</i> (1989)
NO ₂	6.4×10^{-3}	2500	Lelieveld and Crutzen (1991)	0.0015	(at 298 K)	Ponche <i>et al.</i> (1993)
NO ₃	2.0	2000	Thomas <i>et al.</i> (1993)	0.04	(at 273? K)	Rudich <i>et al.</i> (1996)
N ₂ O ₅	∞	—	—	0.1	(at 195-300 K)	DeMore <i>et al.</i> (1997)
HONO	4.9×10^1	4780	Schwartz and White (1981)	0.04	(at 247-297 K)	DeMore <i>et al.</i> (1997)
HNO ₃	1.7×10^5	8694	Lelieveld and Crutzen (1991)	0.5	(at RT)	Abbatt and Waschewsky (1998)
HNO ₄	1.2×10^4	6900	Régimbald and Mozurkewich (1997)	0.1	(at 200 K)	DeMore <i>et al.</i> (1997)
NH ₃	5.8×10^1	4085	Chameides (1984)	0.06	(at 295 K)	DeMore <i>et al.</i> (1997)
CH ₃ OO	6.0	=HO ₂	Pandis and Seinfeld (1989)	0.01	2000	estimated
ROOH	3.0×10^2	5322	Lind and Kok (1994)	0.0046	3273	Magi <i>et al.</i> (1997)
HCHO	7.0×10^3	6425	Chameides (1984)	0.04	(at 260-270 K)	DeMore <i>et al.</i> (1997)
HCOOH	3.7×10^3	5700	Chameides (1984)	0.014	3978	DeMore <i>et al.</i> (1997)
CO ₂	3.1×10^{-2}	2423	Chameides (1984)	0.01	2000	estimated
HCl	1.2	9001	Brimblecombe and Clegg (1989)	0.074	3072	Schweitzer <i>et al.</i> (2000)
HOCl	6.7×10^2	5862	Huthwelker <i>et al.</i> (1995)	=HOBr	=HOBr	estimated
ClNO ₃	∞	—	—	0.1	(at RT)	Koch and Rossi (1998)
Cl ₂	9.1×10^{-2}	2500	Wilhelm <i>et al.</i> (1977)	0.038	6546	Hu <i>et al.</i> (1995)
HBr	1.3	10239	Brimblecombe and Clegg (1989)	0.031	3940	Schweitzer <i>et al.</i> (2000)
HOBr	9.3×10^1	=HOCl	Vogt <i>et al.</i> (1996)	0.5	(at RT)	Abbatt and Waschewsky (1998)
BrNO ₃	∞	—	Dean (1992)	0.8	0	Hanson <i>et al.</i> (1996)
Br ₂	7.6×10^{-1}	4094	Bartlett and Margerum (1999)	0.038	6546	Hu <i>et al.</i> (1995)
BrCl	9.4×10^{-1}	5600	=Cl ₂	=Cl ₂	estimated	De Bruyn <i>et al.</i> (1994)
DMSO	5.0×10^4	=HCHO	De Bruyn <i>et al.</i> (1994)	0.048	2578	De Bruyn <i>et al.</i> (1994)
DMSO ₂	∞	—	assumed	0.03	5388	DeMore <i>et al.</i> (1997)
SO ₂	1.2	3120	Chameides (1984)	0.11	0	Pöschl <i>et al.</i> (1998)
H ₂ SO ₄	∞	—	assumed	0.65	(at 303 K)	Lucas and Prinn (2002)
CH ₃ SO ₂ H	∞	—	assumed	0.0002	0	De Bruyn <i>et al.</i> (1994)
CH ₃ SO ₃ H	∞	—	assumed	0.076	1762	De Bruyn <i>et al.</i> (1994)

For ROOH the values of CH₃OOH have been assumed. The temperature dependence is for the Henry constants is $K_H = K_H^0 \times \exp(-\frac{-\Delta_{soln}H}{R}(\frac{1}{T} - \frac{1}{T_0}))$, $T_0 = 298$ K and for the accommodation coefficients $d\ln(\frac{\alpha}{1-\alpha})/d(\frac{1}{T}) = -\frac{\Delta_{obs}H}{R}$. RT stands for “room temperature”.

D.1 Iodine chemistry

The following tables list the deactivated iodine chemistry. The tables are sorted in the same order as above. Before iodine chemistry is used again it has to be updated. The following mechanism is based on *Vogt et al.* (1999) with the addition as described in *von Glasow et al.* (2002a).

Table D.7: Species

Gas phase
I, IO, OIO, HI, HOI, I ₂ O ₂ , INO ₂ , INO ₃ , I ₂ , ICl, IBr, CH ₃ I, CH ₂ I ₂ , CH ₂ ClI, C ₃ H ₇ I, HIO ₃
Liquid phase
IO, HI, HOI, I ₂ , ICl, IBr
Ions
I ⁻ , IO ₂ ⁻ , IO ₃ ⁻ , ICl ₂ ⁻ , IBr ₂ ⁻ , IClBr ⁻

Table D.8: Gas phase reactions.

no	reaction	n	$A [(\text{cm}^{-3})^{1-n} \text{s}^{-1}]$	$-E_a / R [\text{K}]$	reference
I1	$\text{I} + \text{O}_3 \rightarrow \text{IO} + \text{O}_2$	2	2.3×10^{-11}	-870	DeMore <i>et al.</i> (1997)
I2	$\text{I} + \text{HO}_2 \rightarrow \text{HI} + \text{O}_2$	2	1.5×10^{-11}	-1090	DeMore <i>et al.</i> (1997)
I3	$\text{I} + \text{BrO} \rightarrow \text{IO} + \text{Br}$	2	1.2×10^{-11}		DeMore <i>et al.</i> (1997)
I4	$\text{I} + \text{NO}_2 \xrightarrow{\text{M}} \text{INO}_2$	2			DeMore <i>et al.</i> (1997)
I5	$\text{I} + \text{NO}_3 \rightarrow \text{IO} + \text{NO}_2$	2	4.5×10^{-10}		Chambers <i>et al.</i> (1992)
I6	$\text{HI} + \text{OH} \rightarrow \text{I} + \text{H}_2\text{O}$	2	3.0×10^{-11}		Campuzano-Jost and Crowley (1999)
I7	$\text{IO} + \text{HO}_2 \rightarrow \text{HOI} + \text{O}_2$	2	8.4×10^{-11}		DeMore <i>et al.</i> (1997)
I8	$\text{IO} + \text{NO} \rightarrow \text{I} + \text{NO}_2$	2	9.1×10^{-12}		DeMore <i>et al.</i> (1997)
I9	$\text{IO} + \text{NO}_2 \xrightarrow{\text{M}} \text{INO}_3$	2			DeMore <i>et al.</i> (1997)
I10	$\text{IO} + \text{IO} \rightarrow \text{I}_2\text{O}_2$	2	$0.5 \times 1.5 \times 10^{-11}$	500	DeMore <i>et al.</i> (1997)
I11	$\text{IO} + \text{IO} \rightarrow 2 \text{I} + \text{O}_2$	2	$0.12 \times 1.5 \times 10^{-11}$	500	DeMore <i>et al.</i> (1997)
I12	$\text{IO} + \text{IO} \rightarrow \text{OIO} + \text{I}$	2	$0.38 \times 1.5 \times 10^{-11}$	500	DeMore <i>et al.</i> (1997)
I13	$\text{IO} + \text{ClO} \rightarrow \text{I} + \text{Cl} + \text{O}_2$	2	5.1×10^{-12}	280	DeMore <i>et al.</i> (1997)
I14	$\text{IO} + \text{BrO} \rightarrow \text{OIO} + \text{Br}$	2	8.5×10^{-11}		Bedjanian <i>et al.</i> (1998)
I15	$\text{INO}_2 \rightarrow \text{I} + \text{NO}_2$	1	2.4		estimated from data in Jenkins <i>et al.</i> (1985)
I16	$\text{INO}_3 \rightarrow \text{IO} + \text{NO}_2$	1	$5. \times 10^{-3}$		Barnes <i>et al.</i> (1991)
I17	$\text{IO} + h\nu \xrightarrow{\text{O}_2} \text{I} + \text{O}_3$	1	1		Laszlo <i>et al.</i> (1995)
I18	$\text{HOI} + h\nu \rightarrow \text{I} + \text{OH}$	1	1		Bauer <i>et al.</i> (1998)
I19	$\text{I}_2 + h\nu \rightarrow 2 \text{I}$	1	1		Wesely (1989)
I20	$\text{I}_2\text{O}_2 + h\nu \rightarrow 2 \text{I} + \text{O}_2$	1	1		estimated by Davis <i>et al.</i> (1996), 9 × G79
I21	$\text{ICl} + h\nu \rightarrow \text{I} + \text{Cl}$	1	1		Seery and Britton (1964)
I22	$\text{IBr} + h\nu \rightarrow \text{I} + \text{Br}$	1	1		Seery and Britton (1964)
I23	$\text{INO}_2 + h\nu \rightarrow \text{I} + \text{NO}_2$	1	1		Bröske and Zabel (1998), R. Bröske, pers. comm.
I24	$\text{INO}_3 + h\nu \rightarrow \text{I} + \text{NO}_3$	1	1		same as G114, but redshifted by 50 nm
I25	$\text{CH}_3\text{I} + h\nu \rightarrow \text{I} + \text{CH}_3\text{OO}$	1	1		Roehl <i>et al.</i> (1997)
I26	$\text{C}_3\text{H}_7\text{I} + h\nu \rightarrow \text{I} + \text{ROOH}$	1	1		Roehl <i>et al.</i> (1997)
I27	$\text{CH}_2\text{ClI} + h\nu \rightarrow \text{I} + \text{Cl} + 2 \text{HO}_2 + \text{CO}$	1	1		Roehl <i>et al.</i> (1997)
I28	$\text{CH}_2\text{I}_2 + h\nu \rightarrow 2 \text{I} + 2 \text{HO}_2 + \text{CO}$	1	1		Roehl <i>et al.</i> (1997)
I29	$\text{C}_3\text{H}_7\text{I} + \text{OH} \rightarrow \text{CH}_3\text{OO} + \text{I}$	2	1.2×10^{-12}		J. Crowley, pers. comm.

Table D.8: Continued.

no	reaction	<i>n</i>	$A [(\text{cm}^{-3})^{1-n} \text{s}^{-1}]$	$-E_a / R [\text{K}]$	reference
I30	$\text{I}_2\text{O}_2 \rightarrow 2 \text{IO}$	1	31.0	assumed (thermolysis of Cl_2O_2 at 20 °C)	
I31	$\text{OIO} + \text{OH} \rightarrow 0.5 \text{HIO}_3 + 0.5 \text{HOI}$	2	2.0×10^{-10}	assumed, see caption and <i>von Glasow et al.</i> (2002a)	
I32	$\text{OIO} + \text{NO} \rightarrow \text{NO}_2 + \text{IO}$	2	8.5×10^{-12}	assumed, see caption and <i>von Glasow et al.</i> (2002a)	
I33	$\text{CH}_3\text{SCH}_3 + \text{IO} \rightarrow \text{CH}_3\text{SOCH}_3 + \text{I}$	2	1.2×10^{-14}	<i>DeMore et al.</i> (1997)	

n is the order of the reaction.¹ photolysis rates calculated online,² special rate functions (pressure dependent and/or humidity dependent),³ products after *Pham et al.* (1995). The reactions involving OIO are particularly uncertain (see discussion in *von Glasow et al.* (2002a)). The rate coefficients are calculated with $k = A \times \exp\left(\frac{-E_a}{RT}\right)$.

Table D.9: Aqueous phase reactions.

no	reaction	n	k_0 [$\text{M}^{1-n}\text{s}^{-1}$]	$-E_a / R$ [K]	reference
I1	$\text{HOI} + \text{I}^- + \text{H}^+ \rightarrow \text{I}_2$	3	4.4×10^{12}		<i>Eigen and Kustin</i> (1962)
I2	$\text{HOI} + \text{Cl}^- + \text{H}^+ \rightarrow \text{ICl}$	3	2.9×10^{10}		<i>Wang et al.</i> (1989)
I3	$\text{ICl} \rightarrow \text{HOI} + \text{Cl}^- + \text{H}^+$	1	2.4×10^6		<i>Wang et al.</i> (1989)
I4	$\text{HOI} + \text{Br}^- + \text{H}^+ \rightarrow \text{IBr}$	3	3.3×10^{12}		<i>Troy et al.</i> (1991)
I5	$\text{IBr} \rightarrow \text{HOI} + \text{H}^+ + \text{Br}^-$	1	8.0×10^5		<i>Troy et al.</i> (1991)
I6	$\text{HOCl} + \text{I}^- + \text{H}^+ \rightarrow \text{ICl}$	3	3.5×10^{11}		<i>Nagy et al.</i> (1988)
I7	$\text{HOBr} + \text{I}^- \rightarrow \text{IBr} + \text{OH}^-$	2	5.0×10^9		<i>Troy and Margerum</i> (1991)
I8	$\text{IO} + \text{O}_2^- \xrightarrow{\text{H}^+} \text{HOI} + \text{O}_2$	2	0.		see note
I9	$\text{IO}_2^- + \text{H}_2\text{O}_2 \rightarrow \text{IO}_3^-$	2	6.0×10^1		<i>Farrow</i> (1987)
I10	$\text{IO} + \text{IO} \rightarrow \text{HOI} + \text{IO}_2^- + \text{H}^+$	2	1.5×10^9		<i>Burton et al.</i> (1986)
I11	$\text{I}^- + \text{O}_3 \xrightarrow{\text{H}^+} \text{HOI}$	2	4.2×10^9		<i>Magi et al.</i> (1997)
I12	$\text{Cl}_2 + \text{HOI} \rightarrow \text{IO}_2^- + 2\text{Cl}^- + 3\text{H}^+$	2	1.0×10^6		<i>Lengyel et al.</i> (1996)
I13	$\text{HOI} + \text{HOCl} \rightarrow \text{IO}_2^- + \text{Cl}^- + 2\text{H}^+$	2	5.0×10^5		<i>Citri and Epstein</i> (1988)
I14	$\text{HOI} + \text{HOBr} \rightarrow \text{IO}_2^- + \text{Br}^- + 2\text{H}^+$	2	1.0×10^6		<i>Chinake and Smoysi</i> (1996)
I15	$\text{IO}_2^- + \text{HOCl} \rightarrow \text{IO}_3^- + \text{Cl}^- + \text{H}^+$	2	1.5×10^3		<i>Lengyel et al.</i> (1996)
I16	$\text{IO}_2^- + \text{HOBr} \rightarrow \text{IO}_3^- + \text{Br}^- + \text{H}^+$	2	1.0×10^6		<i>Chinake and Smoysi</i> (1996)
I17	$\text{IO}_2^- + \text{HOI} \rightarrow \text{IO}_3^- + \text{I}^- + \text{H}^+$	2	6.0×10^2		<i>Chinake and Smoysi</i> (1996)
I18	$\text{I}_2 + \text{HSO}_3^- \rightarrow 2\text{I}^- + \text{HSO}_4^- + 2\text{H}^+$	2	1.0×10^6		<i>Olsen and Epstein</i> (1991)

n is the order of the reaction. ¹ photolysis rates calculated online. The temperature dependence is $k = k_0 \times \exp(-E_a / R(\frac{1}{T} - \frac{1}{T_0}))$, $T_0 = 298$ K.

Table D.10: Heterogeneous reactions.

no	reaction	k	reference
Hi1	$\text{INO}_3 \xrightarrow{\text{H}_2\text{O}} \text{HOI}_{aq} + \text{HNO}_3_{aq}$	$\overline{k}_t(\text{INO}_3)w_{l,i}$	
Hi2	$\text{HI} \xrightarrow{\text{H}_2\text{O}} \text{H}^+ + \text{I}^-$	$\overline{k}_t(\text{HI})w_{l,i}$	
Hi3	$\text{I}_2\text{O}_2 \xrightarrow{\text{H}_2\text{O}} \text{HOI}_{aq} + \text{H}^+ + \text{IO}_2^-$	$\overline{k}_t(\text{I}_2\text{O}_2)w_{l,i}$	
Hi4	$\text{INO}_2 \xrightarrow{\text{H}_2\text{O}} \text{HOI}_{aq} + \text{HONO}_{aq}$	$\overline{k}_t(\text{INO}_2)w_{l,i}$	
Hi5	$\text{OIO} \xrightarrow{\text{H}_2\text{O}} \text{HOI}_{aq} + \text{HO}_{2aq}$	$\overline{k}_t(\text{OIO})w_{l,i}, \alpha = 0.01$	assumed, see <i>von Glasow et al.</i> (2002a)
Hi6	$\text{HOI}_3 \xrightarrow{\text{H}_2\text{O}} \text{IO}_3^- + \text{H}^+$	$\overline{k}_t(\text{HOI}_3)w_{l,i}, \alpha = 0.01$	assumed, see <i>von Glasow et al.</i> (2002a)

For a definition of \overline{k}_t and $w_{l,i}$ see section 2. $\text{Het}_T = [\text{H}_2\text{O} + f(\text{Cl}^-)[\text{Cl}^-] + f(\text{Br}^-)[\text{Br}^-]]$, with $f(\text{Cl}^-) = 5.0 \times 10^2$ and $f(\text{Br}^-) = 3.0 \times 10^5$. H4 - H9: the total rate is determined by \overline{k}_t , the distribution among the different reaction paths was assumed to be the same as for reactions H1 - H3. The reaction involving OIO is particularly uncertain (see discussion in *von Glasow et al.* (2002a)).

Table D.11: Aqueous phase equilibrium constants.

no	reaction	<i>m</i>	<i>n</i>	$K_0 [M^{n-m}]$	$-\Delta H/R [K]$	reference
EQi1	$\text{ICl}_{aq} + \text{Cl}^- \rightleftharpoons \text{ICl}_2^-$	2	1	7.7×10^1		<i>Wang et al. (1989)</i>
EQi2	$\text{IBr}_{aq} + \text{Br}^- \rightleftharpoons \text{IBr}_2^-$	2	1	2.9×10^2		<i>Troy et al. (1991)</i>

The temperature dependence is $K = K_0 \times \exp\left(-\frac{\Delta H}{R}\left(\frac{1}{T} - \frac{1}{T_0}\right)\right)$, $T_0 = 298$ K.

Table D.12: Henry constants and accommodation coefficients.

specie	K_H^0 [M/atm]	$-\Delta_{soln}H/R$ [K]	reference	α^0	$-\Delta_{obs}H/R$ [K]	reference
HI	∞	—				
IO	4.5×10^2	=HOI	see note	0.036	4130	<i>Schweitzer et al. (2000)</i>
HOI	4.5×10^2	=HOCl	<i>Chatfield and Crutzen (1990)</i>	0.5	2000	estimated
INO ₂	∞	—		0.1	2000	estimated
INO ₃	∞	—		0.1	2000	estimated
I ₂	3.0	4431	<i>Palmer et al. (1985)</i>	0.01	2000	estimated
ICl	1.1×10^2	=BrCl	see note	0.01	2000	estimated
IBr	2.4×10^1	=BrCl	see note	0.01	2000	estimated
I ₂ O ₂	∞	—		0.1	2000	estimated

The temperature dependence is for the Henry constants is $K_H = K_H^0 \times \exp\left(\frac{-\Delta_{soln}H}{R}\left(\frac{1}{T} - \frac{1}{T_0}\right)\right)$, $T_0 = 298$ K and for the accommodation coefficients $d\ln\left(\frac{\alpha}{1-\alpha}\right)/d\left(\frac{1}{T}\right) = \frac{-\Delta_{obs}H}{R}$.

Appendix E

File unit numbers

unit	file name	description
1	flux.dat	jrate input (SR cross_init)
2	sig0900.dat	jrate input (SR cross_init)
3	cheb_coeff.dat	jrate input (SR cross_init)
4	lookt0900.dat	jrate input (SR cross_init)
7	prof.out	jrate output (SR atm_out)
8	check_four.out	jrate output (SR check_four)
9	f4st.out	jrate output (SR flux_out)
6	profma.out	
11	istart	
8	euler_in.dat	
13	initr.dat	
13	initr.dat	
15	rstma.dat	
16	rstca.dat	
17	pma.out	
18		
18	pta.out	
19	pba.out	
20	pra.out	
30	check_four.out	
33	pifm2.dat	
40	profr.out	
41	f1a.out	
42	f2a.out	
43	f3a.out	
44	fia.out	
50	initc.dat	
50	clarke.dat	
51	urbankw.dat	
52	urbanlw.dat	
53	ruralkw.dat	

54	rurallw.dat	
55	ozeankw.dat	
56	ozeanlw.dat	
60	prof.c.out	
61	sg1a.out	
62	sl1a.out	
63	iona.out	
64	sr1a.out	
65	araa.out	
66	aea.out	
66	gra.out	
67	gsa.out	
67	sle.out	
69	jraa.out	
74	mass.out	
84		
85		
86		
87		
88		
89		
97	pia.out	
99	tima.out	
109	gam.out	

Appendix F

Cross sections

In the following figures an overview of the cross sections used in the model as of **05.03.1999 - update plots** is given. The artificial spikes in the cross sections of BrCl, Br₂, IO, INO₃, CH₃I, and BrO have been corrected in the meantime.

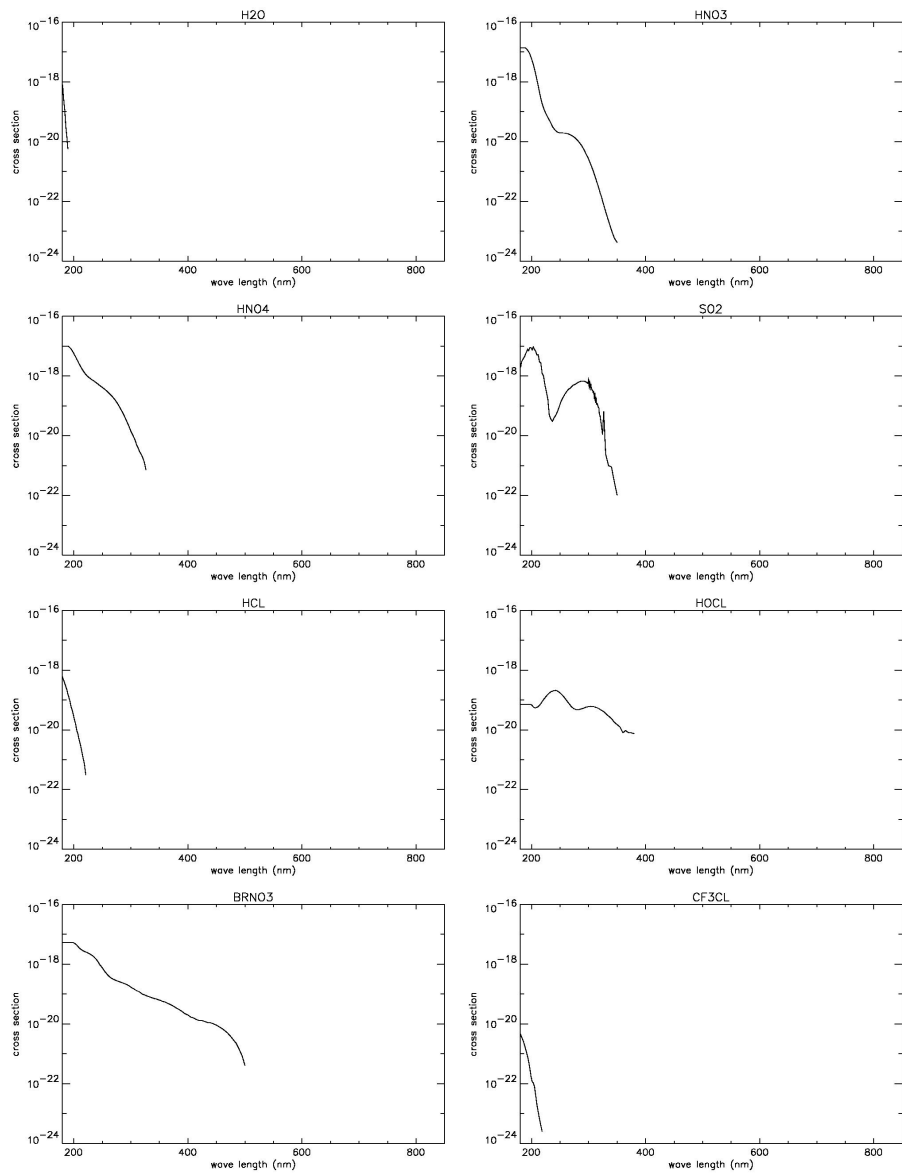


Figure F.1: Cross sections

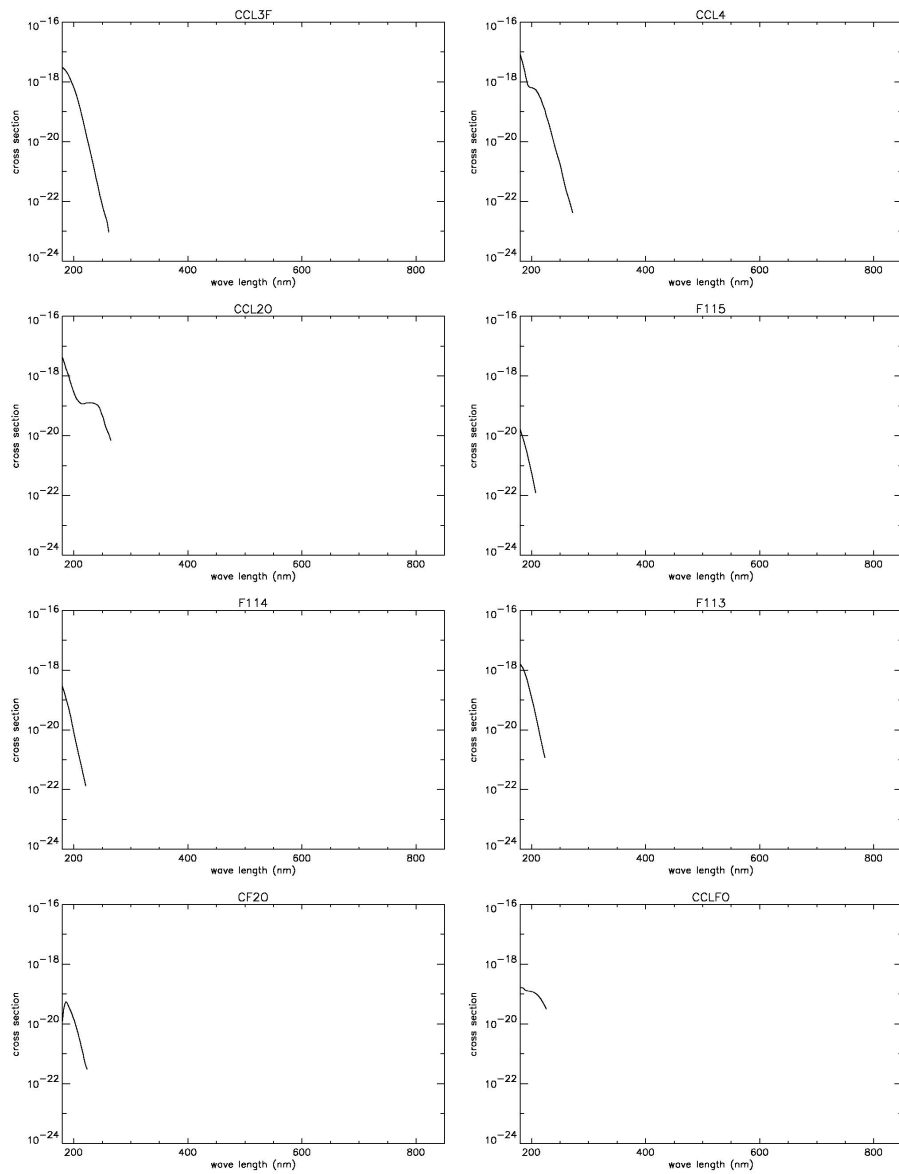


Figure F.2: Cross sections

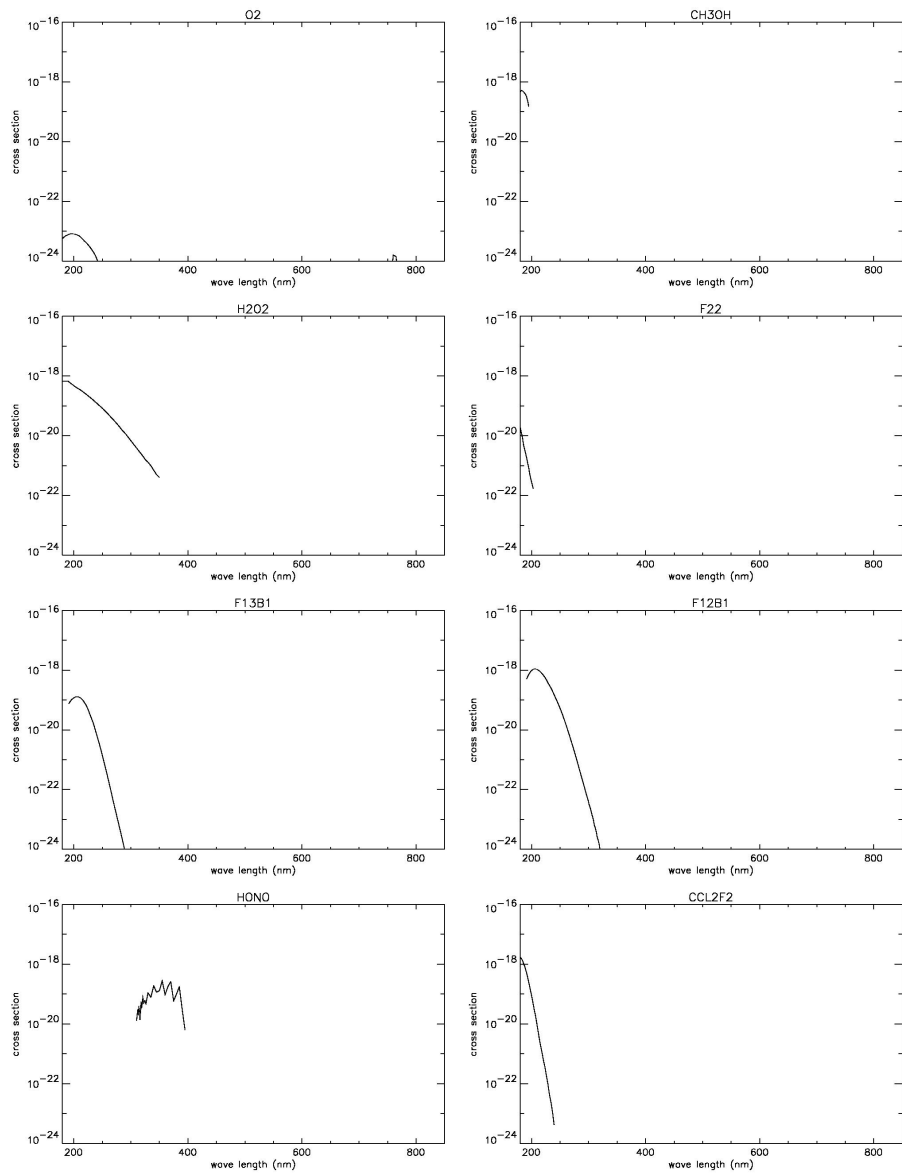


Figure F.3: Cross sections

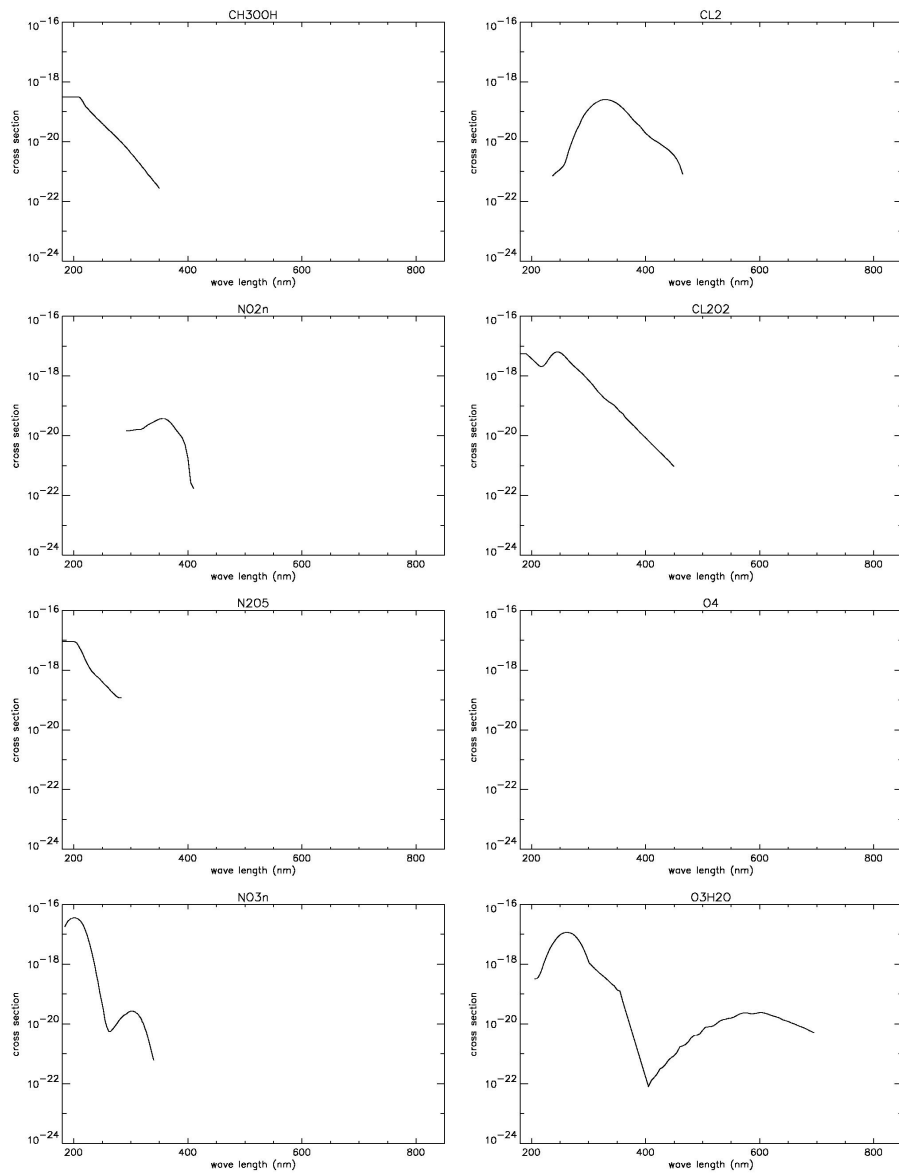


Figure F.4: Cross sections

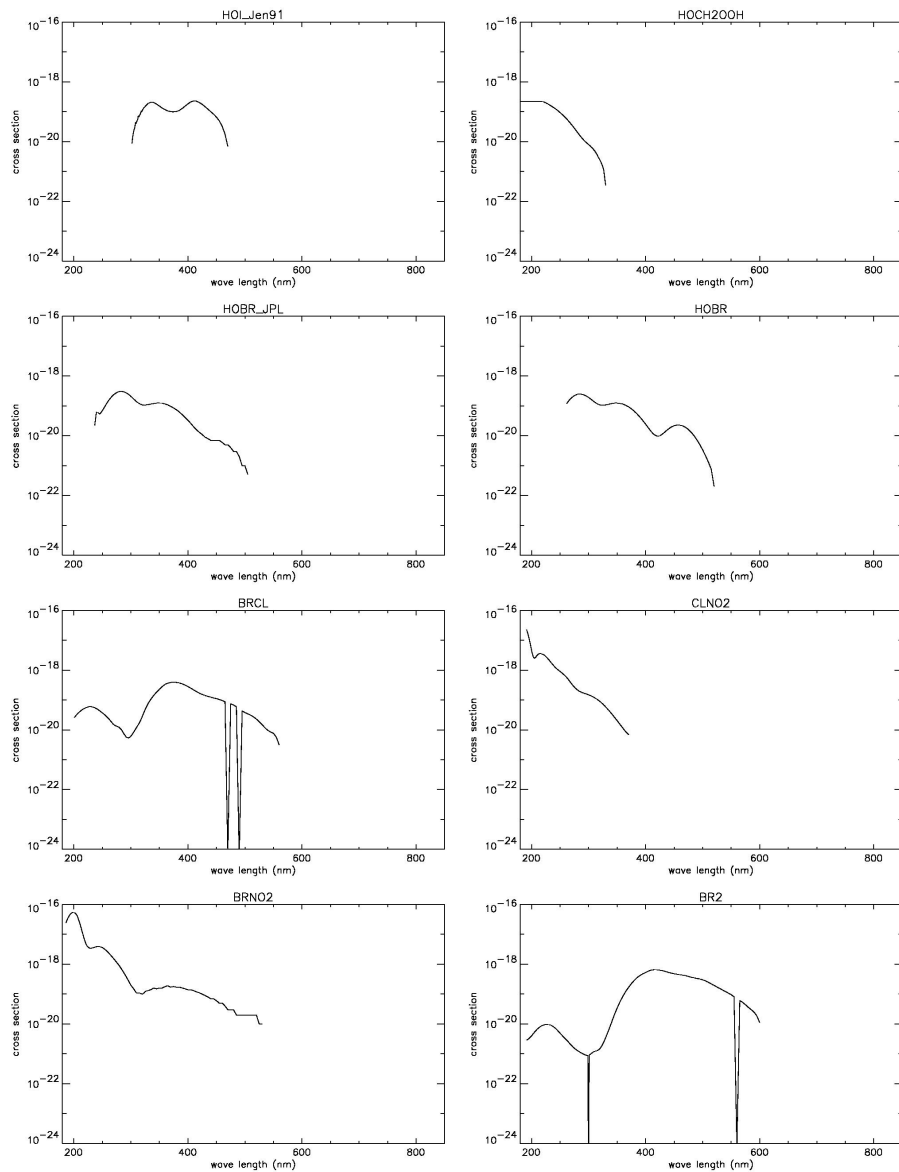


Figure F.5: Cross sections

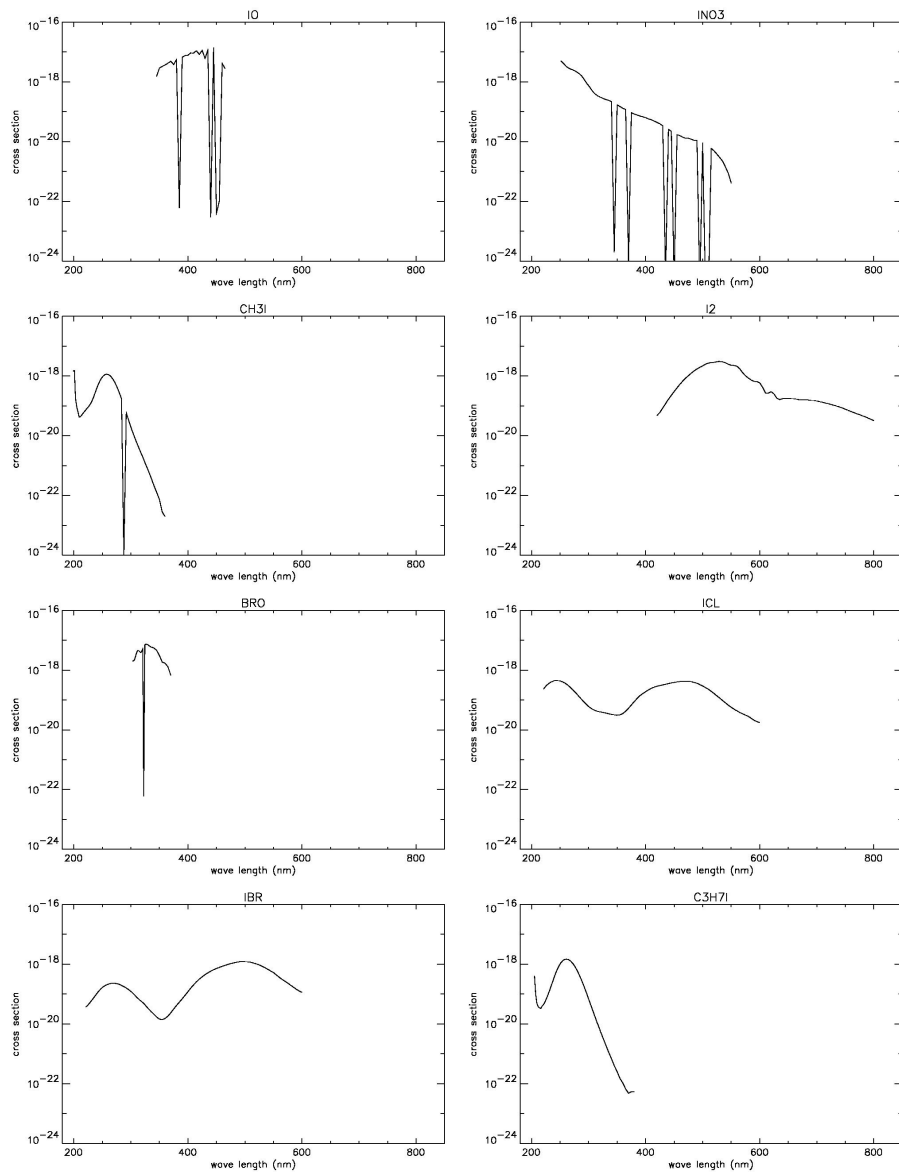


Figure F.6: Cross sections

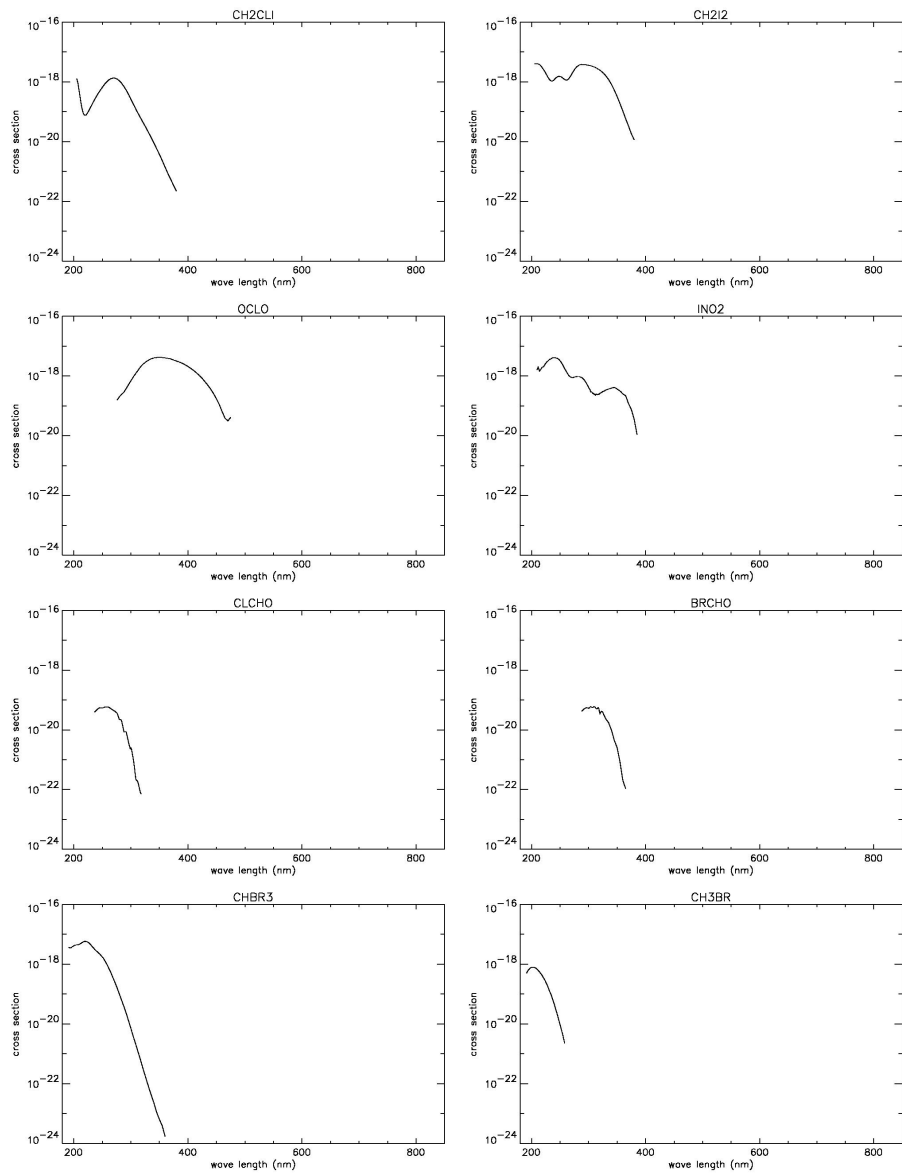


Figure F.7: Cross sections

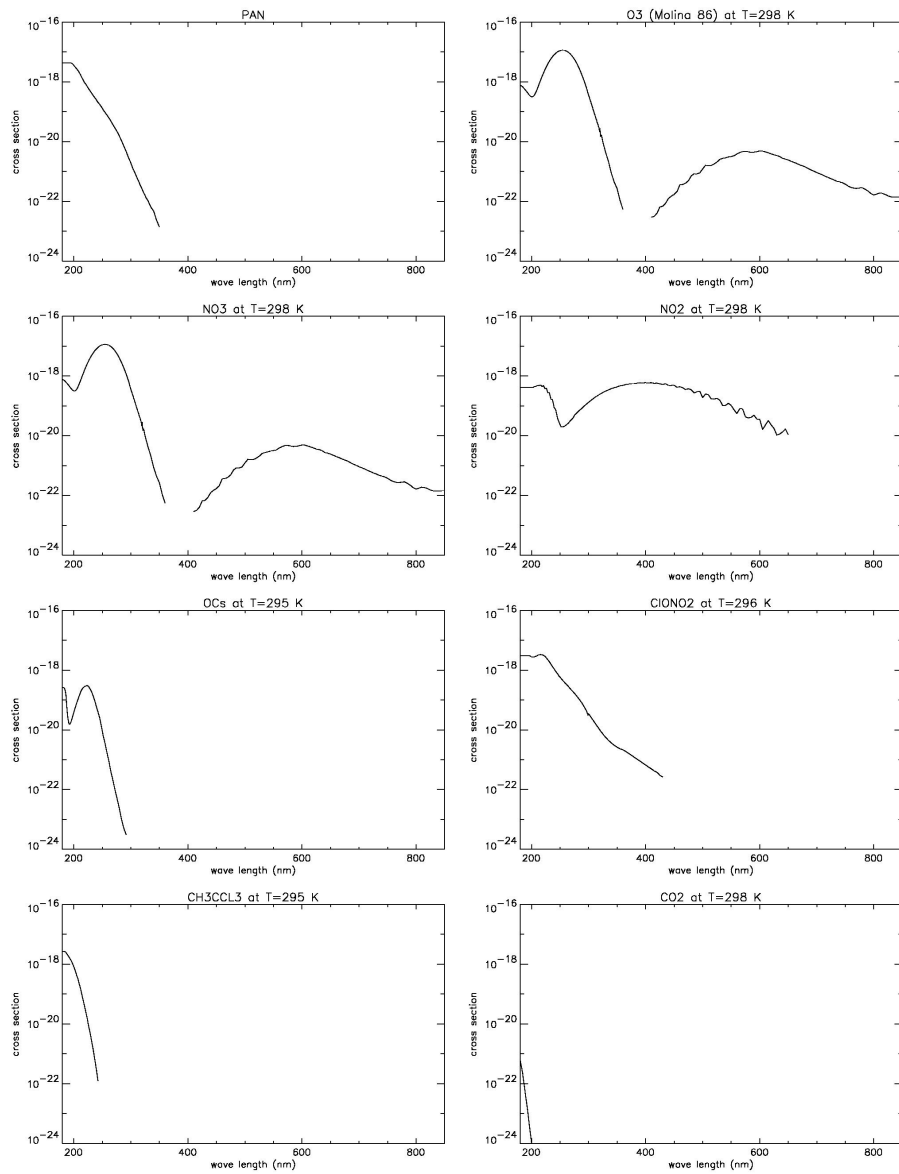


Figure F.8: Cross sections

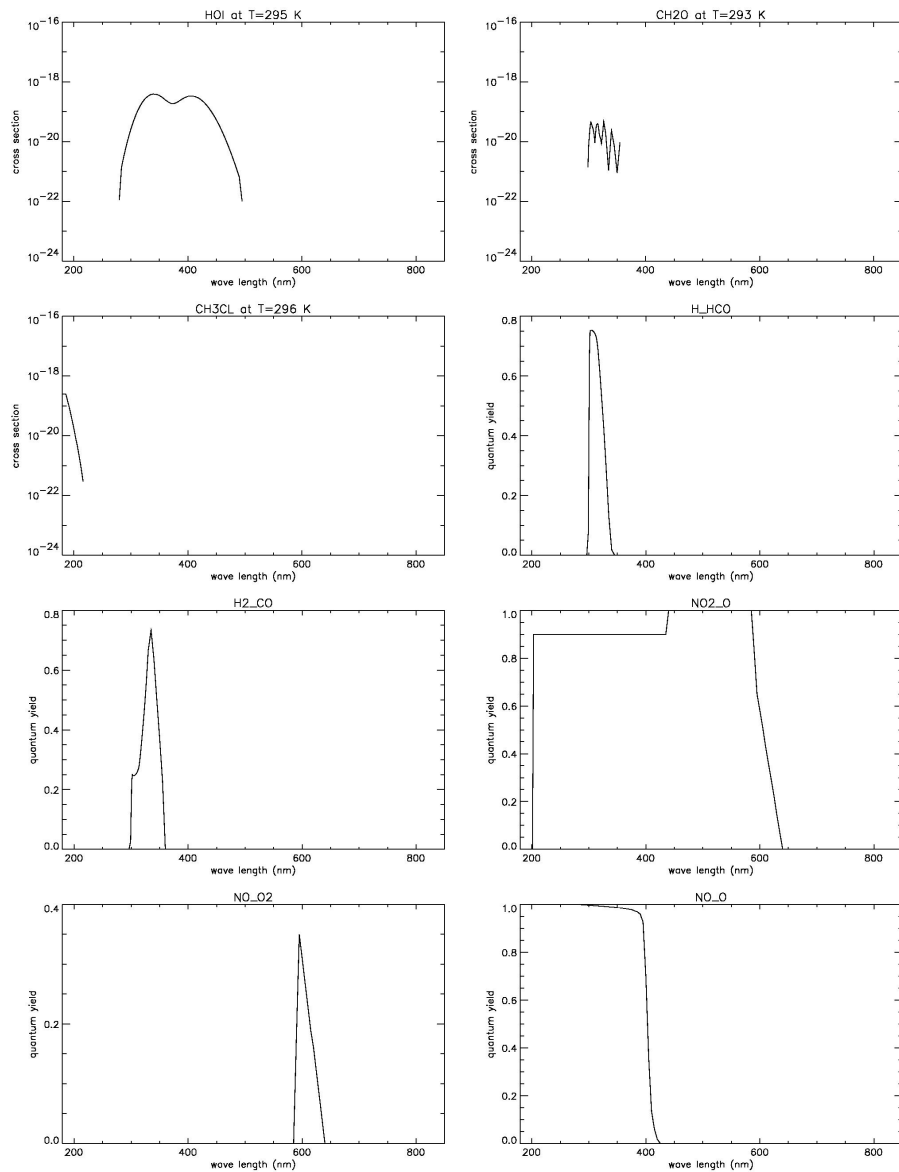


Figure F.9: Cross sections and quantum yields

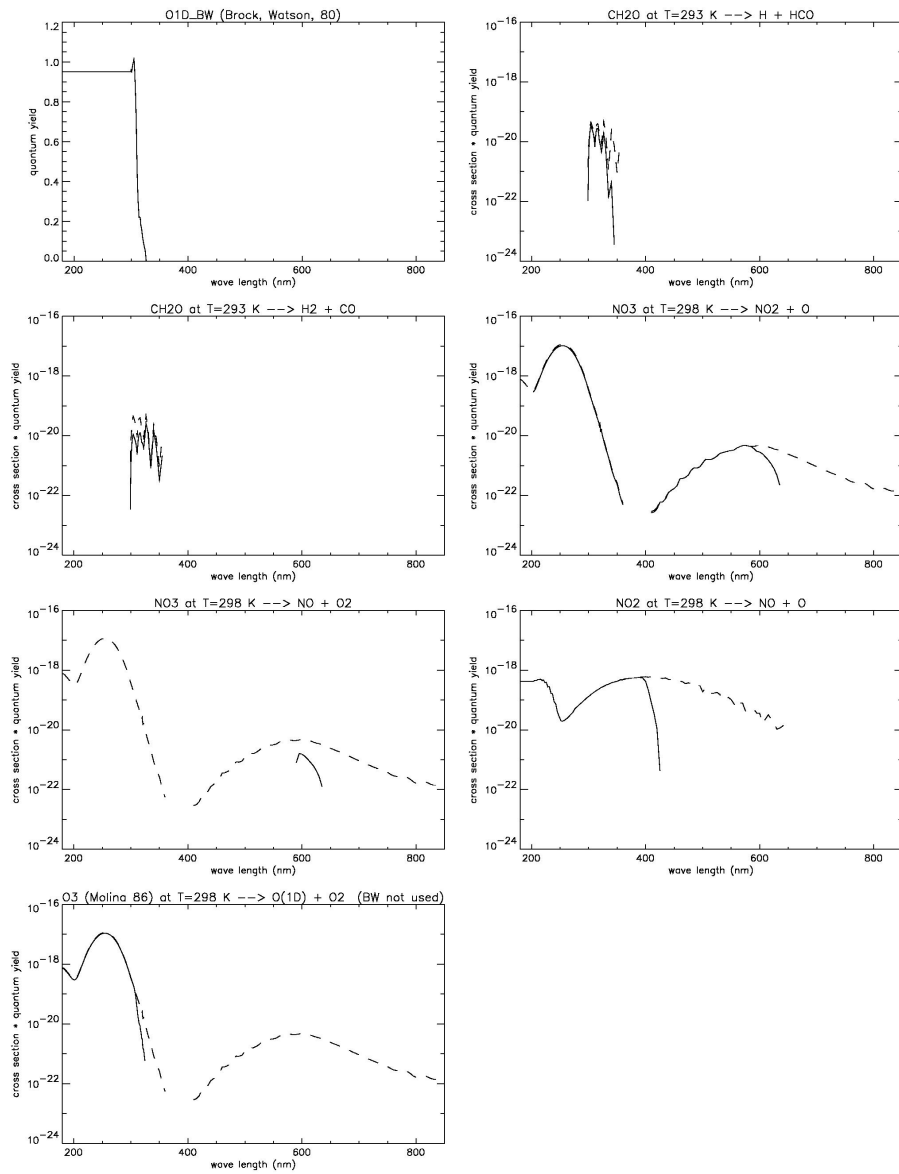


Figure F.10: Cross sections and quantum yields

Appendix G

Photolysis frequencies

Figure G.1 shows photolysis frequencies that are calculated with MISTRA and the above described band module for photolysis for a cloudy and non-cloudy model run near the surface (in 50 m height) and at 750 m, which is below the top of the cloud for the cloudy run (end of July at latitude $\phi = 30^\circ$). The asymmetry of the photolysis rates with respect to local noon in the cloudy MBL is a consequence of the column integrated liquid water content, the so-called liquid water path. It has a minimum after noon, see Figures in *von Glasow (2001)*.

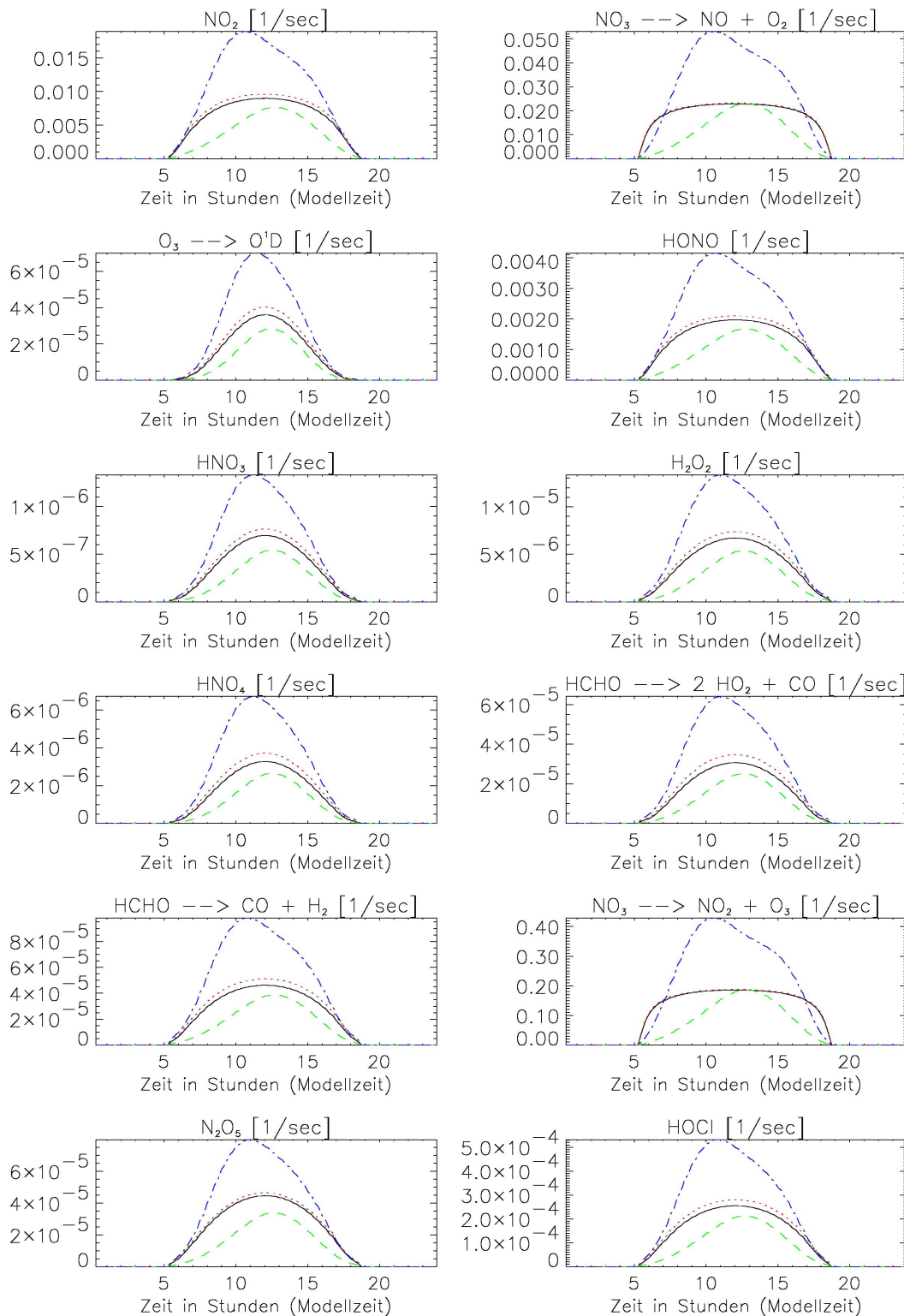


Figure G.1: Photolysis rates for a cloudy and a cloud-free MBL (end of July at latitudte $\phi = 30^\circ$). 50 m cloud-free: black, solid line, 50 m cloudy: green, dashed line; 750 m cloud-free: red, dotted line, 750 m cloudy: blue, dash-dotted line.

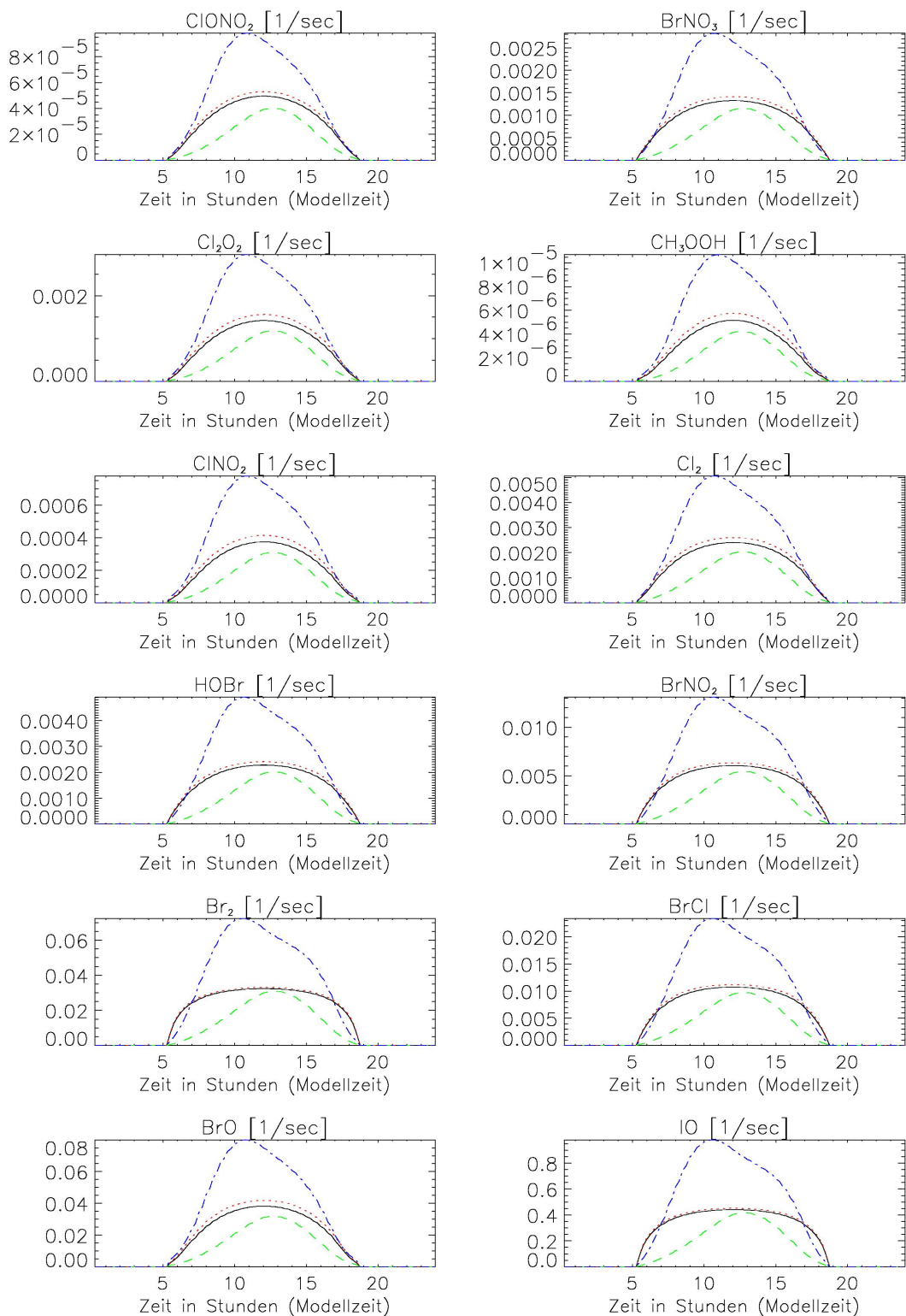


Figure G.1: Continued.

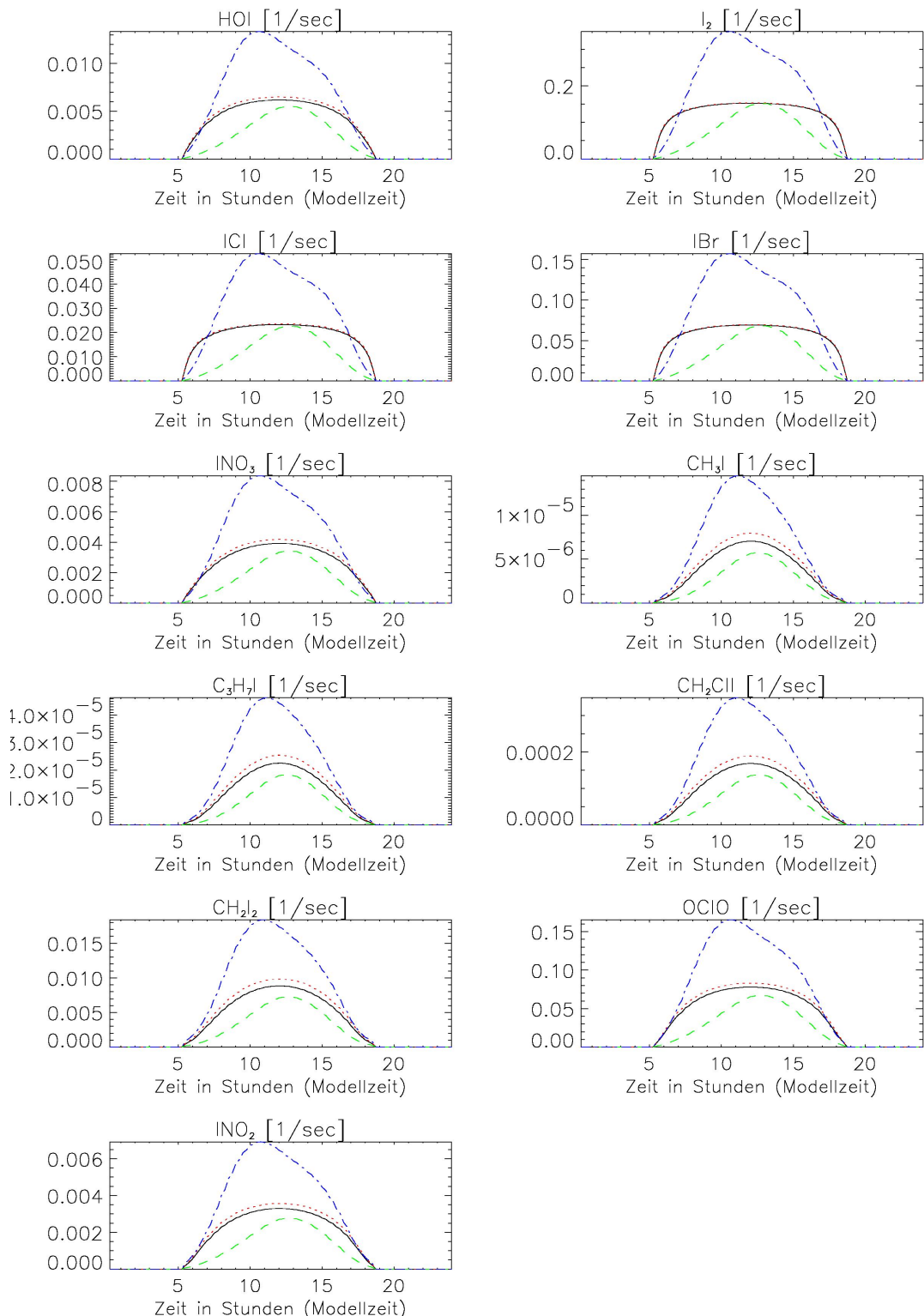


Figure G.1: Continued.

Appendix H

Routines documentation

H.1 claf

The tabled values of fu and ft come from (*Clarke*, 1970, Fig. 1). Note that in the stable part ($xzpd1 \geq 0$), both are equal, thus explaining the tests "if ($zpd1.ge.0..dp$) then ...".

Appendix I

Change log

This section lists the changes that have been made in previous model updates.

u6 ("unified version 6"):

- 3 mechanisms (tot, aer, gas) in one model
- runs on DEC alpha, w/ DEC compiler
- used for von Glasow 2000 (PhD); von Glasow and Sander, 2001; von Glasow et al 2002a,b; Wagner et al. 2002

v7.1.3:

- rate coeff. updates, further automatization of mechanism generation and checking
- same (external) timestep for dynamics, microphysics and chemistry: 10sec
- Intel Xeon, RedHat Linux, Intel Fortran Compiler 5.0
- used for von Glasow and Crutzen, 2004

v7.2.0:

- update of aqueous phase chemistry
UNFINISHED

v7.3.0:

- minor bug fixes
- consistency updates (logical "kpp", "jrate" deleted)
- output additionally in netCDF format; binary output commented
- Intel Xeon, SuSE Linux, Intel Fortran Compiler 8.0

v7.3.1:

- out_netCDF.f: minor changes and adjustment to new plot programs
- box model: if restart, now it can be chosen to use averages over the BL or values from a certain level
- box model: speed-up of roughly 10x by not calling PIFM
- restart: meteo: improvements
chemistry: enabled
WARNING: a restarted run DOES diverge with time from a continuous run, will be improved, but doesn't have an effect if sensitivity runs are made with the same restart files
- minor bug fixes

v7.3.2:

- new name: MISTRAL-IUP
- iodine chemistry and nucleation after Susanne
- several bug fixes (surface reactions, ...)
- some obsolete common blocks deleted
- output: switch for binary output added; changes in levels of mic and rate output; many typos corrected
- "strange" concentrations at k=nf: strongly improved but not completely fixed (main change: NO aqueous phase chemistry anymore in layer k-nf)
- reactions on dry aerosol: upper limit for reaction rate based on Henry's laws constant introduced (results in strongly reduced uptake of HNO₃)
- aerosol above k=nf: now in equilibrium with rel. hum.
- sea salt aerosol: more complete initialization: SO₄²⁻, NO₃⁻ added
- initca.dat: no double CO input anymore
- complete update of rate coefficients for O_x, HO_x, NO_x, SO_x, ClO_x, BrO_x chemistry
- SO₂ + OH --> .. --> H₂SO₄: now all reactions explicitly
- 5 new tracers (2 so far unused): CO₂ (for upcoming volcano studies), SO₃, HOSO₃
- CO_{2,aq} as "additional aqueous" tracer deleted because it's an explicit tracer now
- sea salt aerosol shrinking due to CO₂ degassing improved by using the correct molecular mass for

- degassing CO₂ instead of HC₀₃-
- restart: further corrections; NOT compatible with previous versions

v7.3.3:

- use of v7.3.2 with Intel compiler 8.1 revealed problems: if "array index out of bounds" occurred in 8.0 the value was set to 0. and no warning was given; in 8.1 the value is set to NaN and the model crashes because of this
- with "-check all" all occurrences of "index out of bounds" were found and corrected
- v7.3.3a.tar.gz contains only the above fixes!
- compilation with -fpe0, which is supposed to lead to model crash in case of floating exceptions and usually also crashes
- unexplainable problem in FCT d1mach - replaced with call to a SR including a necessary (sic!) write-out to /dev/null
- minor inconsistencies for dry aerosol reactions for box model solved
- v7.3.3b.tar.gz contains only the above fixes!
- 2 typos in T-dependence of OH + ClO corrected
- no further changes

v7.3.3_ROS3:

- based on v7.3.3
- includes ROS3 as default
- CO₂ is no fixed species anymore (relevant only for plume studies)
- warning if ionic strength is too high, then Pitzer is switched off
- output of 1D particle spectrum in netCDF files
- no creation of .asc files if nuc is off

v7.3.3_ROS3_release_b:

- str.f : correctly calculate the 1D grid
- out_netCDF.f: "long" meteo output
- out_netCDF.f: improved output for 1D microphysics (see ./volcanoes/new_runs/grid_out)
- out_netCDF.f: reaction rates as 1 variable to enable comparisons (see ./NIWA/v7.3.3R(CG)_sum_cl_3_corr)

v7.4.0:

- str.f, SR initm: calculation of thetl after definition of xm1
- str.f, SR difc: all aqueous compounds are being transported to avoid mistakes when changing the number of compounds
- str.f, kpp.f: replaced CB mbl with kinv_i
- str.f, kpp.f: array sizes made consistent (hopefully) everywhere: /cb40/, /k_surf_*/ , bg(2,nlev,nrxn)
- kpp.f: SR set_box_lev_a: correct /kpp_drya/
- kpp.f: SR aer_source: log(rr) --> log10(rr) for Monahan
- kpp.f: SR st_coeff_a/t: alpha=min(1,alpha)
- kpp.f: declare FCN funa in SR dry_rates_a
- kpp.f: avoid potential division by 0. in: FCNs fbck2, fdehtg, fdetha
- out_netcdf.f: SR write_chem_gas: no output of undefined variable #79
- out_netcdf.f: SR write_chem_aq: mliq(19:24) --> mliq(20:25)
- mech/out_netcdf.f: correct I_HOS03 --> I_HOS02
(also in plot_gas_v740.sc)
- ./mech/sedt23: don't replace CO2: I --> F anymore
- istart: fogtype cannot be chosen anymore
- ROS3: "stepmax" corrected (luckily has no effect
(./Mistra/v7.3.3_ROS3_rel_b_stepmax))
- cosmetics:
 - delete unused SRs
 - delete unused functions
 - delete commented print statements
 - delete a few obsolete commented "back-up" calls from ~1998
 - add comments to header of all subroutines in str.f and kpp.f
 - add comments to main program
 - all unused versions of SR initm are now in
./special_versions/SR_initm

Updates from Susanne's last control run

[/data/Susanne/MISTRA/v7.3.3_ROS3.S/control8_v7.3.3_ROS3.S]:

- nuc.f: replaced with her latest version
- jrate.f: 3 more species (but not explicitly calculated, just assumed as linear scaling of other compounds)
- str.f: new calls to nuc; SR photol now every 2^min as standard
- kpp.f: implications from new nuc; update of liq parms every 2^min
- kpp.f: typo correction - r*2 --> r**2 in SR aer_source
- outp.f: a few new iodine species
- out_netcdf.f: a few new iodine species; nuc output
- aqueous phase: check to ensure that reactions are not faster than diffusion limit

Updates from Matthias latest base version

[/data/Roland/Mistra/Arctic_Matthias_final_base_runs/

Base_case_without_halo]

- mainly typos
- gas phase: Br₂ + OH
- aq. phase Br-/Cl- + HNO₄ (very small k though)
- specific changes for polar regions/FF aerosol/re-emission of deposited material are under ./special_versions/polar

Updates from Linda's latest version

[/data2/Linda/TOTES_MEER/LAGRANGE/dead_19]

- none as her changes almost exclusively refer to Dead Sea specifics which are documented under ./special_versions

v7.4.1:

- gas phase mechanism as updated by Roberto
- NO in aq. phase
- gas phase species are included in gas.nc independent on switches halo, iod, nuc
- Hg chemistry prepared but commented and not included in *eqn

v9.0: (to be completed)

- radiation code: correction of several bugs in SR water (radiative effect of cloud droplets). It had been completely switched off with icld (this switch is now removed), probably because the calculation lead to wrong results due to the bugs.
- nrad.f converted to Fortran90
- nuc.f: converted to Fortran90
- ...
- kpp.f: in SR liq_parm, fast_k_mt_* routines were expected to be called once

Appendix J

Troubleshooting and FAQ

J.0.1 Issues when producing the mechanism files

The scripts that generate the mechanism files use sed with GNU extensions. If the resulting files are incorrect, check that GNU extensions are enabled in sed, and that no environment-specific alias is defined for sed command. For instance, if `sed='sed -posix'` (this option disables GNU extensions), some substitutions done in the scripts will fail.

Bibliography

- Abbatt, J. P. D. and G. C. G. Waschewsky. Heterogeneous interactions of HOBr, HNO₃, O₃ and NO₂ with deliquescent NaCl aerosols at room temperature. *J. Phys. Chem. A*, **102**, 3719 – 3725, 1998.
- Aiuppa, A., A. Franco, R. von Glasow, A. G. Allen, W. D'Alessandro, T. A. Mather, D. M. Pyle, and M. Valenza. The tropospheric processing of acidic gases and hydrogen sulphide in volcanic gas plumes as inferred from field and model investigations. *Atmos. Chem. Phys.*, **7**, 1441 – 1450, 2007.
- Albrecht, B. A. Aerosols, Cloud Microphysics, and Fractional Cloudiness. *Science*, **245**, 1227 – 1230, 1989.
- Anastasio, C., B. M. Matthew, J. T. Newberg, and I. George. Photochemical formation of hydroxyl radical in sea-salt particles leads to the release of Br₂. *submitted*, 2003.
- Anderson, L. C. and D. W. Fahey. Studies with ClONO₂: Thermal dissociation rate and catalytic conversion to NO using an NO/O₃ chemiluminescence detector. *J. Phys. Chem.*, **94**, 644 – 652, 1990.
- Andreas, E. L. A New Sea Spray Generation Function for Wind Speeds up to 32 m s⁻¹. *J. Phys. Oceanogr.*, **28**, 2175 – 2184, 1998.
- Andreas, E. L., J. B. Edson, E. C. Monahan, M. P. Rouault, and S. D. Smith. The spray contribution to net evaporation from the sea: A review of recent progress. *Bound. Lay. Met.*, **72**, 3 – 52, 1995.
- Andrews, J. E., P. Brimblecombe, T. D. Jickells, and P. S. Liss. *An Introduction to Environmental Chemistry*. Blackwell Science, Oxford, 1996.
- Aranda, A., G. Le Bras, G. La Verdet, and G. Poulet. The BrO + CH₃O₂ reaction: Kinetics and role in the atmospheric ozone budget. *Geophys. Res. Lett.*, **24**, 2745 – 2748, 1997.
- Atkinson, A., D. L. Baulch, R. A. Cox, R. F. Hampson, Jr., J. A. Kerr, M. J. Rossi, and J. Troe. Evaluated kinetic and photochemical data for atmospheric chemistry: Supplement VI. *J. Phys. Chem. Ref. Data*, **26**, 1329 – 1499, 1997.
- Atkinson, R., D. L. Baulch, R. A. Cox, J. N. Crowley, R. F. Hampson, J. A. Kerr, M. J. Rossi, and J. Troe. Summary of Evaluated Kinetic and Photochemical Data for Atmospheric Chemistry. *Web Version*, Dec. 2002.

- Atkinson, R., D. L. Baulch, R. A. Cox, R. F. Hampson, Jr., J. A. Kerr, M. J. Rossi, and J. Troe. Summary of Evaluated Kinetic and Photochemical Data for Atmospheric Chemistry. *Web Version*, <http://www.iupac-kinetic.ch.cam.ac.uk>, 1999.
- Audriffen, N., M. Renard, E. Buisson, and N. Chaumerliac. Deviations from the Henry's law equilibrium during cloud events: a numerical approach of the mass transfer between phases and its specific numerical effects. *Atmos. Res.*, *49*, 139 – 161, 1998.
- Ayers, G. P., S. A. Penkett, R. W. Gillett, B. Bandy, I. E. Galbally, C. P. Meyer, C. M. Elsworth, S. T. Bentle, and B. W. Forgan. The Annual Cycle of Peroxides and Ozone in Marine Air at Cape Grim, Tasmania. *J. Atmos. Chem.*, *23*, 221 – 252, 1996.
- Bardouki, H., M. B. da Rosa, N. Mihalopoulos, W.-U. Palm, and C. Zetzsch. Kinetics and mechanism of the oxidation of dimethylsulfoxide (DMSO) and methanesulfinate (MSI^-) in aqueous medium. *Atmos. Environ.*, *36*, 4627 – 4634, 2002.
- Barker, G. C., P. Fowles, and B. Stringer. Pulse radiolytic induced transient electrical conductance in liquid solutions. *Trans. Faraday Soc.*, *66*, 1509–1519, 1970.
- Barnes, I., K. H. Becker, and J. Starcke. Fourier-transform IR spectroscopic observation of gaseous nitrosyl iodine, nitryl iodine, and iodine nitrate. *J. Phys. Chem.*, *95*, 9736–9740, 1991.
- Barone, S. B., A. A. Turnipseed, and A. R. Ravishankara. Role of adducts in the atmospheric oxidation of dimethyl sulfide. *Faraday Discuss.*, *100*, 39 – 54, 1995.
- Bartlett, W. P. and D. W. Margerum. Temperature dependencies of the Henry's law constant and the aqueous phase dissociation constant of bromine chloride. *Environ. Sci. Technol.*, *33*, 3410–3414, 1999.
- Bauer, D., T. Ingham, S. A. Carl, G. K. Moortgat, and J. N. Crowley. Ultraviolet-visible absorption cross sections of gaseous HOI and its photolysis at 355 nm. *J. Phys. Chem. A*, *102*, 2857 – 2864, 1998.
- Bedjanian, Y., G. L. Bras, and G. Poulet. Kinetics and Mechanisms of the IO + BrO Reaction. *J. Phys. Chem. A*, *102*, 10 501 – 10 511, 1998.
- Behnke, W., C. George, V. Scheer, and C. Zetzsch. Production and decay of ClNO₂ from the reaction of gaseous N₂O₅ with NaCl solution: Bulk and aerosol experiments. *J. Geophys. Res.*, *102*, 3795 – 3804, 1997.
- Behnke, W., V. Scheer, and C. Zetzsch. Production of BrNO₂, Br₂ and ClNO₂ from the Reaction between Sea Spray Aerosol and N₂O₅. *J. Aerosol Sci.*, *25*, Suppl.1, S277 – S278, 1994.
- Betterton, E. A. and M. R. Hoffmann. Oxidation of aqueous SO₂ by peroxymonosulfate. *J. Phys. Chem.*, *92*, 5962–5965, 1988.
- Bjergbakke, E., S. Navartnam, B. J. Parsons, and A. J. Swallow. Reaction between HO₂· and chlorine in aqueous solution. *J. Am. Chem. Soc.*, *103*, 5926–5928, 1981.

- Bobrowski, N., R. von Glasow, A. Aiuppa, S. Inguaggiato, I. Louban, O. W. Ibrahim, and U. Platt. Reactive halogen chemistry in volcanic plumes. *J. Geophys. Res.*, **112**, D06311, doi:10.1029/2006JD007206, 2007.
- Bonsang, B., D. Martin, G. Lambert, M. Kanakidou, J. de Rouley, and G. Sennequir. Vertical distribution of nonmethane hydrocarbons in the remote marine boundary layer. *J. Geophys. Res.*, **96**, 7313 – 7324, 1991.
- Bott, A. A numerical model of the cloud-topped planetary boundary-layer: Impact of aerosol particles on the radiative forcing of stratiform clouds. *Q. J. R. Meteorol. Soc.*, **123**, 631 – 656, 1997.
- Bott, A. A numerical model of the cloud-topped planetary boundary-layer: Chemistry in marine stratus and the effects on aerosol particles. *Atmos. Environ.*, **33**, 1921 – 1936, 1999.
- Bott, A. A Flux Method for the Numerical Solution of the Stochastic Collection Equation: Extension to Two-Dimensional Particle Distributions. *J. Atmos. Sci.*, **57**, 284 – 294, 2000.
- Bott, A. and G. R. Carmichael. Multiphase Chemistry in a Microphysical Radiation Fog Model - a Numerical Study. *Atmos. Environ.*, **27A**, 503 – 522, 1993.
- Bott, A., U. Sievers, and W. Zdunkowski. A Radiation Fog Model with a Detailed Treatment of the Interaction between Radiative Transfer and Fog Microphysics. *J. Atmos. Sci.*, **47**, 2153–2166, 1990.
- Bott, A., T. Trautmann, and W. Zdunkowski. A numerical model of the cloud-topped planetary boundary-layer: Radiation, turbulence and spectral microphysics in marine stratus. *Q. J. R. Meteorol. Soc.*, **122**, 635–667, 1996.
- Boyce, S. D. and M. R. Hoffmann. Kinetics and mechanism of the formation of hydroxymethanesulfonic acid at low pH. *J. Phys. Chem.*, **88**, 4740–4746, 1984.
- Brasseur, G. P., J. J. Orlando, and G. S. Tyndall, editors. *Atmospheric Chemistry and Global Change*. Oxford University Press, New York, Oxford, 1999.
- Brimblecombe, P. and S. L. Clegg. Erratum. *J. Atmos. Chem.*, **8**, 95, 1989.
- Bröske, R. and F. Zabel. Spectroscopic and kinetic properties of XNO₂ (X = Br, I). *Ann. Geophys. Suppl. II*, **16**, C717, 1998.
- Burkholder, J. B., J. Curtius, A. R. Ravishankara, and E. R. Lovejoy. Laboratory studies of the homogeneous nucleation of iodine oxides. *Atmos. Chem. Phys.*, **4**, 19 – 34, 2004.
- Burley, J. D. and H. S. Johnston. Ionic mechanisms for heterogeneous stratospheric reactions and ultraviolet photoabsorption cross-sections for NO₂⁺, HNO₃, and NO₃⁻ in sulfuric-acid. *Geophys. Res. Lett.*, **19**, 1359 – 1362, 1992.
- Buxton, G. V., M. Bydder, and G. A. Salmon. The reactivity of chlorine atoms in aqueous solution Part II: The equilibrium SO₄²⁻ + Cl⁻ ⇌ Cl + SO₄²⁻. *Phys. Chem. Chem. Phys.*, **1**, 269 – 273, 1999a.

- Buxton, G. V., C. L. Greenstock, W. P. Helman, and A. B. Ross. Critical review of rate constants for reactions of hydrated electrons, hydrogen atoms and hydroxyl radicals ($\cdot\text{OH}/\cdot\text{O}^-$) in aqueous solution. *J. Phys. Chem. Ref. Data*, *17*, 513–886, 1988.
- Buxton, G. V., C. Kilner, and R. M. Sellers. Pulse radiolysis of HOI and IO^- in aqueous solution, formation and characterization of I^{II} . In *6th. Symp. on Radiation Chemistry*, pages 155 – 159. 1986.
- Buxton, G. V., S. McGowan, G. S. Salmon, J. E. Williams, and N. D. Wood. A study of the spectra and reactivity of oxysulphur-radical anions involved in the chain oxidation of S(IV): A pulse and γ -radiolysis study. *Atmos. Environ.*, *30*, 2483–2493, 1996.
- Buxton, G. V., G. A. Salmon, and J. Wang. The equilibrium $\text{NO}_3 + \text{Cl}^- \longleftrightarrow \text{NO}_3^- + \text{Cl}$: A laser flash photolysis and pulse radiolysis study of the reactivity of NO_3 with chloride ion in aqueous solution. *Phys. Chem. Chem. Phys.*, *1*, 3589 – 3593, 1999b.
- Campuzano-Jost, P. and J. N. Crowley. Kinetics of the Reaction of OH with HI between 246 and 353 K. *J. Phys. Chem. A*, *103*, 2712 – 2719, 1999.
- Chambers, R. M., A. C. Heard, and R. P. Wayne. Inorganic gas-phase reactions of the nitrate radical: $\text{I}_2 + \text{NO}_3$ and $\text{I} + \text{NO}_3$. *J. Phys. Chem.*, *96*, 3321–3331, 1992.
- Chameides, W. L. The Photochemistry of a Remote Marine Stratiform Cloud. *J. Geophys. Res.*, *89*, 4739 – 4755, 1984.
- Chameides, W. L. and A. W. Stelson. Aqueous-Phase Chemical Processes in Deliquescent Sea-Salt Aerosols: A Mechanism That Couples the Atmospheric Cycles of S and Sea Salt. *J. Geophys. Res.*, *97*, 20 565 – 20 580, 1992.
- Chatfield, R. B. and P. J. Crutzen. Are There Interactions of Iodine and Sulfur Species in Marine Air Photochemistry? *J. Geophys. Res.*, *95*, 22 319 – 22 341, 1990.
- Chaumerliac, N., M. Leriche, and N. Audriffen. Modeling of scavenging processes in clouds: some remaining questions about the partitioning of gases among gas and liquid phases. *Atmos. Res.*, *53*, 29 – 43, 2000.
- Chin, M. and P. H. Wine. A temperature-dependent competitive kinetics study of the aqueous-phase reactions of OH radicals with formate, formic acid, acetate, acetic acid, and hydrated formaldehyde. In G. R. Helz, R. G. Zepp, and D. G. Crosby, editors, *Aquatic and Surface Photochemistry*, pages 85–96. A. F. Lewis, NY, 1994.
- Chinake, C. R. and R. H. Simoyi. Kinetics and mechanism of the complex bromate-iodine reaction. *J. Phys. Chem.*, *100*, 1643–1656, 1996.
- Christensen, H. and K. Sehested. HO_2 and O_2^- radicals at elevated temperatures. *J. Phys. Chem.*, *92*, 3007–3011, 1988.
- Christensen, H., K. Sehested, and H. Corfitzen. Reactions of hydroxyl radicals with hydrogen peroxide at ambient and elevated temperatures. *J. Phys. Chem.*, *86*, 1588–1590, 1982.

- Citri, O. and I. R. Epstein. Mechanistic study of a coupled chemical oscillator: the bromate-chlorite-iodide reaction. *J. Phys. Chem.*, **92**, 1865–1871, 1988.
- Clarke, R. H. Recommended methods for the treatment of the boundary layer in numerical models. *Australian Meteorological Magazine*, **18**(2), 51–73, 1970.
- Clifton, C. L., N. Altstein, and R. E. Huie. Rate constant for the reaction of NO₂ with sulfur(IV) over the pH range 5.3–13. *Environ. Sci. Technol.*, **22**, 586–589, 1988.
- Curtis, A. R. and W. P. Sweetenham. Facsimile/Chekmat User's Manual. Technical report, Computer Science and Systems Division, Harwell Lab., Oxfordshire, Great Britain, 1987.
- Dal Maso, M., M. Kulmala, K. E. J. Lehtinen, J. Mäkelä, P. Aalto, and C. D. O'Dowd. Condensation and coagulation sinks and formation of nucleation mode particles in coastal and boreal forest boundary layers. *J. Geophys. Res.*, **107** (D19), 8097, doi: 10.1029/2001JD001053, 2002.
- Damian, V., A. Sandu, M. Damian, F. Potra, and G. R. Carmichael. The kinetic preprocessor KPP - a software environment for solving chemical kinetics. *Comp. Chem. Eng.*, **26**, 1567 – 1579, 2002.
- Damian-Iordache, V. KPP - Chemistry Simulation Development Environment. M.S. thesis, University of Iowa, Iowa City, 1996.
- Damschen, D. E. and L. R. Martin. Aqueous aerosol oxidation of nitrous acid by O₂, O₃ and H₂O₂. *Atmos. Environ.*, **17**, 2005–2011, 1983.
- Davies, R. Response of Cloud Supersaturation to Radiative Forcing. *J. Atmos. Sci.*, **42**, 2820–2825, 1985.
- Davis, D., J. Crawford, S. Liu, S. McKeen, A. Bandy, D. Thornton, F. Rowland, and D. Blake. Potential impact of iodine on tropospheric levels of ozone and other critical oxidants. *J. Geophys. Res.*, **101**, 2135 – 2147, 1996.
- Davis, W., Jr. and H. J. de Bruin. New activity coefficients of 0–100 per cent aqueous nitric acid. *J. Inorg. Nucl. Chem.*, **26**, 1069 – 1083, 1964.
- De Bruyn, W. J., J. A. Shorter, P. Davidovits, D. R. Worsnop, M. S. Zahniser, and C. E. Kolb. Uptake of gas phase sulfur species methanesulfonic acid, dimethylsulfoxide, and dimethyl sulfone by aqueous surface. *J. Geophys. Res.*, **99**, 16 927 – 16 932, 1994.
- Dean, J. A. *Lange's Handbook of Chemistry*. McGraw-Hill, Inc., 1992.
- Deister, U. and P. Warneck. Photooxidation of SO₃²⁻ in aqueous solution. *J. Phys. Chem.*, **94**, 2191–2198, 1990.
- DeMore, W. B., S. P. Sander, D. M. Golden, R. F. Hampson, M. J. Kurylo, C. J. Howard, A. R. Ravishankara, C. E. Kolb, and M. J. Molina. Chemical Kinetics and Photochemical Data for Use in Stratospheric Modeling. Technical Report JPL Publication 97-4, Jet Propulsion Laboratory, Pasadena, CA, 1997.

- Driedonks, A. G. M. and P. G. Duynkerke. Current Problems in the Stratocumulus-Topped Atmospheric Boundary Layer. *Bound. Lay. Met.*, **46**, 275 – 303, 1989.
- Eigen, M. and K. Kustin. The kinetics of halogen hydrolysis. *J. Am. Chem. Soc.*, **84**, 1355 – 1361, 1962.
- Espenson, J. H. *Chemical kinetics and reaction mechanisms*. McGraw-Hill, Inc., New York, 1995.
- Exner, M., H. Herrmann, and R. Zellner. Laser-based studies of reactions of the nitrate radical in aqueous solution. *Ber. Bunsenges. Phys. Chem.*, **96**, 470 – 477, 1992.
- Fogelman, K. D., D. M. Walker, and D. W. Margerum. Non-metal redox kinetics: Hypochlorite and hypochlorous acid reactions with sulfite. *Inorg. Chem.*, **28**, 986 – 993, 1989.
- Fortnum, D. H., C. J. Battaglia, S. R. Cohen, and J. O. Edwards. The kinetics of the oxidation of halide ions by monosubstituted peroxides. *J. Am. Chem. Soc.*, **82**, 778–782, 1960.
- Fuchs, N. A. and A. G. Sutugin. *Highly Dispersed Aerosols*. Ann Arbor Science Publishers, Ann Arbor, London, 1970.
- Furrow, S. Reactions of iodine intermediates in iodate-hydrogen peroxide oscillators. *J. Phys. Chem.*, **91**, 2129–2135, 1987.
- Gershenson, M., P. Davidovits, J. T. Jayne, C. E. Kolb, and D. R. Worsnop. Simultaneous Uptake of DMS and Ozone on Water. *J. Phys. Chem. A*, **105**, 7031 – 7036, 2001.
- Gombosi, T. I. *Gaskinetic Theory*. Cambridge University Press, 1994.
- Gong, S. L., L. A. Barrie, and J.-P. Blanchet. Modeling sea-salt aerosols in the atmosphere: 1. Model development. *J. Geophys. Res.*, **102**, 3805 – 3818, 1997.
- Haag, W. R. and J. Hoigné. Ozonation of bromide-containing waters: Kinetics of formation of hypobromous acid and bromate. *Environ. Sci. Technol.*, **17**, 261 – 267, 1983.
- Hanson, D. R., J. B. Burkholder, C. J. Howard, and A. R. Ravishankara. Measurement of OH and HO₂ radical uptake coefficients on water and sulfuric acid surfaces. *J. Phys. Chem.*, **96**, 4979–4985, 1992.
- Hanson, D. R., A. R. Ravishankara, and E. R. Lovejoy. Reaction of BrONO₂ with H₂O on submicron sulfuric acid aerosol and the implications for the lower stratosphere. *J. Geophys. Res.*, **101D**, 9063–9069, 1996.
- Herrmann, H., B. Ervens, H.-W. Jacobi, R. Wolke, P. Nowacki, and R. Zellner. CAPRAM2.3: A Chemical Aqueous Phase Radical Mechanism for Tropospheric Chemistry. *J. Atmos. Chem.*, **36**, 231 – 284, 2000.

- Herrmann, H., B. Ervens, P. Nowacki, R. Wolke, and R. Zellner. A chemical aqueous phase radical mechanism for tropospheric chemistry. *Chemosphere*, *38*, 1223 – 1232, 1999.
- Herrmann, H., A. Reese, and R. Zellner. Time resolved UV/VIS diode array absorption spectroscopy of SO_x^- ($x=3, 4, 5$) radical anions in aqueous solution. *J. Mol. Struct.*, *348*, 183–186, 1995.
- Hoffmann, M. R. On the kinetics and mechanism of oxidation of aquated sulfur dioxide by ozone. *Atmos. Environ.*, *20*, 1145 – 1154, 1986.
- Hoffmann, T., C. O'Dowd, and J. H. Seinfeld. Iodine oxide homogeneous nucleation: An explanation for coastal new particle production. *Geophys. Res. Lett.*, *28*, 1949 – 1952, 2001.
- Hoigné, J., H. Bader, W. R. Haag, and J. Staehelin. Rate constants of reactions of ozone with organic and inorganic compounds in water — III Inorganic compounds and radicals. *Wat. Res.*, *19*, 993–1004, 1985.
- Hoppel, W. A. and G. M. Frick. Submicron aerosol size distributions measured over the tropical and south Pacific. *Atmos. Environ.*, *24A*, 645 – 659, 1990.
- Houze, R. A., Jr. *Cloud Dynamics*. ap, 1993.
- Hu, J. H., Q. Shi, P. Davidovits, D. R. Worsnop, M. S. Zahniser, and C. E. Kolb. Reactive uptake of Cl_2 and Br_2 by aqueous surfaces as a function of Br^- and I^- ion concentration: The effect of chemical reaction at the interface. *J. Phys. Chem.*, *99*, 8768 – 8776, 1995.
- Hubinger, S. and J. B. Nee. Absorption spectra of Cl_2 , Br_2 and BrCl between 190 and 600 nm. *J. Photochem. Photobiol. A: Chem.*, *86*, 1–7, 1995.
- Huie, R. E. and P. Neta. Rate constants for some oxidations of S(IV) by radicals in aqueous solutions. *Atmos. Environ.*, *21*, 1743–1747, 1987.
- Huthwelker, T., S. L. Clegg, T. Peter, K. Carslaw, B. P. Luo, and P. Brimblecombe. Solubility of HOCl in water and aqueous H_2SO_4 to stratospheric temperatures. *J. Atmos. Chem.*, *21*, 81–95, 1995.
- Ingham, T., D. Bauer, R. Sander, P. J. Crutzen, and J. N. Crowley. Kinetics and Products of the Reactions $\text{BrO} + \text{DMS}$ and $\text{Br} + \text{DMS}$ at 298 K. *J. Phys. Chem. A*, *103*, 7199 – 7209, 1999.
- Jacob, D. J. Chemistry of OH in Remote Clouds and Its Role in the Production of Formic Acid and Peroxymonosulfate. *J. Geophys. Res.*, *91*, 9807 – 9826, 1986.
- Jacob, D. J. Heterogeneous chemistry and tropospheric ozone. *Atmos. Environ.*, *34*, 2131 – 2159, 2000.
- Jacobi, H.-W. *Kinetische Untersuchungen und Modellrechnungen zur troposphärischen Chemie von Radikalanionen und Ozon in wässriger Phase*. Ph.D. thesis, Universität Essen, Germany, 1996.

- Jacobi, H.-W., H. Herrmann, and R. Zellner. Kinetic investigation of the Cl_2^- radical in the aqueous phase. In P. Mirabel, editor, *Air Pollution Research Report 57: Homogenous and heterogeneous chemical Processes in the Troposphere*, pages 172–176. Office for official Publications of the European Communities, Luxembourg, 1996.
- Jaenicke, R. Aerosol Physics and Chemistry. In *Landolt-Börnstein "Zahlenwerte und Funktionen aus Naturwissenschaften und Technik"*, V 4b, pages 391–457. Springer, Heidelberg, 1988.
- Jayson, G. G., B. J. Parsons, and A. J. Swallow. Some simple, highly reactive, inorganic chlorine derivatives in aqueous solution. *J. Chem. Soc. Faraday Trans.*, **69**, 1597–1607, 1973.
- Jefferson, A., J. M. Nicovich, and P. H. Wine. Temperature-dependent kinetics studies of the reactions $\text{Br}({}^2\text{P}_{3/2}) + \text{CH}_3\text{SCH}_3 \leftrightarrow \text{CH}_3\text{SCH}_2 + \text{HBr}$. Heat of formation of the CH_3SCH_2 radical. *J. Phys. Chem.*, **98**, 7128 – 7135, 1994.
- Jenkin, M. E., R. A. Cox, and D. E. Candeland. Photochemical Aspects of Tropospheric Iodine behaviour. *J. Atmos. Chem.*, **2**, 359 – 375, 1985.
- Jiang, P.-Y., Y. Katsumura, R. Nagaishi, M. Domae, K. Ishikawa, K. Ishigure, and Y. Yoshida. Pulse radiolysis study of concentrated sulfuric acid solutions. Formation mechanism, yield and reactivity of sulfate radicals. *J. Chem. Soc. Faraday Trans.*, **88**, 1653–1658, 1992.
- Keene, W. C., J. Stutz, A. A. P. Pszenny, J. R. Maben, E. V. Fisher, A. M. Smith, R. von Glasow, S. Pechtl, B. C. Sive, and R. K. Varner. Inorganic chlorine and bromine in coastal New England air during summer. *J. Geophys. Res.*, **112**, D10S12, doi:10.1029/2006JD007689, 2007.
- Kelley, C. M. and H. V. Tartar. On the system: bromine-water. *J. Am. Chem. Soc.*, **78**, 5752–5756, 1956.
- Keppler, F., R. Borchers, P. Elsner, I. Fahimi, J. Pracht, and H. F. Schöler. Formation of volatile iodinated alkanes in soil: Results from laboratory studies. *Chemosphere*, **52**, 477 – 483, 2003.
- Kerminen, V.-M., T. Anttila, K. E. J. Lehtinen, and M. Kulmala. Parameterization for atmospheric new-particle formation: application to a system involving sulfuric acid and condensable water-soluble organic vapors. *Aerosol Sci. Technol.*, **38**, 1001 – 1008, 2004.
- Kerminen, V.-M. and M. Kulmala. Analytical formulae connecting the 'real' and the 'apparent' nucleation rate and the nuclei number concentration for atmospheric nucleation events. *J. Aerosol Sci.*, **33**, 609 – 622, 2002.
- Koch, T. G. and M. J. Rossi. Direct measurement of surface residence times: Nitryl chloride and chlorine nitrate on alkali halides at room temperature. *J. Phys. Chem. A*, **102**, 9193–9201, 1998.

- Kukui, A., D. Borissenko, G. Laverdet, and G. L. Bras. Gas phase reactions of OH radicals with dimethyl sulfoxide and methane sulfonic acid using turbulent flow reactor and chemical ionization mass spectrometry. *J. Phys. Chem. A*, **107**, 5732 – 5742, 2003.
- Kukui, A., V. Bossoutrot, G. Laverdet, and G. L. Bras. Mechanism of the Reaction of CH₃SO with NO₂ in Relation to Atmospheric Oxidation of Dimethyl Sulfide: Experimental and Theoretical Study. *J. Phys. Chem. A*, **104**, 935 – 946, 2000.
- Kumar, K. and D. W. Margerum. Kinetics and mechanism of general-acid-assisted oxidation of bromide by hypochlorite and hypochlorous acid. *Inorg. Chem.*, **26**, 2706 – 2711, 1987.
- Landgraf, J. *Modellierung photochemisch relevanter Strahlungsvorgänge in der Atmosphäre unter Berücksichtigung des Einflusses von Wolken*. Ph.D. thesis, Universität Mainz, Germany, 1998.
- Landgraf, J. and P. Crutzen. An Efficient Method for 'On-Line' Calculations of Photolysis and Heating Rates. *J. Atmos. Sci.*, **55**, 863 – 878, 1998.
- Laszlo, B., M. J. Kurylo, and R. E. Huie. Absorption cross sections, kinetics of formation, and self-reaction of the IO radical produced via the laser photolysis of N₂O/I₂/N₂ mixtures. *J. Phys. Chem.*, **99**, 11701 – 11707, 1995.
- Lax, E. *Taschenbuch für Chemiker und Physiker*. Springer Verlag, Berlin, 1969.
- Lee, C.-T. and W.-C. Hsu. The measurement of liquid water mass associated with collected hygroscopic particles. *J. Aerosol Sci.*, **31**, 189 – 197, 2000.
- Lee, Y.-N. and S. E. Schwartz. Reaction kinetics of nitrogen dioxide with liquid water at low partial pressure. *J. Phys. Chem.*, **85**, 840–848, 1981.
- Lelieveld, J. and P. J. Crutzen. The Role of Clouds in Tropospheric Photochemistry. *J. Atmos. Chem.*, **12**, 229 – 267, 1991.
- Lelieveld, J., P. J. Crutzen, and H. Rodhe. Zonal average cloud characteristics for global atmospheric chemistry modelling. Technical Report CM-76, Dep. of Meteorology, University of Stockholm (MISU), 1989.
- Lengyel, I., J. Li, K. Kustin, and I. R. Epstein. Rate constants for reactions between iodine- and chlorine-containing species: A detailed mechanism of the chlorine dioxide/chlorite reaction. *J. Am. Chem. Soc.*, **118**, 3708–3719, 1996.
- Lind, J. A. and G. L. Kok. Correction to "Henry's law determinations for aqueous solutions of hydrogen peroxide, methylhydroperoxide, and peroxyacetic acid" by John A. Lind and Gregory L. Kok. *J. Geophys. Res.*, **99D**, 21119, 1994.
- Lind, J. A., A. L. Lazarus, and G. L. Kok. Aqueous phase oxidation of sulfur(IV) by hydrogen peroxide, methylhydroperoxide, and peroxyacetic acid. *J. Geophys. Res.*, **92D**, 4171–4177, 1987.

- Liu, Q. and D. W. Margerum. Equilibrium and Kinetics of Bromine Chloride Hydrolysis. *est*, 35, 1127 – 1133, 2001.
- Logager, T., K. Sehested, and J. Holcman. Rate constants of the equilibrium reactions $\text{SO}_4 + \text{HNO}_3 \longleftrightarrow \text{HSO}_4^- + \text{NO}_3$ and $\text{SO}_4 + \text{NO}_3 \longleftrightarrow \text{SO}_4^{2-} + \text{NO}_3$. *Radiat. Phys. Chem.*, 41, 539 – 543, 1993.
- Loughlin, P. E., T. Trautmann, A. Bott, W. G. Panhans, and W. Zdunkowski. The effects of different radiation parameterisations on cloud evolution. *Q. J. R. Meteorol. Soc.*, 123, 1985–2007, 1997.
- Lucas, D. D. and R. G. Prinn. Mechanistic studies of dimethylsulfide oxidation products using an observationally constrained model. *J. Geophys. Res.*, 107, 4201, doi: 10.1029/2001JD000843, 2002.
- Luo, B., K. S. Carslaw, T. Peter, and S. Clegg. Vapour pressures of $\text{H}_2\text{SO}_4/\text{HNO}_3/\text{HCl}/\text{HBr}/\text{H}_2\text{O}$ solutions to low stratospheric temperatures. *Geophys. Res. Lett.*, 22, 247 – 250, 1995.
- Lurmann, F. W., A. C. Lloyd, and R. Atkinson. A Chemical Mechanism for Use in Long-Range Transport/Acid Deposition Computer Modeling. *J. Geophys. Res.*, 91, 10 905 – 10 936, 1986a.
- Lurmann, F. W., J. R. Young, and G. M. Hidy. A Study of Cloudwater Acidity Downwind of Urban and Power Plant Sources. In W. Jaeschke, editor, *Chemistry of Multiphase Atmospheric Systems*, pages ?? – 692. NATO ASI Series, Vol. G6, 1986b.
- Magi, L., F. Schweitzer, C. Pallares, S. Cherif, , P. Mirabel, and C. George. Investigation of the uptake rate of ozone and methyl hydroperoxide by water surfaces. *J. Phys. Chem. A*, 101, 4943–4949, 1997.
- Mallard, W. G., F. Westley, J. T. Herron, R. F. Hampson, and D. H. Frizzel. *NIST Chemical Kinetics Database: Version 5.0*. National Institute of Standards and Technology, Gaithersburg, MD, 1993.
- Mamou, A., J. Rabani, and D. Behar. On the oxidation of aqueous Br^- by OH radicals, studied by pulse radiolysis. *J. Phys. Chem.*, 81, 1447 – 1448, 1977.
- Marsh, A. R. W. and W. J. McElroy. The dissociation constant and Henry's law constant of HCl in aqueous solution. *Atmos. Environ.*, 19, 1075 – 1080, 1985.
- Mason, B. J. The role of sea-salt particles as cloud condensation nuclei over the remote oceans. *Q. J. R. Meteorol. Soc.*, 127, 2023 – 2032, 2001.
- Matthew, B. M., I. George, and C. Anastasio. Hydroperoxyl radical (HO_2) oxidizes dibromide radical anion (Br_2^-) to bromine (Br_2) in aqueous solution: Implication for the formation of Br_2 in the marine boundary layer. *Geophys. Res. Lett.*, 30, 2297, doi: 10.1029/2003GL018572, 2003.
- Mellor, G. L. and T. Yamada. Development of a Turbulence Closure Model for Geophysical Fluid Problems. *Rev. Geoph. Space Ph.*, 20, 851–875, 1982.

- Mentel, T. F., D. Bleilebens, and A. Wahner. A study of nighttime nitrogen oxide oxidation in a large reaction chamber — The fate of NO₂, N₂O₅, HNO₃, and O₃ at different humidities. *Atmos. Environ.*, *30*, 4007 – 4020, 1996.
- Monahan, E. C., D. E. Spiel, and K. L. Davidson. A model of marine aerosol generation via whitecaps and wave disruption. In E. C. Monahan and G. M. Niocaill, editors, *Oceanic Whitecaps*, pages 167 – 174. D. Reidel, Norwell, Mass, 1986.
- Nagy, J. C., K. Kumar, and D. W. Margerum. Non-metal redox kinetics: Oxidation of iodide by hypochlorous acid and by nitrogen trichloride measured by the pulsed-accelerated-flow method. *Inorg. Chem.*, *27*, 2773 – 2780, 1988.
- Napari, I., M. Noppel, H. Vehkämäki, and M. Kulmala. Parametrization of ternary nucleation rates for H₂SO₄ – NH₃ – H₂O vapors. *J. Geophys. Res.*, *107*, 4381, doi: 10.1029/2002JD002132, 2002.
- O'Dowd, C. and M. H. Smith. Physicochemical properties of aerosols over the northeast Atlantic: Evidence for wind-speed-related submicron sea-salt aerosol production. *J. Geophys. Res.*, *98*, 1137 – 1149, 1993.
- O'Dowd, C. D. K. H., J. Mäkelä, M. Väkeva, P. Aalto, G. de Leeuw, G. J. Kunz, E. Becker, H.-C. Hansson, A. G. Allen, R. M. Harrison, H. Berresheim, C. Kleefeld, M. Geever, S. G. Jennings, and M. Kulmala. Coastal new particle formation: Environmental conditions and aerosol physicochemical characteristics during nucleation bursts. *J. Geophys. Res.*, *107*, 8107, doi: 10.1029/2000JD000206, 2002.
- Olsen, R. J. and I. R. Epstein. Bifurcation analysis of chemical reaction mechanisms. I. Steady state bifurcation structure. *J. Chem. Phys.*, *94*, 3083–3095, 1991.
- Orlando, J. J. and G. S. Tyndall. Rate coefficients for the thermal decomposition of BrONO₂ and the heat of formation of BrONO₂. *J. Phys. Chem.*, *100*, 19398 – 19405, 1996.
- Palmer, D. A., R. W. Ramette, and R. E. Mesmer. The hydrolysis of iodine: Equilibria at high temperatures. *J. Nucl. Mater.*, *130*, 280–286, 1985.
- Pandis, S. N. and J. H. Seinfeld. Sensitivity Analysis of a Chemical Mechanism for Aqueous-Phase Atmospheric Chemistry. *J. Geophys. Res.*, *94*, 1105 – 1126, 1989.
- Pechtl, S., E. R. Lovejoy, J. B. Burkholder, and R. von Glasow. Modeling the possible role of iodine oxides in atmospheric new particle formation. *Atmos. Chem. Phys.*, *6*, 503 – 523, 2006.
- Pechtl, S., G. Schmitz, and R. von Glasow. Modeling iodide iodate speciation in atmospheric aerosol. *Atmos. Chem. Phys.*, *7*, 1381 – 1393, 2007.
- Pechtl, S. and R. von Glasow. Reactive chlorine in the marine boundary layer in the outflow of polluted continental air: A model study. *Geophys. Res. Lett.*, *34*, L11813, doi:10.1029/2007GL029761, 2007.
- Peixoto, J. P. and A. H. Oort. *Physics of Climate*. American Institute of Physics, New York, 1991.

- Pham, M., J.-F. Müller, G. P. Brasseur, C. Granier, and G. Mégie. A three-dimensional study of the tropospheric sulfur cycle. *J. Geophys. Res.*, *100*, 26 061 – 26 092, 1995.
- Pielke, R. A. *Mesoscale Meteorological Modeling*. Academic Press, 2002.
- Piot, M. and R. von Glasow. The chemistry influencing ODEs in the Polar Boundary Layer in spring: a model study. *Atmos. Chem. Phys. Discuss.*, *8*, 7391 – 7453, 2008a.
- Piot, M. and R. von Glasow. The potential importance of frost flowers, recycling on snow, and open leads for Ozone Depletion Events. *Atmos. Chem. Phys.*, *8*, 2437 – 2467, 2008b.
- Pitzer, K. S. Ion interaction approach: Theory and data correlation. In *Activity Coefficients in Electrolyte Solutions*, edited by K. S. Pitzer, pages 75 – 153. CRC Press, Boca Raton, 1991.
- Ponche, J. L., C. George, and P. Mirabel. Mass transfer at the air/water interface: Mass accommodation coefficients of SO₂, HNO₃, NO₂ and NH₃. *J. Atmos. Chem.*, *16*, 1–21, 1993.
- Pöschl, U., M. Canagaratna, J. T. Jayne, L. T. Molina, D. R. Worsnop, C. E. Kolb, and M. J. Molina. Mass accommodation coefficient of H₂SO₄ vapor on aqueous sulfuric acid surfaces and gaseous diffusion coefficient of H₂SO₄ in N₂/H₂O. *J. Phys. Chem. A*, *102*, 10 082–10 089, 1998.
- Pruppacher, H. R. and J. D. Klett. *Microphysics of Clouds and Precipitation*. Kluwer Academic Pub., Dordrecht/Boston/London, 1997.
- Quinn, P. K., T. S. Bates, J. E. Johnson, D. S. Covert, and R. J. Charlson. Interactions Between the Sulfur and Reduced Nitrogen Cycles Over the Central Pacific Ocean. *J. Geophys. Res.*, *95*, 16 405 – 16 416, 1990.
- Ray, A., I. Vassalli, G. Laverdet, and G. L. Bras. Kinetics of the Thermal Decomposition of the CH₃SO₂ Radical and Its Reaction with NO₂ at 1 Torr and 298 K. *J. Phys. Chem.*, *100*, 8895 – 8900, 1996.
- Régimbal, J.-M. and M. Mozurkewich. Peroxynitric acid decay mechanisms and kinetics at low pH. *J. Phys. Chem. A*, *101*, 8822–8829, 1997.
- Roehl, C. M., J. B. Burkholder, G. K. Moortgat, A. R. Ravishankara, and P. J. Crutzen. The temperature dependence of the UV absorption cross sections and the atmospheric implications of several alkyl iodides. *J. Geophys. Res.*, *102D*, 12 819–12 829, 1997.
- Ross, A. B., W. G. Mallard, W. P. Helman, B. H. J. Bielski, G. V. Buxton, D. E. Cabelli, C. L. Greenstock, R. E. Huie, and P. Neta. *NDRL-NIST Solution Kinetics Database: - Ver. 1*. National Institute of Standards and Technology, Gaithersburg, MD, 1992.
- Ross, A. B., W. G. Mallard, W. P. Helman, G. V. Buxton, R. E. Huie, and P. Neta. *NDRL-NIST Solution kinetics database: Version 3.0*. Notre Dame Radiation Laboratory, Notre Dame, and National Institut of Standards and Technology, Gaithersburg, 1998.

- Rudich, Y., R. K. Talukdar, T. Imamura, R. W. Fox, and A. R. Ravishankara. Uptake of NO_3^- on KI solutions: Rate coefficient for the $\text{NO}_3^- + \text{I}^-$ reaction and gas-phase diffusion coefficients for NO_3^- . *Chem. Phys. Lett.*, **261**, 467–473, 1996.
- Ruggaber, A., R. Dlugi, A. Bott, R. Forkel, H. Herrmann, and H.-W. Jacobi. Modelling of radiation quantities and photolysis frequencies in the aqueous phase in the troposphere. *Atmos. Environ.*, **31**, 3137 – 3150, 1997.
- Sander, R. Modeling Atmospheric Chemistry: Interactions between Gas-Phase Species and Liquid Cloud/Aerosol Particles. *Surv. Geophys.*, **20**, 1 – 31, 1999.
- Sander, R. and P. J. Crutzen. Model study indicating halogen activation and ozone destruction in polluted air masses transported to the sea. *J. Geophys. Res.*, **101**, 9121 – 9138, 1996.
- Sander, R., W. C. Keene, A. A. P. Pszenny, R. Arimoto, G. P. Ayers, E. Baboukas, J. M. Cainey, P. J. Crutzen, R. A. Duce, G. Hönniger, B. J. Huebert, W. Maenhaut, N. Mihalopoulos, V. C. Turekian, and R. V. Dingenen. Inorganic bromine compounds in the marine boundary layer: A critical review. *Atmos. Chem. Phys.*, **3**, 1301 – 1336, 2003.
- Sander, S. P., R. R. Friedl, W. B. DeMore, D. M. Golden, M. J. Kurylo, R. F. Hampson, R. E. Huie, G. K. Moortgat, A. R. Ravishankara, C. E. Kolb, and M. J. Molina. Chemical Kinetics and Photochemical Data for Use in Stratospheric Modeling. Technical Report JPL Publication 00-3, Jet Propulsion Laboratory, Pasadena, CA, 2000.
- Sandu, A. and R. Sander. Technical note: Simulating chemical systems in Fortran90 and Matlab with the Kinetic PreProcessor KPP-2.1. *Atmos. Chem. Phys.*, **6**, 187 – 195, 2006.
- Scheffler, D., H. Grothe, H. Willner, A. Frenzel, and C. Zetzsch. Properties of Pure Nitryl Bromide. Thermal Behaviour, UV/Vis and FTIR Spectra, and Photoisomerization to *trans*-BrONO in an Argon Matrix. *Inorg. Chem.*, **36**, 335 – 338, 1997.
- Schwartz, S. E. Mass-Transport Considerations Pertinent to Aqueous Phase Reactions of Gases in Liquid-Water Clouds. In W. Jaeschke, editor, *Chemistry of Multiphase Atmospheric Systems*, pages 415 – 471. NATO ASI Series, Vol. G6, 1986.
- Schwartz, S. E. and W. H. White. Solubility equilibria of the nitrogen oxides and oxyacids in dilute aqueous solution. In J. R. Pfafflin and E. N. Ziegler, editors, *Advances in Environmental Science and Engineering*, volume 4, pages 1–45. Gordon and Breach Science Publishers, NY, 1981.
- Schwarz, H. A. and B. H. J. Bielski. Reactions of HO_2 and O_2^- with iodine and bromine and the I_2^- and I atom reduction potentials. *J. Phys. Chem.*, **90**, 1445 – 1448, 1986.
- Schweitzer, F., P. Mirabel, and C. George. Uptake of hydrogen halides by water droplets. *J. Phys. Chem. A*, **104**, 72–76, 2000.
- Seery, D. J. and D. Britton. The continuous absorption spectra of chlorine, bromine, bromine chloride, iodine chloride, and iodine bromide. *J. Phys. Chem.*, **68**, 2263–2266, 1964.

- Sehested, K., J. Holcman, E. Bjergbakke, and E. J. Hart. A pulse radiolytic study of the reaction OH + O₃ in aqueous medium. *J. Phys. Chem.*, **88**, 4144–4147, 1984.
- Sehested, K., J. Holcman, and E. J. Hart. Rate constants and products of the reactions of e_{aq}⁻, O₂⁻ and H with ozone in aqueous solutions. *J. Phys. Chem.*, **87**, 1951–1954, 1983.
- Sehested, K., O. L. Rasmussen, and H. Fricke. Rate constants of OH with HO₂, O₂⁻, and H₂O₂⁺ from hydrogen peroxide formation in pulse-irradiated oxygenated water. *J. Phys. Chem.*, **72**, 626–631, 1968.
- Seinfeld, J. H. and S. N. Pandis. *Atmospheric Chemistry and Physics*. John Wiley & Sons, New York, Chichester, Weinheim, 1998.
- Shaw, M. A. and M. J. Rood. Measurement of the crystallization humidities of ambient aerosol particles. *Atmos. Environ.*, **24A**, 1837 – 1841, 1990.
- Shoute, L. C. T., Z. B. Alfassi, P. Neta, and R. E. Huie. Temperature dependence of the rate constants for reaction of dihalide and azide radicals with inorganic reductants. *J. Phys. Chem.*, **95**, 3238 – 3242, 1991.
- Singh, H. B. and P. B. Zimmerman. Atmospheric distribution and sources of non-methane hydrocarbons. *Adv. Environ. Sci. Technol.*, **24**, 177 – 235, 1992.
- Smith, M. H., P. M. Park, and I. E. Consterdine. Marine aerosol concentrations and estimated fluxes over the sea. *Q. J. R. Meteorol. Soc.*, **119**, 809 – 824, 1993.
- Smoydzin, L. *Modelling Gas Phase and Aerosol Phase Chemistry in the Atmospheric Boundary Layer*. Ph.D. thesis, Universität Heidelberg, Germany, <http://www.ub.uni-heidelberg.de/archiv/8501>, 2008.
- Smoydzin, L. and R. von Glasow. Do organic surface films on sea salt aerosols influence atmospheric chemistry? A model study. *Atmos. Chem. Phys.*, **7**, 5555 – 5567, 2007.
- Stull, R. B. *An Introduction to Boundary Layer Meteorology*. Kluwer Academic Pub., Dordrecht/Boston/London, 1988.
- Stutz, J., O. Pikelnaya, S. C. Hurlock, S. Trick, S. Pechtl, and R. von Glasow. Daytime OIO in the Gulf of Maine. *Geophys. Res. Lett.*, **34**, L22816, doi:10.1029/2007GL031332, 2007.
- Takami, A., S. Kato, A. Shimono, and S. Koda. Uptake coefficient of OH radical on aqueous surface. *Chem. Phys.*, **231**, 215–227, 1998.
- Tang, I. N. Thermodynamic and optical properties of mixed-salt aerosols of atmospheric interest. *J. Geophys. Res.*, **102**, 1883 – 1893, 1997.
- Thomas, K., A. Volz-Thomas, and D. Kley. *Zur Wechselwirkung von NO₃-Radikalen mit wässrigen Lösungen: Bestimmung des Henry- und des Massenakkommodationskoeffizienten*. Ph.D. thesis, Institut für Chemie und Dynamik der Geosphäre 2, Forschungszentrum Jülich GmbH, FRG, 1993.

- Trautmann, T., I. Podgorny, J. Landgraf, and P. J. Crutzen. Actinic fluxes and photodissociation coefficients in cloud fields embedded in realistic atmospheres. *J. Geophys. Res.*, **104**, 30 173 – 30 192, 1999.
- Troy, R. C., M. D. Kelley, J. C. Nagy, and D. W. Margerum. Non-metal redox kinetics: Iodine monobromide reaction with iodide ion and the hydrolysis of IBr. *Inorg. Chem.*, **30**, 4838 – 4845, 1991.
- Troy, R. C. and D. W. Margerum. Non-metal redox kinetics: Hypobromite and hypobromous acid reactions with iodide and with sulfite and the hydrolysis of bromosulfate. *Inorg. Chem.*, **30**, 3538 – 3543, 1991.
- Urbanski, S., R. E. Stickel, and P. H. Wine. Mechanistic and kinetic study of the gas-phase reaction of hydroxyl radical with dimethyl sulfoxide. *J. Phys. Chem. A*, **102**, 10 522 – 10 529, 1998.
- Urbanski, S., R. E. Stickel, Z. Z. Zhao, and P. H. Wine. Mechanistic and kinetic study of formaldehyde production in the atmospheric oxidation of dimethyl sulfide. *J. Chem. Soc. Faraday Trans.*, **93**, 2813 – 2819, 1997.
- van Dingenen, R., N. R. Jensen, J. Hjorth, and F. Raes. Peroxynitrate Formation During the Night-Time Oxidation of Dimethylsulfide: Its Role as a Reservoir Species for Aerosol Formation. *J. Atmos. Chem.*, **18**, 211 – 237, 1994.
- Verwer, J. G., E. J. Spee, J. G. Blom, and W. H. Hundsorfer. A second order Rosenbrock method applied to photochemical dispersion problems. Technical Report MAS-R9717, Centrum voor Wiskunde en Informatica, Amsterdam, The Netherlands, <http://www.cwi.nl>, 1997.
- Vogt, R., P. J. Crutzen, and R. Sander. A mechanism for halogen release from sea-salt aerosol in the remote marine boundary layer. *Nature*, **383**, 327 – 330, 1996.
- Vogt, R., R. Sander, R. von Glasow, and P. Crutzen. Iodine Chemistry and its Role in Halogen Activation and Ozone Loss in the Marine Boundary Layer: A Model Study. *J. Atmos. Chem.*, **32**, 375 – 395, 1999.
- von Glasow, R. *Modeling the gas and aqueous phase chemistry of the marine boundary layer*. Ph.D. thesis, Universität Mainz, Germany, <http://www.rolandvonglasow.de>, 2001.
- von Glasow, R. Importance of the surface reaction OH + Cl⁻ on sea salt aerosol for the chemistry of the marine boundary layer - a model study. *Atmos. Chem. Phys.*, **6**, 3571 – 3581, 2006.
- von Glasow, R. Pollution meets sea salt. *Nature Geosc.*, **1**, 292, 2008.
- von Glasow, R. and A. Bott. Interaction of radiation fog with tall vegetation. *Atmos. Environ.*, **33**, 1333 – 1346, 1999.
- von Glasow, R. and P. J. Crutzen. Model study of multiphase DMS oxidation with a focus on halogens. *Atmos. Chem. Phys.*, **4**, 589 – 608, 2004.

- von Glasow, R. and P. J. Crutzen. Tropospheric halogen chemistry. In Treatise on Geochemistry Update 1, vol.4.02 (eds. H. D. Holland and K. K. Turekian), pages 1 – 67. Elsevier-Pergamon, Oxford, 2007.
- von Glasow, R. and R. Sander. Variation of sea salt aerosol pH with relative humidity. *Geophys. Res. Lett.*, 28, 247 – 250, 2001.
- von Glasow, R., R. Sander, A. Bott, and P. J. Crutzen. Modeling halogen chemistry in the marine boundary layer. 1. Cloud-free MBL. *J. Geophys. Res.*, 107, 4341, doi: 10.1029/2001JD000942, 2002a.
- von Glasow, R., R. Sander, A. Bott, and P. J. Crutzen. Modeling halogen chemistry in the marine boundary layer. 2. Interactions with sulfur and cloud-covered MBL. *J. Geophys. Res.*, 107, 4323, doi: 10.1029/2001JD000943, 2002b.
- von Gunten, U. and Y. Oliveras. Advanced oxidation of bromide-containing waters: Bromate formation mechanisms. *Environ. Sci. Technol.*, 32, 63 – 70, 1998.
- Wagner, I. and H. Strehlow. On the flash photolysis of bromide ions in aqueous solution. *Ber. Bunsenges. Phys. Chem.*, 91, 1317 – 1321, 1987.
- Wagner, V., R. von Glasow, H. Fischer, and P. J. Crutzen. Are CH₂O Measurements in the Marine Boundary Layer Suitable for Testing the Current Understanding of CH₄ Photooxidation? *J. Geophys. Res.*, 107, 4029, doi: 10.1029/2001JD000722, 2002.
- Wallington, T. J., J. M. Andino, J. C. Ball, and S. M. Japar. Fourier transform infrared studies of the reaction of Cl atoms with PAN, PPN, CH₃OOH, HCOOH, CH₃COCH₃ and CH₃COC₂H₅ at 295±2 K. *J. Atmos. Chem.*, 10, 301 – 313, 1990.
- Wang, T. X., M. D. Kelley, J. N. Cooper, R. C. Beckwith, and D. W. Margerum. Equilibrium, kinetic, and UV-spectral characteristics of aqueous bromine chloride, bromine, and chlorine species. *Inorg. Chem.*, 33, 5872 – 5878, 1994.
- Wang, Y. L., J. C. Nagy, and D. W. Margerum. Kinetics of hydrolysis of iodine monochloride measured by the pulsed-accelerated-flow method. *J. Am. Chem. Soc.*, 111, 7838 – 7844, 1989.
- Warneck, P. The relative importance of various pathways for the oxidation of sulfur dioxide and nitrogen dioxide in sunlit continental fair weather clouds. *Phys. Chem. Chem. Phys.*, 1, 5471 – 5483, 1999.
- Wayne, R. P., I. Barnes, P. Biggs, J. P. Burrows, C. E. Canosa-Mas, J. Hjorth, G. Le Bras, G. K. Moortgat, D. Perner, G. Poulet, G. Restelli, and H. Sidebottom. The nitrate radical: Physics, chemistry, and the atmosphere. *Atmos. Environ.*, 25A, 1–203, 1991.
- Weast, R. C., editor. *CRC Handbook of Chemistry and Physics, 61st Edition*. CRC Press, Inc., Boca Raton, FL, 1980.
- Weinstein-Lloyd, J. and S. E. Schwartz. Low-intensity radiolysis study of free-radical reactions in cloudwater: H₂O₂ production and destruction. *Environ. Sci. Technol.*, 25, 791–800, 1991.

- Wesely, M. L. Parameterization of surface resistances to gaseous deposition in regional-scale numerical models. *Atmos. Environ.*, **23**, 1293 – 1304, 1989.
- Wilhelm, E., R. Battino, and R. J. Wilcock. Low-pressure solubility of gases in liquid water. *Chem. Rev.*, **77**, 219–262, 1977.
- Wine, P. H., Y. Tang, R. P. Thorn, J. R. Wells, and D. D. Davis. Kinetics of aqueous phase reactions of the SO_4^- radical with potential importance in cloud chemistry. *J. Geophys. Res.*, **94D**, 1085–1094, 1989.
- Woodcock, A. H., C. F. Kientzler, A. B. Arons, and D. C. Blanchard. Giant Condensation Nuclei from Bursting Bubbles. *Nature*, **172**, 1144 – 1145, 1953.
- Worsnop, D. R., M. S. Zahniser, C. E. Kolb, J. A. Gardner, L. R. Watson, J. M. van Doren, J. T. Jayne, and P. Davidovits. The temperature dependence of mass accommodation of SO_2 and H_2O_2 on aqueous surfaces. *J. Phys. Chem.*, **93**, 1159–1172, 1989.
- Wu, D., D. Wong, and B. Di Bartolo. Evolution of Cl_2^- in aqueous NaCl solutions. *J. Photochem.*, **14**, 303–310, 1980.
- Wu, J. Production of Spume Drops by the Wind Tearing of Wave Crests: The Search for Quantification. *J. Geophys. Res.*, **98**, 18 221 – 18 227, 1993.
- Yin, F., D. Grosjean, and J. H. Seinfeld. Photooxidation of Dimethyl Sulfide and Dimethyl Disulfide. I: Mechanism Development. *J. Atmos. Chem.*, **11**, 309 – 364, 1990.
- Yokelson, R. J., J. B. Burkholder, L. Goldfarb, R. W. Fox, M. K. Gilles, and A. R. Ravishankara. Temperature dependent rate coefficient for the $\text{Cl} + \text{ClONO}_2$ reaction. *J. Phys. Chem.*, **99**, 13 976–13 983, 1995.
- Yu, X.-Y. *Kinetics of free radical reactions generated by laser flash photolysis of $\text{OH} + \text{Cl}^-$ and $\text{SO}_4^- + \text{Cl}^-$ in the aqueous phase – Chemical mechanism, kinetics data and their implications*. Ph.D. thesis, University of Michigan, Ann Arbor, 2001.
- Zdunkowski, W. G., W.-G. Panhans, R. M. Welch, and G. J. Korb. A Radiation Scheme for Circulation and Climate Models. *Contr. Physics Atm.*, **55**, 215–238, 1982.
- Zehavi, D. and J. Rabani. Oxidation of aqueous bromide ions by hydroxyl radicals. Pulse radiolytic investigation. *J. Phys. Chem.*, **76**, 312 – 319, 1972.
- Zellner, R., M. Exner, and H. Herrmann. Absolute OH Quantum Yield in the Laser Photolysis of Nitrate, Nitrite and Dissolved H_2O_2 at 308 and 351 nm in the Temperature Range 278–353 K. *J. Atmos. Chem.*, **10**, 411 – 425, 1990.

List of Tables

1.1	Ionic composition of sea water.	7
2.1	Subdivision of the spectral range of the photolysis module.	17
2.2	Initial mixing ratios of gas phase species (in nmol/mol).	20
2.3	Initial size distribution of the aerosol.	20
3.1	Brief description of the files. ¹ The routines in <code>bud_*.f</code> are for output of the rates in 8 predefined levels only, whereas <code>bud_s_*.f</code> ensure output of the sulfur rates for all model layers.	25
5.1	Subdivision of the spectral range $178.6 \text{ nm} \leq \lambda \leq 752.5 \text{ nm}$ in eight intervals; λ_a and λ_b are the initial and the final, and λ_i the fixed wavelength in interval I_i . σ_{O_2} and σ_{O_3} are the oxygen and ozone cross section for the wavelengths λ_i .	45
5.2	What to change for a new NOT temperature dependent species in the band model (<code>jrate.f</code>)	49
5.3	What to change additionally for a new temperature dependent species in the band model (<code>jrate.f</code>)	51
C.2	The variables of KPP are not listed here.	65
D.1	Species	68
D.2	Gas phase reactions.	69
D.2	Continued.	70
D.2	Continued.	71
D.2	Continued.	72
D.2	Continued.	73
D.3	Aqueous phase reactions.	74
D.3	Continued.	75
D.3	Continued.	76
D.3	Continued.	77
D.3	Continued.	78
D.3	Continued.	79
D.4	Heterogeneous reactions.	80
D.5	Aqueous phase equilibrium constants.	81
D.6	Henry constants and accommodation coefficients.	82
D.7	Species	83
D.8	Gas phase reactions.	84
D.8	Continued.	85

D.9 Aqueous phase reactions.	86
D.10 Heterogeneous reactions.	87
D.11 Aqueous phase equilibrium constants.	88
D.12 Henry constants and accommodation coefficients.	89

Index

- actinic flux, 17, 44
- add reaction, 34
- add species, 34
- aerosol processing, 15
- bubble bursting, 6
- crystallisation, 15
- deliquescence, 15
- dry deposition, 18
- emission, gases, 17
- emission, sea salt aerosol, 17
- grid, 21, 29, 59
- Henry's law, 14
- initialisation, 15, 19
- inversion, 5
- KPP, 21, 31
- marine boundary layer, 5
- microphysics, treatment of, 11
- model grid, 29
- multiple scattering, 52
- ozone hole, 7
- particle grid, 14, 29
- photolysis, 16, 44
- PIFM2, 12, 59
- prognostic equations, 9
- prognostic variables, 9, 13, 14, 29
- radiation, treatment of, 12
- reaction cycles, major, 66
- sea salt aerosol production, 6
- sea water composition, 6
- soil, 25
- subroutine kpp_driver, 30
- subroutine liq_parm, 30
- subsidence, large scale, 10
- timestep, 21
- turbulence, treatment of, 10
- uptake coefficient, 13